RÉPUBLIQUE ALGÉRIENNE DÉMOCRATIQUE ET POPULAIRE
MINISTÈRE DE L'ENSEIGNEMENT SUPÉRIEUR ET DE LA RECHERCHE SCIENTIFIQUE
UNIVERSITÉ MOHAMED BOUDIAF - M'SILA
FACULTÉ DE MATHÉMATIQUES ET DE L'INFORMATIQUE
DÉPARTEMENT DE MATHÉMATIQUES

N° d'ordre : .....

# T H È S E

*Présentée pour l'obtention du diplôme*
*de Doctorat de Troisième Cycle (LMD)*

**Domaine**
*Mathématiques et Informatique*

**Spécialité**
*Analyse numérique, EDPs et applications*

**Par**

HOSSEMDDINE ACHOUR

**Thème**

# Étude d'EDPs liées à l'amélioration de contour d'image par auto similarité intermediaire.

Soutenue le 08/05/2025 devant le jury composé de :

| | | | |
|---|---|---|---|
| **Merzougui Abdelkrim** | **Prof.** | **Université de Msila** | **Président** |
| **Benhamidouche Noureddine** | **Prof.** | **Université de Msila** | **Directeur** |
| **Chouder Rafaa** | **MCA** | **Université de Msila** | **Co-Directeur** |
| **Benterki Djamel** | **Prof.** | **Université de Setif** | **Examinateur** |
| **Gagui Bachir** | **MCA** | **Université de Msila** | **Examinateur** |

Année Universitaire : 2024/2025

DEMOCRATIC AND POPULAR REPUBLIC OF ALGERIA
MINISTRY OF HIGHER EDUCATION AND SCIENTIFIC RESEARCH
MOHAMED BOUDIAF UNIVERSITY - M'SILA
FACULTY OF MATHEMATICS AND COMPUTER SCIENCE
DEPARTMENT OF MATHEMATICS

Order No.: .....

# THESIS

*Submitted in partial fulfillment of the requirements for the degree of Doctorate (Third Cycle LMD)*

**Domain**

*Mathematics and Computer Science*

**Specialty**

*Numerical Analysis, PDEs and Applications*

**By**

HOSSEMDDINE ACHOUR

**Title**

## Study of PDEs Related to Image Contour Enhancement Through Intermediate Self-Similarity.

Defended on 08/05/2025 before the committee composed of:

| | | | |
|---|---|---|---|
| **Merzougui Abdelkrim** | **Prof.** | **University of Msila** | **Chairman** |
| **Benhamidouche Noureddine** | **Prof.** | **University of Msila** | **Supervisor** |
| **Chouder Rafaa** | **Assoc. Prof.** | **University of Msila** | **Co-Supervisor** |
| **Benterki Djamel** | **Prof.** | **University of Setif** | **Examiner** |
| **Gagui Bachir** | **Assoc. Prof.** | **University of Msila** | **Examiner** |

Academic Year: 2024/2025

# *Acknowledgements*

*I acknowledge the presence of God who created me and gave me this rare privilege to achieve my dream of attaining the highest qualification. All praises are due to Almighty God Allah, Who provided me with the strength and willingness to undertake this work and the opportunity to contribute a drop in the sea of knowledge.*

*Firstly, I would like to express my sincere gratitude to my advisor, Prof. Benhamidouche Noureddine, for the continuous support of my Ph.D study and related research, for his patience, motivation, and immense knowledge. His guidance helped me throughout the research and writing of this thesis. I could not have imagined having a better advisor and mentor for my Ph.D study; it has been a great pleasure working with him.*

*I am equally deeply grateful to my co-advisor, Prof. Chouder Rafaa, who was a true mentor in every sense. He never hesitated to share his knowledge and supported me tirelessly throughout my work. His humanity and dedication left a lasting impact on my academic journey.*

*I sincerely thank the chairman of the jury committee, Prof. Merzougui Abdelkrim, and the other jury members, Prof. Benterki Djamel, Dr. Gagui Bachir, for agreeing to read the manuscript.*

*I extend my heartfelt thanks to all faculty members of the Department of Mathematics for their continuous encouragement, inspiring motivation, and invaluable advice and guidance throughout my academic journey.*

*Last but not least, I would like to thank my family: my parents, my brothers, for supporting me spiritually throughout writing this thesis and my life in general. To my precious wife, I owe boundless gratitude for her unwavering patience, sacrifices, and emotional support during every step of this Ph.D journey—her presence was my greatest strength.*

# Contents

# List of Figures

# List of Symbols

## Mathematical Symbols

| | |
|---|---|
| $u(x, y, t)$ | **Image intensity: Gray level value at pixel** $(x, y)$**, time** $t$ |
| $u_0(x, y)$ | **Initial image: Original input image data** |
| $\nabla u$ | **Gradient:** $\left(\frac{\partial u}{\partial x}, \frac{\partial u}{\partial y}\right)^T$ |
| $\|\nabla u\|$ | **Gradient magnitude:** $\|\nabla u\| = \sqrt{\left(\frac{\partial u}{\partial x}\right)^2 + \left(\frac{\partial u}{\partial y}\right)^2}$ |
| $\Delta u$ | **Laplacian:** $\Delta u = \Delta u = \frac{\partial^2 u}{\partial x^2} + \frac{\partial^2 u}{\partial y^2}$ |
| $\partial_t u$**,** $u_t$ | **Time derivative:** $\frac{\partial u}{\partial t} = \lim_{h \to 0} \frac{u(t+h) - u(t)}{h}$ |
| $\partial_x u$**,** $u_x$ | **Spatial derivative:** $\frac{\partial u}{\partial x} = \lim_{h \to 0} \frac{u(x+h, y) - u(x, y)}{h}$ |
| div | **Divergence:** $\operatorname{div}(\mathbf{F}) = \frac{\partial F_x}{\partial x} + \frac{\partial F_y}{\partial y}$ |
| $\Omega$ | **Image domain: Typically** $\Omega \subseteq \mathbb{R}^2$ **rectangle** |
| $\xi$ | **Similarity variable:** $\xi = x / t^\beta$ **for self-similar solutions** |
| $\phi(\xi)$ | **Profile function: Solution form** $u(x, t) = t^\alpha \phi(\xi)$ |
| $\alpha, \gamma, \mu, \nu$ | **Scaling exponents in self-similar solutions** |
| $T$ | **Final time or critical time** |
| $\sigma$ | **Standard deviation (Gaussian kernel)** |
| $\theta$ | **Gradient angle:** $\theta = \arctan\left(\frac{\partial_y u}{\partial_x u}\right)$ |

## Model Parameters

| | |
|---|---|
| $p, q$ | **Diffusion exponents: In** $\frac{\partial u}{\partial t} = \frac{1}{\|\nabla u\|^q} \operatorname{div}\left(\frac{\nabla u}{\|\nabla u\|^p}\right)$ |
| $k$ | **Edge threshold: In** $g(\|\nabla u\|) = e^{-(\|\nabla u\|/k)^2}$ **(Perona-Malik)** |
| $\lambda$ | **Regularization weight: In energy minimization** |
| $\delta$ | **Noise level/contrast parameter** |
| $\omega$ | **Flux exponent:** $\omega = -(q + p - 1)$ **in** $\Psi(u_x) = \frac{1}{\omega} u_x^\omega$ |

## Special Functions and Operators

| | |
|---|---|
| $G(x, y, t)$ | **Gaussian kernel:** $G(x, y, t) = \frac{1}{4\pi t} \exp\left(-\frac{x^2 + y^2}{4t}\right)$ |
| $g(\|\nabla u\|)$ | **Diffusivity:** $g(s) = \frac{1}{1 + (s/k)^2}$ **(Perona-Malik)** |
| $\mathbf{erf}(x)$ | **Error function:** $\mathbf{erf}(x) = \frac{2}{\sqrt{\pi}} \int_0^x e^{-t^2} \, dt$ |

## Free Boundary

| | |
|---|---|
| $l(t), r(t)$ | **Moving boundaries: Solutions of free boundary problem** |
| $a(t)$ | **Scaling function:** $a(t) = [\alpha(q+p-2)\,t + A_0]^{1/(q+p-2)}$ |
| $C$ | **Integration constant in profile solutions** |
| $A_0$ | **Initial condition constant** |

# *Introduction*

Partial differential equations (PDEs) offer a natural and systematic framework for modeling diverse real-world phenomena, with applications spanning physics, life sciences, and economics. Hence, it is unsurprising that they have made significant contributions to the mathematical foundations of signal and image analysis. They appear in the form of Euler-Lagrange equations when dealing with continuous optimization problems arising from variational models [8, 18] or from the regularization of ill-posed problems [14]. They have been demonstrated to be the inherent framework for scale-spaces [2], effectively employed for image enhancement [56], inpainting [51], and image compression [27]. PDE-based models derive advantages from extensive study on their theoretical underpinnings and effective numerical techniques spanning several decades. Due to their continuous nature, it is straightforward to incorporate advantageous invariances, including rotation invariance.

One of the most compelling characteristics of PDE-based image analysis lies in its capacity to unify and integrate a wide range of established techniques within the domain of image processing. This integrative framework has not only facilitated deeper structural understanding of image features but has also driven the advancement of innovative algorithms. Notable examples of PDE formulations and their applications in image analysis include Gaussian smoothing [31], morphological operations such as dilation and erosion [2, 6, 54], morphological amoebas [58], mean curvature motion [40, 2], and nonlinear diffusion filtering [47, 17].

Diffusion equations have been widely utilised in image processing since their introduction by Perona and Malik [47], who demonstrated that edge enhancement is achievable when the image intensity flux opposes the intensity gradient. Key approaches, such as mean curvature motion and nonlinear diffusion filtering, emphasise the significance of directional information in images. Research into mean curvature motion (MCM) and mean curvature flow (MCF) has established their foundational role in image processing and surface evolution, alongside related geometric flows like the Beltrami flow and the Perona-Malik model. Alvarez et al. [3] proposed an alternative approach, directing image flux orthogonally to the intensity gradient to enhance edges. Concurrently, Malladi and Sethian [39, 40] introduced a curvature-driven model grounded in differential geometry. Further generalisations were explored by Barenblatt and Vazquez [9, 55], whose numerical and asymptotic studies [35, 40] revealed the emergence of high-intensity contrast regions. This

led to the identification of boundary layers, where large gradients concentrate, enabling model simplification within these regions [9].

Authors in [9, 55] proposed a model for image contour enhancement where a free boundary problem. Their theory addresses the existence and uniqueness of solutions to the appropriate problem, the existence and characteristics of bounding interfaces, and the behaviour over extended time periods. In [20, 21], the authors generalized Barenblatt results to improve contour enhancement techniques in image processing. This generalization enables the modeling of more complex edge behaviors, making it possible to detect and enhance contours even in images with poor quality or irregular boundaries. Additionally, they presented generalized results concerning the free boundary problem, which deals with the mathematical description of boundaries that evolve over time.

Our contribution to this work is to introduce a new evolution model based on the nonlinear diffusion equation, considered a generalization of mean curvature motion:

$$\frac{\partial u}{\partial t} = \frac{1}{|\nabla u|^q} \operatorname{div}\left(\frac{\nabla u}{|\nabla u|^p}\right). \tag{1}$$

The parameters $p$ and $q$ play a crucial role in controlling the nature of the diffusion process. This model is particularly effective in analysing the contour enhancement process in images, allowing for more precise control over the diffusion process around image contours. We formulated a free boundary problem that describes the evolution of image intensity within boundary layers around the contour. This formulation offers a more dynamic and adaptable method for handling image contour. The free-boundary approach provides a robust framework for accurately modeling the inherent variations and structural complexities present in images. By allowing the boundary to evolve dynamically based on the underlying image features, this method effectively captures subtle changes in texture, contrast, and contour sharpness that are often challenging to model using fixed-boundary techniques. In this context, we aim to determine exact solutions to nonlinear diffusion equations relevant to image processing. Our methodology relies on the application of general self-similar solutions, following the pioneering approach of Barenblatt. This approach facilitates the derivation of precise analytical solutions for specific classes of nonlinear partial differential equations (PDEs), enhancing our understanding of the diffusion dynamics that govern image contour behavior and intensity transitions.

This work is organized into four chapters:

In the first chapter, we introduce the fundamental concepts that underscore the importance of mathematics in image processing and computer vision. The chapter highlights the essential role of mathematical models, such as differential equations and optimisation techniques, in addressing the challenges inherent in these fields. We also provide a comprehensive overview of various

image enhancement methods proposed in the literature, giving the reader insight into how these techniques have evolved. Furthermore, we define the notation used throughout this manuscript, ensuring consistency and clarity in the presentation of mathematical formulations. Additionally, we revisit classical mathematical principles that are crucial for understanding the more advanced concepts discussed in the subsequent chapters.

In the second chapter, we introduce a novel approach to image intensity evolution by formulating a new model based on nonlinear diffusion equations, which serves as a generalisation of mean curvature motion. This model is particularly suited for describing the evolution of image intensity in boundary layers located near contours, where abrupt changes in intensity typically occur. To account for the evolving boundary, we have formulated a free boundary problem, which represents an important advancement in the field. This formulation offers a more dynamic, flexible, and efficient approach for handling image contours, addressing some of the limitations of traditional methods. As part of the analysis, we examine the asymptotic behaviour of a simplified one-dimensional case. We also present results for varying parameter values $p$ and $q$, specifically considering the condition where $1-p \geq q$ and $p < 1$, providing further insights into how the parameters influence the solution of the problem.

In the third chapter, we conducted a study on the free boundary problem that describes the evolution of image intensity in the boundary layer, when $q > 1-p$ and $p < 1$, by presenting self-similar general solutions. The contour enhancement is represented by three different kinds of self-similar solutions. We also presents some numerical simulations for the proposed model on 2-D gray-level images to validate the theoretical findings. The results found are submitted by Achour , Chouder and Benhamidouche [1].

The concluding chapter is dedicated to the examination of cases where $p > 1$. Within this context, a novel model is introduced, which emerges from the principal problem under investigation. This model is closely associated with the category of inverse problems involving free boundaries or boundary value problems. A detailed analysis is provided regarding the enhancement of image contours, which holds significant potential for future advancements in the development of "Schoc filter" models. These models are renowned for their efficacy in the domain of image restoration, and the findings presented herein may contribute to further progress in this area. The study underscores the potential of this approach to offer meaningful insights and serve as a valuable contribution to the ongoing evolution of image processing and restoration.

We end this thesis with a general conclusion in which we discuss the results of our contribution.

Chapter 1

# *General context and mathematical notations*

The goal of this Chapter is to introduce the general concepts of image processing and to present the fundamental mathematical concepts that will be used in the subsequent chapters. In this chapter, we try to describe the usefulness and importance of mathematics in image processing. We define most of the notations used in the rest of this manuscript and we also recall some classic notions useful for a good understanding of this thesis.

## 1.1 Mathematical Modelling of an Image

A digital image is fundamentally constituted by elementary units known as pixels, with each pixel representing a discrete, specific portion of the overall image. These pixels collectively form the structure of the image, and their individual characteristics significantly influence the image resolution, quality, and detail.
The definition and description of a digital image are primarily determined by two critical parameters:
1. Spatial Resolution: This refers to the total number of pixels that constitute the image along its width and height. The arrangement of pixels in a two-dimensional grid defines the image's dimensions, with the potential for an almost infinite variation in pixel count. Higher pixel density typically correlates with greater image clarity and detail, allowing for finer distinctions in visual content.
2. Dynamic Range (Image Dynamics): This parameter pertains to the spectrum of grey shades or colour variations that each individual pixel can represent. The dynamic range determines the depth and richness of the image, influencing its capacity to display subtle gradations in tone and colour. A broader dynamic range enhances the image visual fidelity, providing more accurate and nuanced representations of the original scene or subject.

### 1. Binary images (black or white)

For instance, in the most basic forms of digital images, each pixel is capable of assuming only one of two possible values: black or white. This binary representation characterises what is known as a *bi-level* image, where no intermediate shades of grey are present. Such images are particularly

suitable for applications that do not require colour or tonal variations.
A common use of this type of image is in the scanning of textual documents composed of a single colour, typically black text on a white background. In this context, bi-level imaging efficiently captures the structural details of the text, ensuring high contrast and clarity, which are essential for processes such as Optical Character Recognition (OCR) and digital archiving.

## 2. Images in shades of gray

In general, grayscale images contain 256 shades of gray. 256-color image, simply each of these 256 colors is defined in the gray range. By convention, the value zero represents black (zero light intensity) and the value 255 represents white (maximum light intensity).

## Definition:

Let $\Omega$ be a bounded open set in $\mathbb{R}^2$, (specifically considering the case where $\Omega$ is an open rectangle). An image is represented as a function $u : \Omega \longrightarrow \mathbb{R}$. The function u is defined on the domain $\Omega$; however, in the context of image processing, access is limited to discrete values $\left(u\left(x_i; y_j\right)\right)$ of the function $u$.

## The pixel

The pixel is the abbreviation of "Picture element"; image element. It is the low-level primitive with the least information because its only attributes are the position in the image matrix ($n°$ of rows, $n°$ of columns) (Fig1.1) and the numerical value indicating its color, or its gray level.
It can be represented in memory on: - One bit (0 or 1) for monochrome images: 0 for black and 1 for white. - One byte, or 256 gray levels for a gray-level image: 0 black and 255 white.

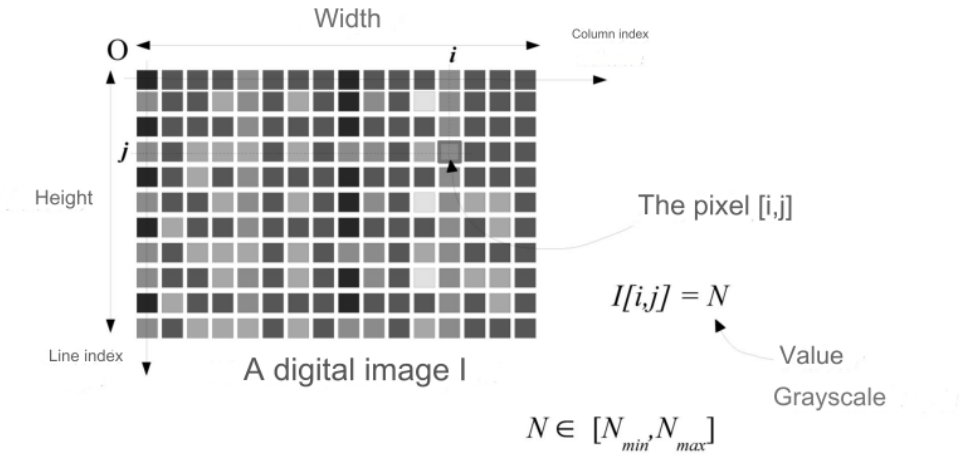


Figure 1.1: An image matrix representation

## 1.2 Concept of contour in image processing

The "contour" approach focuses on extracting primitives defined as contrast lines that delineate areas with varying and relatively uniform grey levels or differing textures. It is essential to identify the transition zones and accurately determine the boundaries between the regions.
Therefore, a contour can approximately be defined as an area of the image where the intensity of the pixels changes abruptly, this discontinuity in the image is the passage from one gray level to another, more or less quickly, giving rise to three interpretations of step, ramp, roof or line.

### Definition

The contour is defined as a variation (or discontinuity) of the image intensity. If $f(x;y)$ is an image, the contour is the locus of strong variations of $f$, and which can also be described by the Laplacian zeros.
We distinguish three types of simple contour [Fig 1.2]
1. Stair step: the contour is sharp (ideal contour).
2. Ramp: The contour is more blurred.
3. Roof: it is a line on a uniform background.

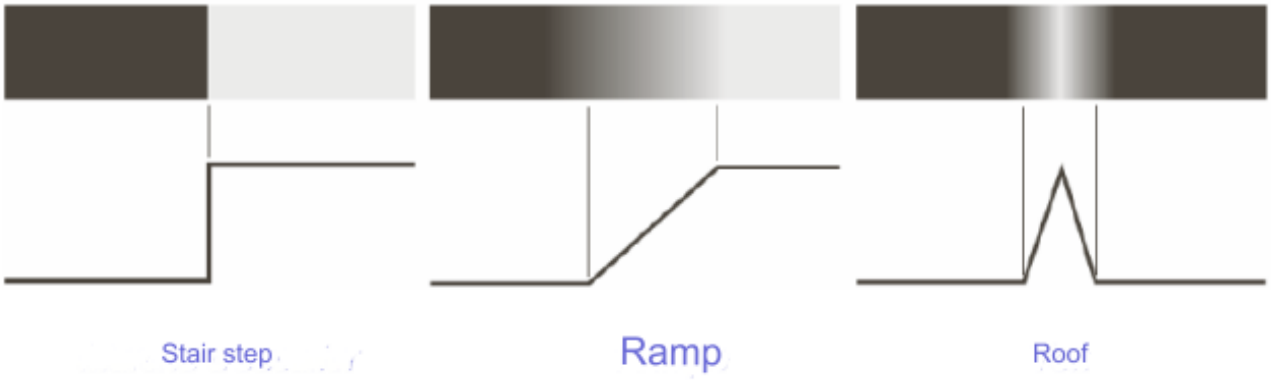


Figure 1.2: Some contour models. The most used is the stair step one. Models representing a step, a ramp, and a roof contour, along with their corresponding intensity profiles, are displayed from left to right.

### 1.2.1 Contour detection method

### Definition

Contour detection constitutes a fundamental preliminary step in a wide range of image analysis applications. Contours serve as valuable indicators, comparable to points of interest, providing critical information for the subsequent interpretation and understanding of image content. They are characterised by discontinuities in the intensity function within the image, which typically

correspond to significant changes in brightness or colour, delineating the boundaries of objects or regions.

The underlying principle of contour detection is rooted in the analysis of the derivatives of the image intensity function. Specifically, it involves identifying local extrema in the gradient of the intensity function, which indicate areas of rapid intensity change, and detecting zero-crossings in the Laplacian of the intensity function, which highlight transitions in curvature. These mathematical operations facilitate the precise localisation of contours, making them indispensable in tasks such as object recognition, image segmentation, and computer vision applications.

## Contour detection models

In a given image $f(x,y)$, a contour manifests as a line corresponding to regions where significant variations in $f$ occur. Mathematically, these variations are characterised by the gradient of the intensity function. Let $G$ denote the gradient of $f$, which is defined as:

$$G = \vec{\nabla} f = \left( \frac{\partial f}{\partial x}, \frac{\partial f}{\partial y} \right)^T$$

We associate with $f$ an image of the gradient modulus of $f$

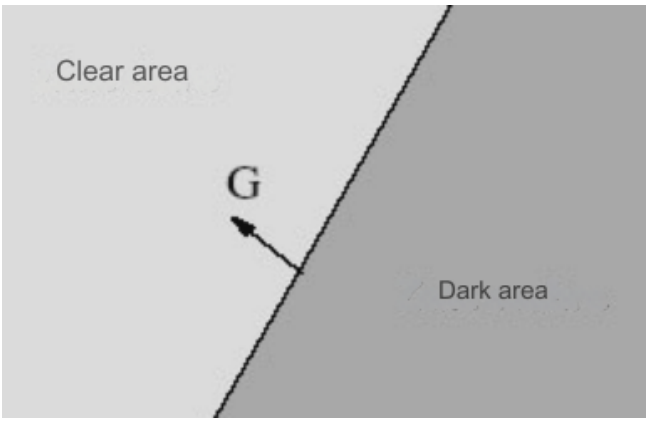


Figure 1.3

$$G = |\vec{\nabla} f| = \sqrt{\left( \frac{\partial f}{\partial x} \right)^2 + \left( \frac{\partial f}{\partial y} \right)^2}$$

As well as an image of the gradient directions from

$$\vec{g} = \frac{\overrightarrow{\nabla f}}{|\overrightarrow{\nabla f}|}$$

A contour is then defined as the locus of the gradient maxima in the direction $\vec{g}$ of the gradient. A contour point therefore verifies

$$\frac{\partial G}{\partial g} = 0 \quad \text{and} \quad \frac{\partial^2 G}{\partial g^2} \leq 0 \quad \text{with} \quad \frac{\partial}{\partial g} = \vec{g} \cdot \vec{\nabla} \tag{1.1}$$

The equation obtained is complex and nonlinear

$$\frac{\partial f}{\partial x}\frac{\partial}{\partial x}\sqrt{\left(\frac{\partial f}{\partial x}\right)^2+\left(\frac{\partial f}{\partial y}\right)^2}+\frac{\partial f}{\partial y}\frac{\partial}{\partial y}\sqrt{\left(\frac{\partial f}{\partial x}\right)^2+\left(\frac{\partial f}{\partial y}\right)^2}=0$$

Location of the maximums of the gradient in the direction $\vec{g}$ of the gradient. Where $\vec{g}$ the normal to the surface defined for $f(x,y)$.

To guarantee the double derivation even in the presence of staircase-type discontinuities, the image $f$ is preprocessed by convolution with a function at least twice derivable. For this, the Gaussian was used.

We can also place ourselves in the local axes defined by the tangent $\vec{t}$ and the normal $\vec{g}$ to the surface $f(x,y)$, This frame is rotated by an angle $\theta$ relative to the frame $\{x,y\}$

$$\theta=\text{arctg}\left(\frac{\frac{\partial f}{\partial x}}{\frac{\partial f}{\partial y}}\right)$$

We then have

$$\frac{\partial f}{\partial g}=\frac{\partial f}{\partial x}\cos\theta+\frac{\partial f}{\partial y}\sin\theta$$

and equations (1.1) give

$$\frac{\partial^2 f}{\partial g^2}=\frac{\partial^2 f}{\partial x^2}\cos^2\theta+\frac{\partial^2 f}{\partial y^2}\sin^2\theta+2\frac{\partial^2 f}{\partial x\partial y}\cos\theta\sin\theta$$

This equation is not simpler to solve than the previous one; however, it is related to the equation of the Laplacian of $f$

$$\triangle f=\frac{\partial^2 f}{\partial x^2}+\frac{\partial^2 f}{\partial y^2}$$

By a change of Euclidean reference (the reference $\{t,g\}$ )

$$\triangle f=\frac{\partial^2 f}{\partial g^2}+\frac{\partial^2 f}{\partial t^2}$$

We neglect the tangential component $\left(\frac{\partial^2 f}{\partial t^2}=0\right)$, i.e. the contour has a very low curvature, so

$$\triangle f=0 \quad \Leftrightarrow \quad \frac{\partial^2 f}{\partial g^2}=0$$

## The goal of contour detection

Contour detection aims to identify points in a digital image that indicate a change in light intensity. Contour detection effectively minimises data volume and removes extraneous information this may be deemed less pertinent while maintaining essential structural characteristics of the image. There are a large number of image detection methods. In the following, some methods will be discussed.

### 1.2.2 Image filtering

- Filtering is an operation that consists of reducing the noise contained in an image. It is considered as a transformation of the image. - Two categories of methods: - spatial domain methods: these methods refer to the image itself, and are based on the direct manipulation of pixels. - frequency domain methods: are based on the modification of the Fourier transform of the image. - We will also talk about: - linear filters expressed in the form of convolution - nonlinear filters

### 1.2.3 Why image processing?

The purpose of image processing is to: - Eliminate or reduce noise and interference introduced during its acquisition (Fig 1.4). - Better interpret the image and its content by detecting the presence of certain shapes.

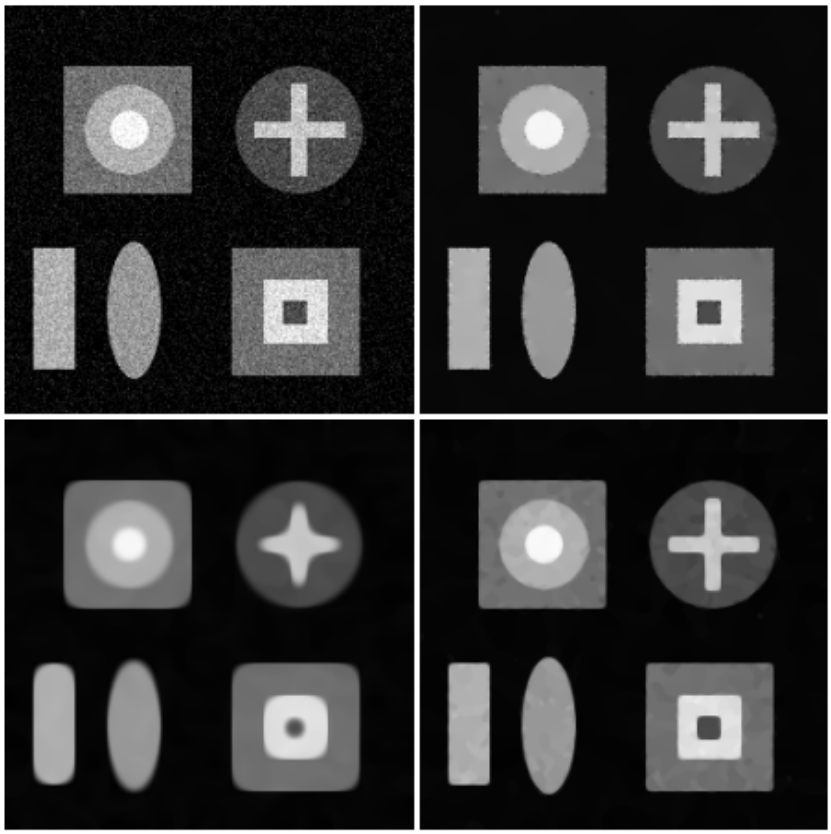

Figure 1.4: Filters based on classical partial differential equations (PDEs). Left: The original image, sized $256 \times 256$ pixels, affected by Gaussian noise with a standard deviation of $\sigma = 20$. Second from left: Image processed using Perona-Malik filtering with parameters $\lambda = 1$ and $t = 50$. Second from right: Result obtained through mean curvature motion at $t = 20$. Right: Output of the self-snakes model with $\lambda = 1$ and $t = 50$.

The fields of application of image processing are diverse, among others, physics, biology, etc.,(See Figure 1.5 ). Since the massive development of imaging techniques (satellite, medical, industrial, etc.), the generalization of systematic tasks has highlighted the interest of image processing tech-

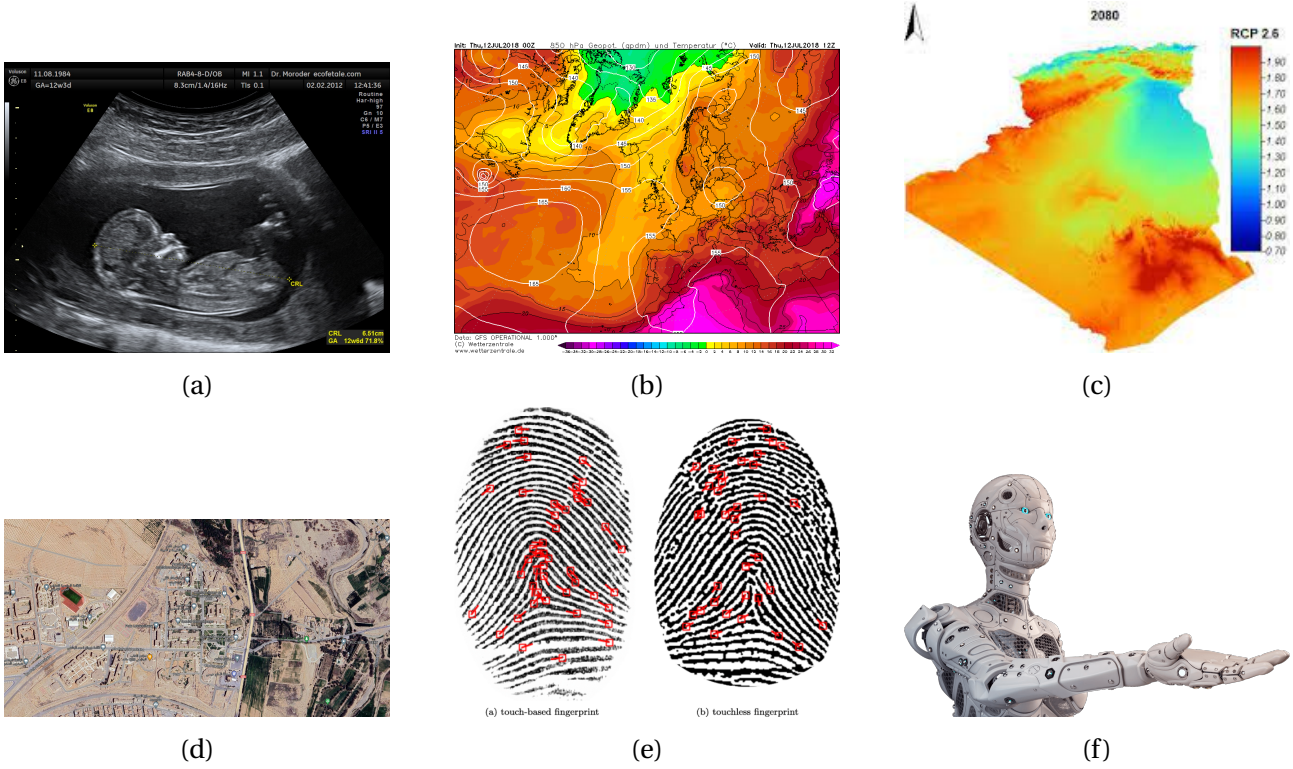


Figure 1.5: Some applications where image processing is concerned.

niques (filtering, compression, restoration, segmentation, classification, reconstruction, etc.). Indeed, more and more, the partitions that separated the various methods used in image processing are becoming permeable and unifying approaches are emerging. We show that partial differential equation (PDE) and variational techniques are the most capable of federating and unifying a large number of approaches. They make it possible to treat a large class of problems in the fields of image processing within a single and coherent formalism.

## 1.3 The framework of PDEs in image processing

Image contour enhancement is one of the central problems in digital image processing. It aims to improve the quality of an image. The essential aspect of this approach is to differentiate between significant image features that must be retained, or even enhanced, with certain elements of the image content regarded as noise and necessitating removal. In this section, we give a brief overview of several classes of image processing methods based on the PDE formalism that guide our thinking to build image contour enhancement approaches presented in the following chapters.

### 1.3.1 Modeling

We consider the image to be processed as a function $u_0$ which, at each point $(x, y)$ of the image, associates its gray level $u_0(x, y)$. It is then a question of constructing from the known function $u_0$ a new, smoother image, represented by a new function $u$. We first assume that $u$ depends on three variables: $x$ and $y$ (like $u_0$ ), and a third variable $t$ which will correspond to a sort of "degree" of smoothing. In the absence of smoothing, that is to say for $t = 0, u$ must correspond to the initial noisy image. This condition is written: $u(x, y, t = 0) = u_0(x, y)$ for all $x$ and $y$. Next, we seek to find $u(x, y, t)$ as a solution to a partial differential equation (PDE). The desired solution is a smoother and clearer image. Finding such a PDE is the most difficult step, even more so than actually solving it. One of the first ideas was to draw an analogy with a physical phenomenon, the diffusion of heat, in the same way that, in a material, heat diffuses from one point to another, from near to near, and thus tends to spread uniformly as time passes, by analogy we seek to make the gray levels in an image "diffuse" from near to near. Thus, the differences between the gray levels will decrease, and we will find a more uniform gray level: which corresponds to erasing the small spots. A smoothing method therefore consists in determining the function $u(x, y, t)$ as a solution to the equation that describes the propagation of heat. The function $u$ should thus verify the following partial differential equation:

$$u_t = \Delta u$$

with the initial condition $u(x, y, t = 0) = u_0(x, y)$ for all $(x, y)$. To find $u$ we move on to numerical resolution. This smoothing method, modeled on heat diffusion, presents some problems in particular the diffusion of gray levels also applies to the contours of the objects represented in the image, which makes the contours more blurred and modifies the equation imposed on $u$ so that the diffusion does not occur at the contours.

How to choose a new model to avoid this problem?

From a mathematical point of view, an outline is recognizable: it corresponds to a region of the image where the gray level varies greatly, therefore to high values of the norm of the gradient of $u$ thus, the gradient of $u$ measures the degree of variation of $u$ and its direction. The researchers therefore modified the equation calculating $u$, they replaced its right-hand side with a more complicated expression, involving among other things the gradient of $u$.

There are various ways to do this, and it then requires fairly complex studies, for example to prove the existence and uniqueness of the solution to the equation, or to find an efficient and fast (numerical) resolution method, the desired result is an anisotropic diffusion, that is to say, which does not occur in the same way in all directions.

Complex models but the smoothing results obtained are quite convincing!

To clearly show the improvement of image contours, several methods were used using PDE, which will be presented as follows:

### 1.3.2 Use of PDEs for image enhancement

Nonlinear methods are considered powerful tools in the field of signal and image processing. Technological advances in terms of computing speed and power have allowed the practical implementation of more complex algorithms that can overcome the limitations inherent in linear invariant approaches. The application of nonlinear methods to contour-preserving smoothing, contour enhancement or image segmentation clearly shows their superiority. Among these approaches, we will focus on those that rely on the use of nonlinear partial differential equations (PDEs).In the context of gray-scale image enhancement, the PDE formulation classically involves modeling the image by a discrete set of points (pixels). Considering the luminance as a function of the spatial coordinates $(x, y)$ and time $t$, the properties of the restored image are obtained through a PDE having as arguments the luminance function and its partial derivatives; the solution of this PDE, at a certain time $t$, represents the restored (enhanced) image. Let $u_0 : \mathbb{R}^2 \to \mathbb{R}$ be the image to be processed where $u(x, y)$ is the gray-scale associated with the pixel with coordinates $(x, y)$. The general model of image evolution can be put in the form [16] :

$$u_t = F(u(x, y, t)) \tag{1.2}$$

This very general writing is based on the operator $F$ specific to the algorithm and linked to the original image and its first and second spatial derivatives.
$u(x, y, t) : \mathbb{R}^2 \times [0, \tau] \to \mathbb{R}$ represents the state of the resulting image at a time t. Finally, the solution of equation (1.2) is nothing other than a simplified version of the original image corresponding to a given evolution time (i.e. at a given scale). As the temporal evolution progresses, the transformation of the image leads to noise reduction (and/or signal enhancement) while preserving the relevant information.
In the PDE formulation, time can be assimilated to an observation scale and consequently, the methods assimilated to multi-scale analysis tools defined by a family of transformations $(T_t)_t \geqslant 0$ which, applied to an original image, gives a family of images dependent on the parameter t. The properties necessary for a multi-scale analysis have been formally stated by Morel [43].
The representation of images in the form of a multi-scale smoothing was introduced by Marr and Hildreth [42], Witkin [59] and then developed by Koenderink [36]. The Method proposed by Witkin makes it possible to obtain images at increasingly coarse scales by performing a series of convolutions between the original image and Gaussian kernels of increasing size $\sigma$.

The following parts of this section will be devoted to presenting a number of approaches combining PDEs in image processing and the ideas of isotropic, anisotropic diffusion and mean curvature filters.

## 1.4 Some models of contour detection

We will introduce some mathematical models for contour detection.

### 1.4.1 Linear (Isotropic) Diffusion-Based Filter

A classical approach in the field of image restoration uses a linear convolution (smoothing) operation to reduce the effect of noise, considered to be high frequency.

$$u(x,y,t) = \int_{\Omega} G(x-\xi, y-\eta, t)\, u_0(\xi,\eta)\, d\Omega, \quad (x,y) \in \Omega \tag{1.3}$$

where we denote by $u_0(x,y)$, the function of $\mathbb{R}^2$ in $\mathbb{R}$, defined on $\Omega = [0,a] \times [0,b]$. The value of the function $u_0$ represent for example the gray level intensities of the original noisy image, $u(x,y,t)$ represents the restored image, and $t$ a parameter that controls the importance of the smoothing of the operator $G(x,y,t)$.

An example of an operator often used due to its performance, separability and isotropy properties is the Gaussian operator $G$ given by:

$$G(x,y,t) = \frac{1}{4\pi t} e^{-\frac{x^2+y^2}{4t}}$$

Koenderink [36] was the first to notice that a convolution operator of an image by a Gaussian operator of a certain variance (here $\sigma^2 = 2t$ ) can be rewritten as a diffusion process of the image intensity around neighboring pixels during a time $t$ in direct relation to the spatial variance $\sigma^2$. This diffusion equation, known as the heat equation, can be expressed as the following linear parabolic PDE:

$$\begin{cases} \frac{\partial u}{\partial t} = u_{xx}(x,y,t) + u_{yy}(x,y,t) \\ u(x,y,0) = u_0(x,y) \end{cases} \tag{1.4}$$

So Koenderink [36] demonstrated the equivalence between the solution of the heat diffusion PDE at time $t$ and the convolution with a Gaussian kernel of standard deviation $\sqrt{2t}$. This linear diffusion equation is expressed in the form of a divergence:

$$\begin{cases} \frac{\partial u}{\partial t} = \operatorname{div}(\nabla u(x,y,t)) \\ u(x,y,0) = u_0(x,y) \end{cases} \tag{1.5}$$

The linear parabolic equation (1.4) induces an isotropic diffusion. This diffusion thus operates identically in all directions and has no preferred direction. For noisy image restoration tasks, this clearly presents drawbacks. Indeed, in regions of homogeneous intensity, this process will effectively reduce the effect of noise but in regions presenting discontinuities in the intensity at the

gray level, these will also be smoothed and the visual contrast of these parts will be significantly reduced, consequently reducing the qualitative and visual interest of such a process. To address this problem, ideas of anisotropic diffusion have been proposed. The principle as well as the work in this framework are the subject of the following paragraph.

## 1.5 Filter based on nonlinear (anisotropic) diffusion

The first idea to solve problems arising from isotropic diffusion was proposed by Perona and Malik in [47].

The adaptive smoothing method with contour enhancement of Perona and Malik [47] is perhaps one of the most relevant in the context of contour detection theory. For the first time, a PDE formalism leads to select a diffusion intensity and therefore a diffusion scale adapted according to the neighborhood. For this, the algorithm uses a nonlinear diffusion function which leads to a significant smoothing in areas of low gradients and allows to limit the effects of this smoothing on the useful signal (contours).

The principle of the approach proposed by Perona and Malik consists in introducing into equation (1.5) a conductivity term $c$ depending on the local context. This diffusion mode has been formalized as follows:

$$\begin{cases} \frac{\partial u}{\partial t} = \text{div}(c(|\nabla u(x,y,t)|)\nabla u(x,y,t)) \\ , u(x,y,0) = u_0(x,y) \end{cases} \tag{1.6}$$

In this context, $div$ and $\nabla$ indicate the divergence and gradient operators with respect to the spatial variables respectively., $u(x,y,t)$ signifies the smoothed image at time step $t$, $|\nabla u|$ indicates the gradient magnitude of $u$. To obtain the desired result, the conductivity is defined as a decreasing function, dependent on the norm of the gradient vector $c(x,y,t) = g(|\nabla u|)$; where $g(x)$ refers to the diffusivity function. The function $g(x)$ must be nonnegative and monotonically decreasing, with the condition that $g(0) = 1$. This ensures that diffusion is maximized in uniform regions and approaches zero as $x$ approaches infinity, effectively halting diffusion across contours.

The functions initially proposed by Perona-Malik are:

$$g(|\nabla u|) = e^{-\left(\frac{|\nabla u|}{k}\right)^2}$$

and

$$g(|\nabla u|) = \frac{1}{1+\left(\frac{|\nabla u|}{k}\right)^2}$$

The parameter $K$ is a so-called "threshold or diffusion barrier" allows to parameterize the value of the gradient from which the behavior of the PDE varies between diffusion and possible enhancement.

Note the interest of the directional interpretation of anisotropic diffusion: we will see that it is from this interpretation that we introduced the principle of diffusion directional $1D$. Directional interpretation: an interpretation of (1.6) that allows to grasp more easily the differences with isotropic diffusion is obtained by writing the equation in terms of directional second derivatives in the direction of the gradient $\vec{\eta} = \left(\frac{u_x}{|\nabla u|}, \frac{u_y}{|\nabla u|}\right)^T$ and in the orthogonal direction $\vec{\zeta} = \left(\frac{u_y}{|\nabla u|}, -\frac{u_x}{|\nabla u|}\right)^T$ which will be assimilated to the direction of the structures (Fig 1.6). $u_x$ and $u_y$ are respectively the derivatives of $u$ in $x$ and in $y$. This classic notation is presented in several works (see [53]).

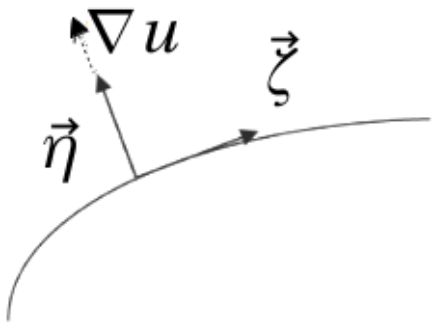


Figure 1.6: Gradient direction and orthogonal direction.

The Perona-Malik diffusion equation for a 1-D signal can be expressed as

$$\frac{\partial u}{\partial t} = \frac{\partial}{\partial x}\left(g\left(u_x\right) u_x\right) \tag{1.7}$$

$$= \frac{\partial g\left(u_x\right)}{\partial x} u_x + g\left(u_x\right) u_{xx} \tag{1.8}$$

To facilitate comprehension, we establish the flux function $f(x) = g(x).x$, where $g(x)$ represents the diffusivity function. Consequently, we can express (1.7) in the following manner

$$\frac{\partial u}{\partial t} = f'\left(u_x\right) u_{xx}. \tag{1.2.10}$$

The variation of the gradients at any point along the contour is expressed by:

$$\frac{\partial\left(u_x\right)}{\partial t} = f''\left(u_x\right) u_{xx}^2 + f'\left(u_x\right) u_{xxx}. \tag{1.9}$$

The sign on the right-hand side of Equation (1.9) provides critical information about the temporal evolution of the gradient $u_x$ at a specific location $x$. Specifically, it determines whether the gradient is increasing $\left(\frac{\partial(u_x)}{\partial t} > 0\right)$ or decreasing $\left(\frac{\partial(u_x)}{\partial t} < 0\right)$. This behavior is directly linked to the blurring or enhancing characteristics of the Perona-Malik filter, which are governed by the sign of the derivative $f'\left(u_x\right)$.

At an contour, the second derivative $u_{xx}$ equals zero, and the third derivative $u_{xxx}$ is less than or equal to zero. This indicates that the gradient $u_x$ reaches its maximum value at the contour, as illustrated in Figure 1.7. The subsequent evolution of the gradient depends on the sign of $f'\left(u_x\right)$:

- If $f'(u_x) > 0$, the gradient at the contour decreases over time, resulting in a blurring effect. This occurs because the filter attenuates the gradient magnitude, leading to a smoothing of the contour.
- Conversely, if $f'(u_x) < 0$, the gradient at the contour increases over time, while the gradients in neighboring regions decrease. This process enhances the contour, making it sharper and more pronounced, as depicted in Figure 1.8.

In summary, the sign of $f'(u_x)$ plays a pivotal role in determining whether the Perona-Malik filter blurs or sharpens contours. This behavior is intrinsically tied to the temporal dynamics of the gradient $u_x$ and its spatial derivatives, providing a mathematical foundation for understanding contour enhancement and smoothing in image processing.

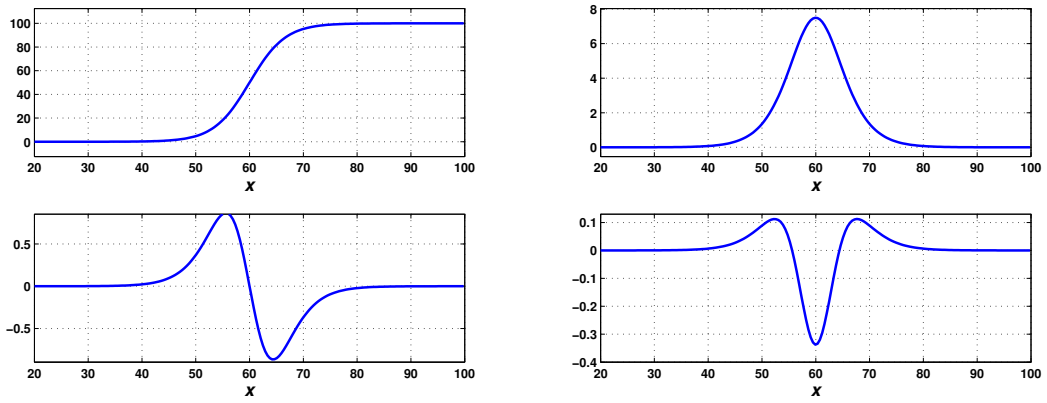


Figure 1.7: In the first row, from left to right, and in the second row, from left to right, the contour function $u(x)$ is depicted alongside its first, second, and third derivatives, respectively.

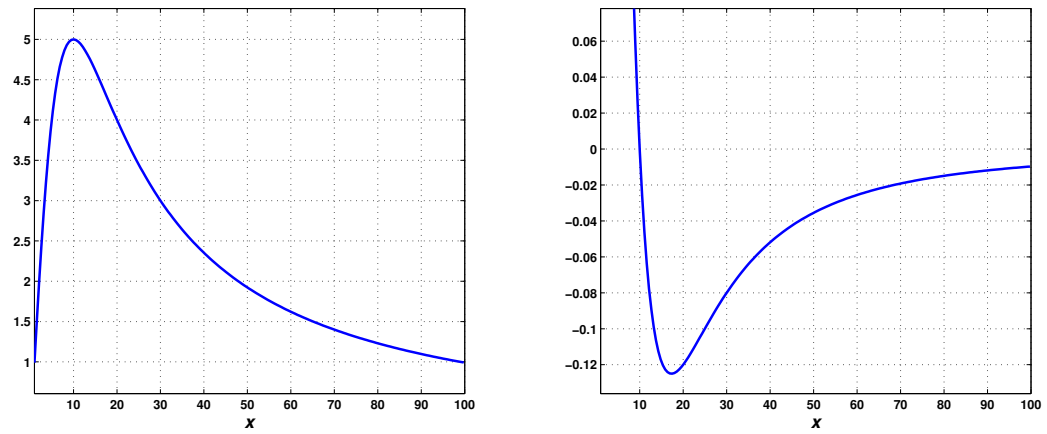


Figure 1.8: Flux function $f$ (left) and its derivative $f'$ (right).

Nonlinear diffusion filtering effectively reduces noise while preserving region boundaries and small structures in the image, provided that key parameters are accurately determined or estimated. Perona and Malik indicate that the selection of functions $g$ for which $f$ meets certain properties results in effective contour enhancement. The following table presents the most frequently utilised

diffusivity functions found in the literature.

| Function | Reference |
|---|---|
| $g(x) = 1$ | Linear Diffusion |
| $g(x) = \frac{1}{\sqrt{1+\frac{x^2}{\delta^2}}}$ | |
| $g(x) = \frac{1}{1+\frac{x^2}{\delta^2}}$ | Perona- Malik |
| $g(x) = \exp\left(-\frac{x^2}{\delta^2}\right)$ | Perona- Malik |
| $g(x) = \begin{cases} 1-\exp\left[\frac{-3.15}{\left(\frac{x}{\delta^2}\right)^4}\right], & x>0 \\ 1 & x\leq 0 \end{cases}$ | Weickert J |
| $g(x) = 0.5[(\tanh[0.2(\delta - x)]) + 1]$ | Fischl and Schwartz |
| $g(x) = \begin{cases} \frac{1}{2}\left[1-\left(\frac{x}{\delta}\right)^2\right]^2, & \lvert x\rvert > \delta \\ 0 & \text{otherwise} \end{cases}$ | Black Sapiro |

Note: The parameter $\delta$ is known as the noise levels or contrast parameter.

### 1.5.1 Mean curvature diffusion

The classical evolution model gives rise to a nonlinear parabolic equation, which can exhibit degeneracy or singularity depending on the specific conditions. The inherent nonlinearity stems from the dependence of the image intensity flow on the intensity itself, making the equation highly sensitive to variations in image structures.

Perona and Malik demonstrated that a carefully chosen nonlinearity within this framework could significantly enhance image contours. This property is particularly valuable in various image processing applications, including noise reduction and denoising, where preserving important structural details while suppressing noise is crucial.

The anisotropic diffusion model introduced by Perona and Malik has had a substantial impact on the field, serving as the foundation for numerous advancements. Among these is the model developed by Malladi and Sethian [40], which extends the principles of anisotropic diffusion to more sophisticated formulations. Under the appropriate scaling, this model leads to the following governing equation for image intensity:

$$\frac{\partial u}{\partial t} = \left(1 + |\nabla u|^2\right)^{\frac{1}{2}} k$$

where $\nabla u$ indicates the spatial gradient of $u$, whereas $k$ signifies the curvature of the surface $z = u(x, y)$, such that:

$$k = \operatorname{div}\left(\frac{\nabla u}{\sqrt{1 + |\nabla u|^2}}\right)$$

The equation representing the motion by the curvature (curvature flow) can be written as follows :

$$\begin{aligned}
\frac{\partial u}{\partial t} &= \sqrt{\left(1+|\nabla u|^2\right)}\,\mathrm{div}\left(\frac{\nabla u}{\sqrt{1+|\nabla u|^2}}\right)\\
&= \sqrt{1+u_x^2+u_Y^2}\,\mathrm{div}\left(\frac{u_x}{\sqrt{1+u_x^2+u_Y^2}},\frac{u_y}{\sqrt{1+u_x^2+u_Y^2}}\right)\\
&= \frac{1+u_x^2+u_Y^2}{\sqrt{1+u_x^2+u_Y^2}}\left(\frac{u_{xx}\sqrt{1+u_x^2+u_Y^2}-\frac{u_xu_{xx}+u_xu_yu_{xy}}{\sqrt{1+u_x^2+u_Y^2}}}{\sqrt{1+u_x^2+u_Y^2}}-\frac{u_{yy}\sqrt{1+u_x^2+u_Y^2}-\frac{u_yu_{yy}+u_xu_yu_{xy}}{\sqrt{1+u_x^2+u_Y^2}}}{\sqrt{1+u_x^2+u_Y^2}}\right)\\
&= \frac{\left(1+u_Y^2\right)u_{xx}-2u_xu_yu_{xy}+\left(1+u_x^2\right)u_{yy}}{1+u_x^2+u_Y^2}
\end{aligned}$$

This model therefore describes contour filtering based on this geometric approach. There is a more general form of this model based on the same technique.

Due to a specific degeneracy in the asymptotic forms of this equation, Barenblatt and Vazquez in [9, 55], proposed to explore a more general flow produced by the following equation:

$$\frac{\partial u}{\partial t} = \left(1+|\nabla u|^2\right)^{\frac{1-2\gamma}{2}}k.$$

Where $\gamma > \frac{-1}{2}$ is a constant parameter, which is written in the form:

$$\frac{\partial u}{\partial t} = \frac{\left(1+u_Y^2\right)u_{xx}-2u_xu_yu_{xy}+\left(1+u_x^2\right)u_{yy}}{\left(1+u_x^2+u_Y^2\right)^{1+\gamma}}, \tag{1.10}$$

where $u(x,y)$ denotes the image intensity, $x$ and $y$ represent the Cartesian coordinates inside the image plane, with $t$ representing time. If $\gamma = 0$ we find the previous model (maen curvature flow), the case $\gamma = 1$ is also getting the attention of researchers (Beltrami flow, cf. Sochen et al. [35]).

### 1.5.2 Linear versus Nonlinear Diffusion

To facilitate a comparative analysis of linear and nonlinear diffusion filtering techniques and their impact on contour sharpness, we present two illustrative examples. The first example examines a noisy one-dimensional contour profile, represented by the function $u(x)$, alongside its filtered counterparts, as depicted in Figure (1.9). The second example demonstrates the application of both linear and nonlinear diffusion filtering to a grayscale image, illustrated in Figure (1.10).

Figures (1.9) and (1.10) reveal that linear diffusion filtering tends to blur contours, whereas nonlinear diffusion filtering effectively preserves contour sharpness. The model introduced by Malik and Perona, however, presents several practical and theoretical challenges:

1. In the presence of noise, such as white noise, the signal generates significant gradients $|\nabla u|$. Since $\nabla u$ is theoretically unbounded, the conditional smoothing employed by the model often fails

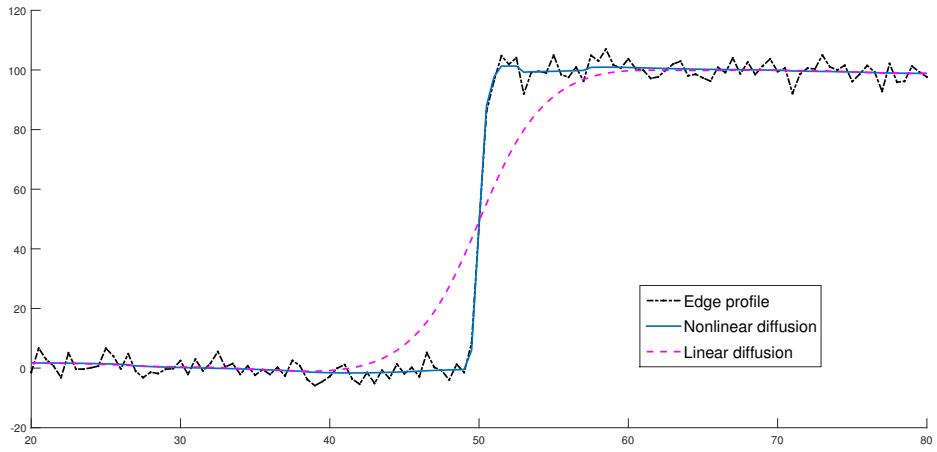


Figure 1.9: One-dimensional edge profile $u(x)$ (solid line) alongside its filtered counterparts, illustrating the results of nonlinear diffusion filtering (ADF, dot-dash) and linear diffusion filtering (dashed line).

to produce satisfactory results. This is because the noise-induced contours are retained, compromising the filtering efficacy.

2. The function $g$ within the model requires careful analysis to ensure the existence and uniqueness of solutions. Specifically, $g$ must satisfy the condition that $x \cdot g(x)$ is non-decreasing. In practical , if $g$ is such that $x \cdot g(x)$ is non-increasing, similar images may yield divergent solutions, leading to inconsistent contour detection outcomes [17].

### 1.5.3 Self-Similar Solutions for Nonlinear Partial Differential Equations

Self-similarity arises when the inherent symmetry of a physical system reduces the number of independent variables. This reduction often leads to a significant simplification of the problem, frequently enabling an analytical approach to its solution. In scenarios where the specific details of initial or boundary conditions become negligible, self-similar behaviour typically emerges in the intermediate asymptotics of the phenomenon, rendering the associated parameters inconsequential.

The nature of the transition to the limiting state, which defines the intermediate asymptotics of a particular problem, allows for the classification of similarity solutions into two types: first-kind and second-kind self-similarities. The self-similarity of the first kind can typically be determined via dimensional analysis, with further validation through symmetry considerations. In contrast, conventional methods are insufficient for deriving second-order self-similarities. To obtain these, it is essential to track the evolution of the solution-whether through experimental or numerical techniques-until it reaches its self-similar asymptotics. Alternatively, second-kind self-similarities can be derived through direct construction, which leads to the formulation of a nonlinear eigen-

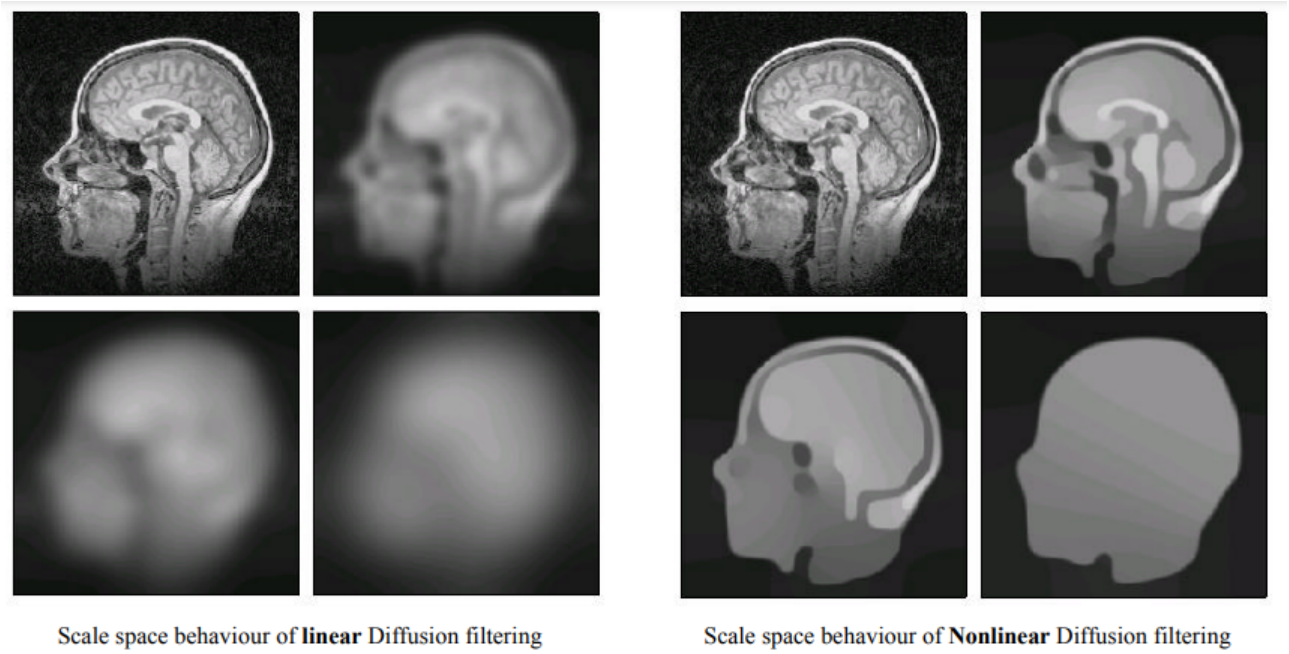


Figure 1.10: gray-scale image and its filtered versions. Linear diffusion filtering (Left) and nonlinear diffusion filtering (Right).

value problem.

A technique employing self-similar solutions offers a powerful approach for deriving exact solutions to partial differential equations (PDEs). This method is particularly valuable in the study of PDEs, as it simplifies complex problems by reducing them to more manageable forms. Consider the general PDE:

$$\frac{\partial u}{\partial t} = A_x u,$$

where $A_x u$ represents a linear or nonlinear differential operator acting on the function $u(x,t)$. The self-similarity approach is widely utilised in solving such equations. It involves seeking solutions to (1.5.3) in a specific form that exploits the scaling symmetry of the problem. One such form is:

$$u(x,t) = t^{\mu} f(\xi), \quad \xi = x t^{-\nu},$$

for $x \in \mathbb{R}$ and $t > 0$, where $\mu$ and $\nu$ are constants determined by the problem's scaling properties. Here, the function $f(\xi)$ satisfies an ordinary differential equation (ODE) derived from the original PDE:

$$A_\xi f - \mu f + \nu \xi f_\xi = 0,$$

where $A_\xi f$ represents the differential operator $A_x u$ expressed in terms of the similarity variable $\xi$. This transformation reduces the PDE to an ODE, which is often easier to solve analytically or numerically.

Another variant of self-similar solutions arises in problems with finite-time behaviour, such as those involving singularities or blow-up phenomena. In such cases, the solution can be expressed as:

$$u(x,t) = (T-t)^{\mu} f(\xi), \quad \xi = x(T-t)^{-\nu},$$

for $x \in \mathbb{R}$ and $0 < t < T$, where $T$ represents a critical time (e.g., the time of singularity formation). Here, $\mu$ and $\nu$ are again constants determined by the scaling properties of the problem. This form is particularly useful for analysing the behaviour of solutions as $t$ approaches $T$.

More generally, self-similar solutions can be expressed in the following unified form:

$$u(x,t) = c(t) f(\xi), \quad \xi = \frac{x}{a(t)},$$

where $c(t)$ and $a(t)$ are time-dependent scaling functions chosen to simplify the problem. The selection of $c(t)$ and $a(t)$ is guided by the specific structure of the PDE and the desired properties of the solution. This general form encapsulates the essence of self-similarity, where the solution maintains its shape while being rescaled in space and time.

The self-similarity method is a cornerstone in the analysis of PDEs, as it leverages the inherent scaling symmetries of the equations to reduce their complexity. By transforming the original PDE into an ODE, this approach enables the identification of exact solutions, which are often challenging to obtain through direct methods. Furthermore, self-similar solutions provide deep insights into the qualitative behaviour of solutions, such as their long-time asymptotics or the formation of singularities. This makes the method indispensable in fields ranging from fluid dynamics and heat conduction to nonlinear wave propagation and mathematical biology.

In summary, the self-similarity technique, as outlined above, offers a systematic and powerful framework for solving PDEs, making it a fundamental tool in both theoretical and applied mathematics.

Chapter 2

# *Study of image contour enhancement with degenerate parabolic equation*

In this chapter, we introduce a novel evolution model based on the nonlinear diffusion equation, which generalises mean curvature motion. This approach is particularly effective in analysing contour enhancement in images. The free boundary problem is formulated to investigate the evolution of image intensity within the boundary layer. By integrating concepts from Total Variation Minimisation (TVM) and Mean Curvature Motion (MMC), we develop a refined framework that enhances the effectiveness of contour enhancement techniques. Furthermore, we employ asymptotic analysis following the methodology introduced by Barenblatt (2001) to explore the impact of the proposed model. We then present a comprehensive examination of the resulting mathematical formulation, which extends previous research findings. This chapter systematically explores the interplay between TVM and MMC in the context of image processing, offering a deeper understanding of their combined effects on contour preservation and noise reduction. We present the results obtained, which are a generalisation of the research presented in [1].

## 2.1 Generalized mean curvature motion

A widely used denoising approach involves minimising a functional of the image gradient, expressed as follows:

$$\min_u \mathscr{F}_\alpha(u), \quad \mathscr{F}_\alpha(u) = \int_\Omega |\nabla u|^\alpha \, dx \tag{2.1}$$

where $\mathscr{F}_1(u)$ represents the total variation (TV); see [52] and [32] To solve equation (2.1), it is often beneficial to reformulate the minimisation problem as a differential equation, specifically the Euler-Lagrange equation:

$$\frac{\partial u}{\partial t} = \operatorname{div}\left(\frac{\nabla u}{|\nabla u|^{2-\alpha}}\right) \tag{2.2}$$

where an artificial time parameter $t$ has been introduced to guide the iterative descent process. This model is known to induce a certain degree of blurring during noise removal.

Despite its effectiveness, the Total Variation Minimisation (TVM) model described by (2.2) may struggle to suppress impulse noise effectively. This is because impulse noise in the initial image $u_0$ acts as a persistent anomaly, potentially leading to significant degradation in the reconstructed image $u$.

Moreover, TVM can introduce substantial distortions to the image structure. Consequently, it is advisable to first eliminate impulse noise before applying TVM. To achieve this, an alternative approach based on motion by mean curvature (MMC) can be considered:

$$u_t = |\nabla u| \operatorname{div}\left(\frac{\nabla u}{|\nabla u|}\right) \tag{2.3}$$

For a comprehensive review of MMC and related techniques, refer to [2] and [41]. By integrating TVM with MMC, we propose a generalised framework that extends their applicability to more complex image processing tasks. This is formulated as follows:

$$\frac{\partial u}{\partial t} - \frac{1}{|\nabla u|^q} \operatorname{div}\left(\frac{\nabla u}{|\nabla u|^p}\right) = 0. \tag{2.4}$$

In this study, we refer to this model as the generalised mean curvature motion. The parameters $p$ and $q$ serve as enhancement factors, governing the behaviour of the diffusion term. Specifically, these constants regulate the rate at which diffusion decreases as the gradient magnitude $|\nabla u|$ increases. In essence, for regions with high gradient values (such as contours), the diffusion process slows down, preserving structural details. The parameters $p$ and $q$ thus control the adaptive nature of the diffusion, ensuring a balance between noise removal and contour preservation.

Equation (2.4) can be considered a generalisation of both the mean curvature motion (MCM) and the total variation model (TVM). To understand this generalisation, let us first examine specific cases. When $q = -1$ and $p = 1$, the equation reduces to the mean curvature motion (MCM). On the other hand, for $q = 0$ and $p = 2 - \alpha$, it corresponds to the total variation model (TVM). Additionally, setting $q = 1$ and $p = 1$ yields the Beltrami flow equation. The key distinction between equation (2.4) and the TVM lies in the presence of the term $|\nabla u|^q$ on the right-hand side of the equation. This term plays a crucial role in enhancing the contours within the image, which is a central feature of this generalisation. Specifically, $|\nabla u|^q$ influences the diffusion process by modulating its rate. To elaborate, in regions of the image where $|\nabla u|$ is relatively small, such as the interior points of a smooth area, the diffusion process is strong, as the gradient is low and diffusion is more pronounced. Conversely, at the location of an contour, where $|\nabla u|$ is large, the effect of the diffusion diminishes because $|\nabla u|^q$ becomes smaller for $q > 0$, thereby reducing the spread of diffusion. This ensures that the diffusion is suppressed near sharp transitions, which is a desired property in image processing tasks such as denoising or contour-preserving smoothing. For

values of $q \leq 0$, the situation changes significantly. In this case, the factor $|\nabla u|^q$ becomes much larger than 1, especially when $|\nabla u|$ is large, which leads to a higher rate of diffusion evolution in proximity to contours. This enables enhanced contour evolution, making the equation particularly useful for applications that require high sensitivity to contours or sharper transitions in the data.

We mention that, a nonlinear extension of mean curvature motion, which generalize equation (2.3), in a different way have been proposed by Didas and Weickert [23], where a combine curve shrinkage properties of mean curvature motion with denoising filter has investigated.

We consider a more general flow given by equation:

$$\partial_t u = \frac{1}{\left(1+|\nabla u|^2\right)^{\frac{q}{2}}} div\left(\frac{\nabla u}{\left(1+|\nabla u|^2\right)^{\frac{p}{2}}}\right), \tag{2.5}$$

$u$ : denotes the intensity of the image.

$\nabla u$ : denotes the spatial gradient of $u$. The gradient gives the direction and amplitude of variation of the image (analogy with the slope of a relief).

$|\nabla u|$ : the gradient norm which gives the amplitude of variation, used for contour detection, The amplitude (i.e. modulus) of the gradient is related to the amount of local variation of the intensity: the larger the modulus, the stronger the contour.

Then equation (2.5) is rewritten as follows:

$$\begin{aligned}
\frac{\partial u}{\partial t} &= \frac{1}{\left(1+|\nabla u|^2\right)^{\frac{q}{2}}} \operatorname{div}\left(\frac{\nabla u}{\left(1+|\nabla u|^2\right)^{\frac{p}{2}}}\right) \\
&= \frac{1}{\left(1+u_x^2+u_y^2\right)^{\frac{q}{2}}} \operatorname{div}\left(\frac{u_x}{\left(1+u_x^2+u_y^2\right)^{\frac{p}{2}}}, \frac{u_y}{\left(1+u_x^2+u_y^2\right)^{\frac{p}{2}}}\right) \\
&= \frac{\left(1+u_x^2+u_y^2\right)^{\frac{p}{2}-1}}{\left(1+u_x^2+u_y^2\right)^{\frac{q}{2}}} \left(\frac{u_{xx}\left(1+u_x^2+u_y^2\right)-p\left(u_x^2u_{xx}+u_xu_yuxy\right)+u_{yy}\left(1+u_x^2+u_y^2\right)-p\left(u_y^2u_{yy}+u_xu_yuxy\right)}{\left(1+u_x^2+u_y^2\right)^p}\right) \\
&= \frac{\left[1+u_y^2+(1-p)\,u_x^2\right]u_{xx}-2pu_xu_yu_{xy}+\left[1+u_x^2+(1-p)\,u_y^2\right]u_{yy}}{\left(1+u_x^2+u_y^2\right)^{\frac{q}{2}+\frac{p}{2}+1}},
\end{aligned}$$

This will be called the generalised mean curvature motion here. In image enhancement techniques, the constants $p$ and $q$ are introduced as critical parameters that modulate image intensity. These constants determine how the intensity values are transformed, directly affecting the image contrast dynamics and brightness distribution. Adjusting $p$ and $q$ enables fine-tuning of image characteristics. The corresponding equation for image intensity is presented below:

$$\partial_t u = \frac{\left[1+u_y^2+(1-p)\,u_x^2\right]u_{xx}-2pu_xu_yu_{xy}+\left[1+u_x^2+(1-p)\,u_y^2\right]u_{yy}}{\left(1+u_x^2+u_y^2\right)^{\frac{q}{2}+\frac{p}{2}+1}}. \tag{2.6}$$

### 2.1.1 The asymptotic representation of the fundamental equation

The asymptotic and numerical analyses conducted in the works [35, 40] shown that a boundary layer consistently occurs along the margins of pictures (see Figure 2.1), characterised by a substantial normal component of the intensity gradient within the image. Focusing on the boundary layer where gradient changes are most significant, [9] developed a streamlined version of model (1.10). This study demonstrated that within this layer, the gradients are particularly large, which supports the feasibility of reducing model complexity while still maintaining accurate descriptions of the phenomenon. Using Cartesian coordinates at the boundary layer contour, where the $x$-axis is aligned normal to the boundary layer, it becomes clear that the $y$-derivatives have a negligible impact compared to the $x$-derivatives in equation (1.10). Therefore, within this region, the equation (1.10) reduces to its one-dimensional representation:

$$\partial_t u = \frac{u_{xx}}{u_x^{2(1+\gamma)}}. \tag{2.7}$$

Authors in [9, 55] proposed a model for image contour enhancement where a free boundary problem has been formulated with equation (2.7). Their theory addresses the existence and uniqueness of solutions to the appropriate problem, the existence and behaviour of bounding interfaces, and the behaviour over extended time periods. A self-similar solution is identified for equation (2.7), applicable for any $\gamma > 0$. It remains consistently 0 or 1 outside a transition region (the grey zone) defined by two curves, $l(t)$ and $r(t)$. The width of the transition region diminishes over time, indicating that contour enhancement is occurring. The intensity function $u$ is continuous across the two delimiting curves; however, its derivative $u_x$ experiences an infinite discontinuity.

In the paper [20, 21] a travelling profile solutions are found for equation (2.7) for $\gamma > -\frac{1}{2}$, they also presented general results obtained for the free boundary problem.

Then we can now neglect $u_{xy}, u_{yy}$ and $u_y$ in equation (2.6). The simplified equation obtained is the one-dimensional form of (2.6):

$$\partial_t u = (1-p)\frac{u_x^2 u_{xx}}{\left(1+u_x^2\right)^{\frac{q+p}{2}+1}}, \tag{2.8}$$

The model contains various dimensional constants; however, they have been normalized to unity without loss of generality.

Equations like (2.8), along with other related models, have been extensively studied and are commonly referred to as nonlinear parabolic equations of diffusion type, or nonlinear diffusion equations. These models are frequently used in the analysis of physical processes such as the diffusion of matter or heat conduction. A well-known one-dimensional formulation within the domain of partial differential equations is:

$$u_t = (\Phi(x,t,u,u_x))_x$$

Under suitable conditions, the equation can be formally classified as parabolic, for instance, when $\frac{\partial \Phi}{\partial u_x} > 0$. In many practical scenarios, including the one at hand, the function $\Phi$ satisfies $\frac{\partial \Phi}{\partial u_x} \geqslant 0$. However, extreme values such as zero or infinity may also arise, leading to the categorisation of such equations as degenerate parabolic or singular parabolic, respectively (cf. [22, 33]). A defining feature of this wide class of equations is their inherent diffusive behaviour, which results in the spreading or dispersion of the level sets of solutions over time. This inherent diffusion, however, runs counter to the desired enhancement effect, necessitating the introduction of an additional mechanism to enable enhancement. In the Perona-Malik model, this enhancement mechanism is characterised by a form of negative diffusion.

The equation (2.8) is classified as a ***degenerate parabolic equation***, characterised by a degeneracy at the value $u_x = \infty$, which corresponds to the critical limit value associated with the enhancement of contours.

The gradient enhancement phenomenon in equation (2.8) is investigated in [9], where a relationship is established between this phenomenon and the convergence towards self-similar asymptotic behaviour in an approximated model. As the solutions evolve towards a state with increasingly significant gradients, it becomes justifiable to approximate the expression $1 + u_x^2$ in (2.8) as $u_x^2$. Therefore, the simplified equation is derived as follows:

$$\partial_t u = \left(1 - p\right) \frac{u_{xx}}{u_x^{(q+p)}}. \tag{2.9}$$

Equation (2.9) governs the evolution of the image intensity in the boundary layer. We can obtain the equation (2.7) for $p = 0$ and $q = 2\left(1+\gamma\right)$. This version explains that the analysis of gradient enhancement connects to the self-similar behaviour of an approximate model. The solution's evolution toward large gradients justifies the simplification of the term $1 + u_x^2$, as the latter term becomes dominant in such configurations.

### 2.1.2 Nonlinear diffusion equations

As previously stated, we shall develop a mathematical theory pertaining to the one-dimensional evolution problem characterised by the aforementioned initial and boundary conditions. However, we will extend our focus from the specific category of equations denoted as (2.9) to encompass a broader class of nonlinear diffusion equations represented in the following form:

$$u_t = \left(\Psi\left(u_x\right)\right)_x \tag{2.10}$$

The nonlinear function $\Psi$ governs the relationship between the image flux and the gradient of the image intensity. This relationship is often referred to as the flux law or, alternatively, as the constitutive function of the model. In this broad framework, $\Psi$ can represent any monotonically

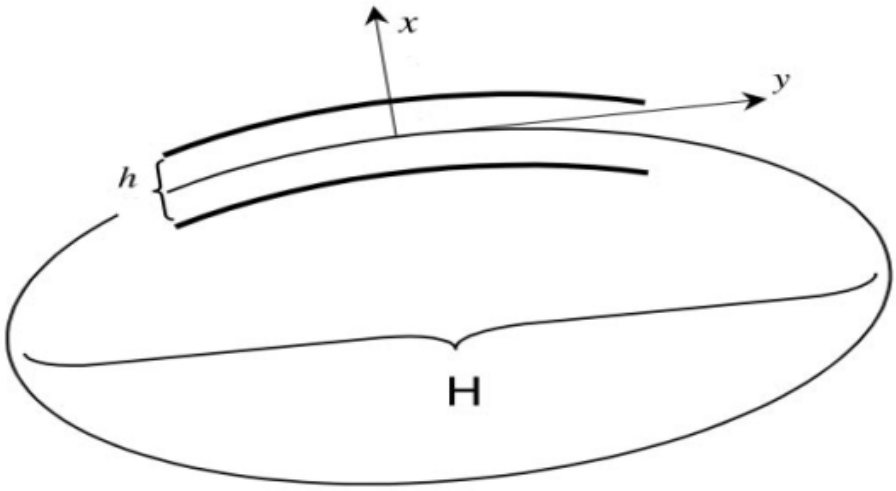


Figure 2.1: The contour of the image in the border layer.

increasing real-valued function that is defined over an appropriate gradient interval. To facilitate the analysis, we make the following assumption:

($\mathbf{H}_1$) $\Psi(s)$ *is* $C^\infty$*: The function* $\Psi(s)$ *is smooth and differentiable to all orders, i.e., it belongs to the class* $C^\infty$*, and it is strictly increasing on both the positive interval* $0 < s < \infty$ *and the negative interval* $-\infty < s < 0$*. This assumption allows for arbitrary behaviour as* $s \to 0$ *or* $|s| \to \infty$*, without imposing specific constraints on the asymptotic limits of the function.* In practical terms, the assumption that $\Psi(s)$ is $C^\infty$ implies that the function is not only smooth, but its derivatives of all orders exist and are continuous, providing a high level of regularity. The fact that it is strictly increasing in the specified intervals suggests that for any two distinct values of $s$, say $s_1$ and $s_2$, with $s_1 < s_2$, we have $\Psi(s_1) < \Psi(s_2)$, meaning that the flux is more sensitive to larger gradients. This property is important for the mathematical model as it ensures that the flux will respond predictably to increases in the gradient, which is a key factor in the process of enhancing the image features.

In this study, we aim to systematically characterise the class of functions $\Psi$ that allow for the derivation of solutions exhibiting pronounced gradient enhancement. A critical aspect of our investigation is the analysis of the temporal rates at which sharp gradients or steep profiles develop, as these dynamics are central to understanding the underlying diffusion processes. By doing so, we intend to corroborate and expand upon the results established in [9], applying our findings not only to specific instances such as the equation (2.9) but also to a broader spectrum of initial data configurations. The mathematical framework of this problem is rooted in solving the nonlinear parabolic equation (2.10), accompanied by rigorously defined initial conditions.

$$u(x,0) = u_0(x)$$

satisfying the conditions $0 \le u_0 \le 1$ and other appropriate criteria (as detailed below), along with

boundary conditions where $u = 0$ on the left side of the contour and $u = 1$ on the right side. Concerning the initial data, we note that our primary focus is on monotone solutions, specifically those for which $u_x \geq 0$ in the context of equation (2.9). This condition will inherently arise from a corresponding monotonicity criterion applied to the initial data. Regarding the boundary conditions, it has been determined that, contingent upon the specific form of $\Psi$, the boundary may be designated to reside either at infinity or at a finite distance. This latter case will be of particular interest to us, necessitating that the problem be appropriately formulated as a free boundary problem.

Now, we introduce the function $\Psi$. Since:

$$\frac{\partial}{\partial x}\left(\Psi\left(u_x\right)\right) = \left(1-p\right)\frac{u_{xx}}{\left(1+u_x^2\right)^{\frac{q+p}{2}}}.$$

$\Psi$ is then given by:

$$\Psi(v) := \int_0^v \frac{ds}{\left(1+s^2\right)^{\frac{q+p}{2}}}$$

Similarly, and since:

$$\frac{\partial}{\partial x}\left(\Psi\left(u_x\right)\right) = \frac{u_{xx}}{\left(u_x\right)^{(q+p)}}$$

We find:

$$\Psi(v) := -\int_v^\infty \frac{ds}{(s)^{q+p}} = -\frac{1}{q+p-1}v^{-(q+p-1)}$$

we set $\omega = -(q+p-1)$ we write

$$\Psi(s) = \frac{1}{\omega}s^\omega,$$

defined for $s \geq 0$, so that it is suitable with (2.9) with $\omega = -(q+p-1)$

$$\Psi'(s) = s^{\omega-1}$$

## Remark

1. If $\omega = 0$ we have $\Psi(s) = \log(s)$ with $\Psi'(s) = \frac{1}{s}$.

2. For $\omega < 0$, the function $\Psi$ is negative, but $\Psi'\left(u_x\right) > 0$ is the important quantity for the parabolic character of the equation.

3. Equation (2.8) corresponds to $\Psi'(s) = \left(1+s^2\right)^{-\left(\frac{q+p}{2}\right)}$ degenerates if $s \longrightarrow \infty$ with $(q \geq 2-p)$ and even if ( $q > -p$ ), But this equation is perfectly parabolic in the regions of bounded $u_x$. the general form of equations (2.8) and (2.9) can be written as follows:

$$u_t = \left(\Psi\left(u_x\right)\right)_x,$$

it is known in the literature as "nonlinear diffusion ".

### Existence of sharp interfaces

There exists a notable subclass of equations (2.10) in which sharp interfaces manifest. We will first examine power nonlinearities. For exponents $\omega > 1$, solutions to the Cauchy problem for equation (2.10) with initial data of compact support will maintain this property for all times. In contrast, infinite propagation occurs when $\omega \leqslant 1$ (cf. [11, 33]). In the initial case, considering an integrable function $u_0 \geqslant 0$ with an integral one, the solution to the problem can be interpreted as a classical solution of equation (2.10) within a specified domain.

$$\Omega = \{(x,t) : -l(t) < x < r(t)\},$$

with initial conditions $u(x,0) = u_0(x)$ and boundary conditions

$$\begin{cases} u(x,t) = 0, & \Psi(u_x) = 0 \quad \text{for } x = l(t) \\ u(x,t) = 1, & \Psi(u_x) = 0 \quad \text{for } x = r(t) \end{cases}$$

The lines $x = l(t)$ and $x = r(t)$ are referred to as interfaces or moving boundaries, and they are fully defined by the conditions specified above. These functions are recognised as smooth (analytic) functions of $t$ [5, 7] and exhibit divergence as $t \to \infty$ in the manner of $O\left(t^{\gamma}\right)$, providing a quantitative assessment of the dispersion effect. The presence of interfaces indicates that the equation is not uniformly parabolic at those points, resulting in limited regularity of the solutions.
Conversely, for $\omega \leqslant 1$, the identical Cauchy problem results in positive solutions where $l(t) = -\infty$ and $r(t) = \infty$. The null flux condition is equivalent to setting $u_x = 0$ at $\pm\infty$, which is a reasonable requirement given the boundary values of $u = 0, 1$ at $\pm\infty$. This condition holds automatically for $\omega > 0$.

## 2.2 Intermediate-Asymptotic Solutions

To thoroughly investigate the phenomenon of contour enhancement, it is imperative to analyse the temporal evolution of the gradient and its associated support. A pivotal approach in this context is the use of intermediate-asymptotic solutions, which are derived through dimensional analysis. This method, initially introduced by Barenblatt [9], provides a framework for understanding the behaviour of solutions to partial differential equations over intermediate time scales. In this section, we apply this methodology to derive an exact solution for Eq. (2.9), focusing on the linear case and its implications for contour enhancement.

### 2.2.1 Linear case

We commence by presenting a detailed derivation of the classical intermediate-asymptotic solution for the linear heat equation, which is given by:

$$u_t = (1-p)\,u_{xx}.$$

This equation formally corresponds to Eq. (2.9) under the condition $q+p=0$ with $p<1$. The analysis is conducted for a "smoothed step" initial condition, which is defined by the following initial and boundary conditions:

$$u(x,0)=\begin{cases}0, & -\infty<x\le -a_1\\ u_0, & -a_1\le x\le a_2\\ 1, & a_2\le x<+\infty\end{cases}, \tag{2.11}$$
$$u(-\infty,t)=0, u(+\infty,t)=1,$$

where $a_1$ and $a_2$ are positive constants that parameterise the problem. The function $u_0(x)$ is assumed to be smooth within the interval $-a_1\le x\le a_2$, satisfying $u_0(-a_1)=0$ and $u_0(a_2)=1$. Furthermore, it is assumed that the derivatives at the boundaries are $u_0'(-a_1)=0, u_0'(a_2)=1$, with the latter being negative.

Through dimensional analysis, as elucidated by Barenblatt [9], the intermediate-asymptotic solution can be expressed in the form:

$$u(x,t)=\phi(\xi)\ \ ,\xi=\frac{x-x_0}{a(t)}, \tag{2.12}$$

where $x_0$ is a parameter to be determined, and $\phi(\xi)$ is an increasing function that describes the profile of the solution. Substituting (2.12) into (2.9) (the linear heat equation formally corresponding to (2.9) for $q+p=0$ with $p<1$) leads to the following equation for the function $\phi(\xi)$

$$-\dot{a}a\xi\frac{d\phi}{d\xi}=(1-p)\frac{d^2\phi}{d\xi^2}. \tag{2.13}$$

A separation of variables argument necessitates that:

$$\dot{a}a=\alpha \tag{2.14}$$

where $\alpha$ is an arbitrary positive constant. This leads to the following equation for the profile $\phi$:

$$-\alpha\xi\frac{d\phi}{d\xi}=(1-p)\frac{d^2\phi}{d\xi^2}. \tag{2.15}$$

Integrating this equation under the boundary conditions $\phi(-\infty)=0$ and $\phi(+\infty)=1$ allows us to express $\phi$ explicitly in terms of the error function:

$$\phi(\xi)=\frac{1}{\pi}\int_{-\infty}^{\frac{\xi}{2\sqrt{1-p}}}e^{-\eta^2}d\eta, \tag{2.16}$$

This integral representation facilitates the expression of the solution $u(x,t)$ in a closed form:

$$u(x,t)=\frac{1}{2}\left[erf\left(\frac{x-x_0}{\sqrt{2(1-p)}\,(2\alpha t+1)^{\frac{1}{2}}}\right)+1\right]. \tag{2.17}$$

This solution elucidates several key features of the evolution of the initial smoothed stepwise distribution. Firstly, the width of the transition region increases proportionally to $\sqrt{2t+1}$, indicating

that the distribution broadens over time. Secondly, the gradient of the solution, $u_x(x,t)$, assumes a Gaussian shape in space, given by:

$$u_x(x,t) \sim t^{-1/2} e^{-x^2/(4t)}.$$

As time progresses, the gradient diminishes and approaches zero at a rate of $t^{-1/2}$. This decay in the gradient explains the absence of contour enhancement in the linear case. Specifically, as the gradient becomes increasingly diffuse over time, the sharpness of the contours is lost, leading to a smoothing effect rather than an enhancement.

Figure 2.2 illustrates the evolution of the image intensity distribution $u(x,t)$ over time for the heat equation in the case $p = 0$. The initial stepwise profile undergoes diffusion, leading to a progressive broadening of the transition region. This result underscores the importance of nonlinear effects

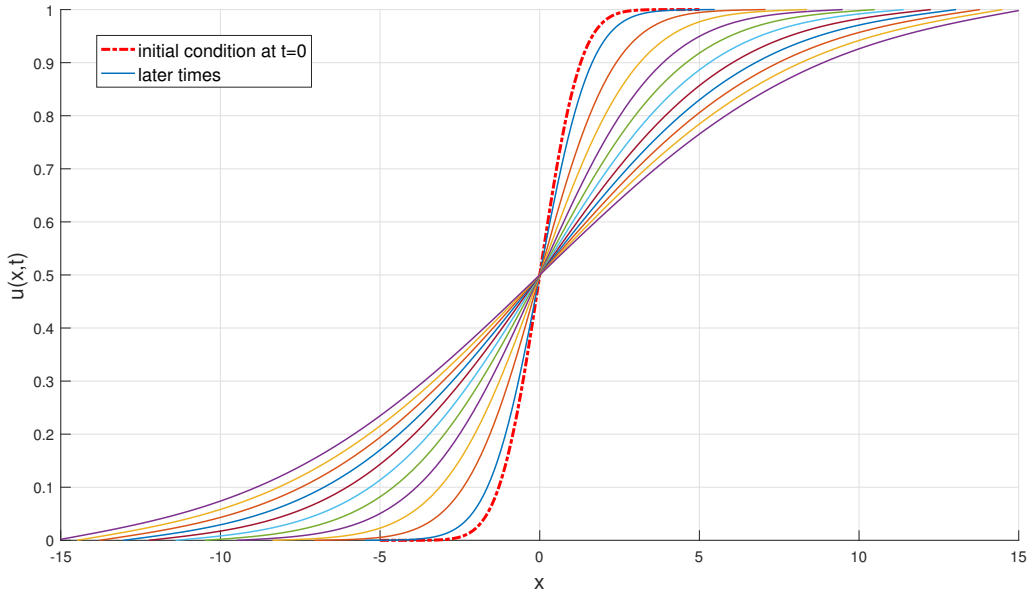


Figure 2.2: The evolution of the image intensity distribution $u(x,t)$ for heat equation (for $p = 0$).

in achieving contour enhancement, as linear diffusion alone is insufficient to maintain or amplify the sharpness of features in the solution.

In summary, the intermediate-asymptotic solution for the linear heat equation provides valuable insights into the temporal evolution of smoothed stepwise initial conditions. The broadening of the transition region and the decay of the gradient highlight the limitations of linear diffusion in preserving contour sharpness. These findings set the stage for further exploration of nonlinear mechanisms that may facilitate contour enhancement .

### 2.2.2 Non-linear case

Based on the idea shown in the linear case (heat equation for $q + p = 0$), now in the next, we consider the nonlinear case defined by equation (2.9). We try now to solve the equation in (2.23)

by using the self-similar solution under the form (2.12). Taking account this form, by replacing (2.12) into equation (2.23), we obtain, the equation:

$$-\frac{\dot{a}}{a}\xi\frac{d\phi}{d\xi}=(1-p)\frac{1}{a^{-(q+p)+2}}\frac{d^2\phi}{d\xi^2}\left(\frac{d\phi}{d\xi}\right)^{-(q+p)}. \tag{2.18}$$

A separation of variables argument implies that the following conditions must hold :

$$\frac{\dot{a}}{a}=-\alpha\frac{1}{a^{-(q+p)+2}}, \tag{2.19}$$

where $\alpha$ is arbitrary constant.

We notice that when we take the case where the initial condition in self-similar form, for example for $p+q=4$ and $\alpha<0$, we get an enhancement of the contour.

After easy integration, we get:

$$\frac{d\phi}{d\xi}=\left[\frac{-2\alpha}{1-p}\right]^{\frac{-1}{4}}C^{\frac{-1}{2}}\left[1-\left(\frac{\xi}{C}\right)^2\right]^{\frac{-1}{4}}, \tag{2.20}$$

for

$$-C\leq\xi\leq C.$$

Here, $C$ is a positive integration constant. For $\xi=\frac{x-x_0}{a(t)}$, we have:

$$x_0-Ca(t)\leq x\leq x_0+Ca(t). \tag{2.21}$$

The problem (2.20) – (2.21) indicates a free-boundary problem aimed at determining the evolution of image intensity within the boundary layer $l(t)$ and $r(t)$ such that $l(t)\leq x\leq r(t)$; with $l(t)=x_0-Ca(t)$ and $r(t)=x_0+Ca(t)$.

Further integration of (2.20) and using the boundary conditions $\phi(-C)=0$, $\phi(C)=1$, then we obtain:

$$\phi(\xi)=\left[\frac{-2\alpha}{1-p}\right]^{\frac{-1}{4}}C^{\frac{1}{2}}\int_{-1}^{\frac{\xi}{C}}\left[1-\eta^2\right]^{\frac{-1}{4}}d\eta,$$

where

$$C=\left[\frac{-2\alpha}{1-p}\right]^{-\frac{1}{2}}\left[2\int_0^1\left[1-\eta^2\right]^{\frac{-1}{4}}d\eta\right]^2,$$

The self-similar solution assumes the form

$$u(x,t)=\left[\frac{-2\alpha}{1-p}\right]^{\frac{-1}{4}}C^{\frac{1}{2}}\int_{-1}^{\frac{x-x_0}{Ca(t)}}\left[1-\eta^2\right]^{\frac{-1}{4}}d\eta, \tag{2.22}$$

In figure (2.3), the phenomenon of gradient enhancement takes place: The spatial gradient of the solutions $u_x$, increases with time, and its support shrinks.

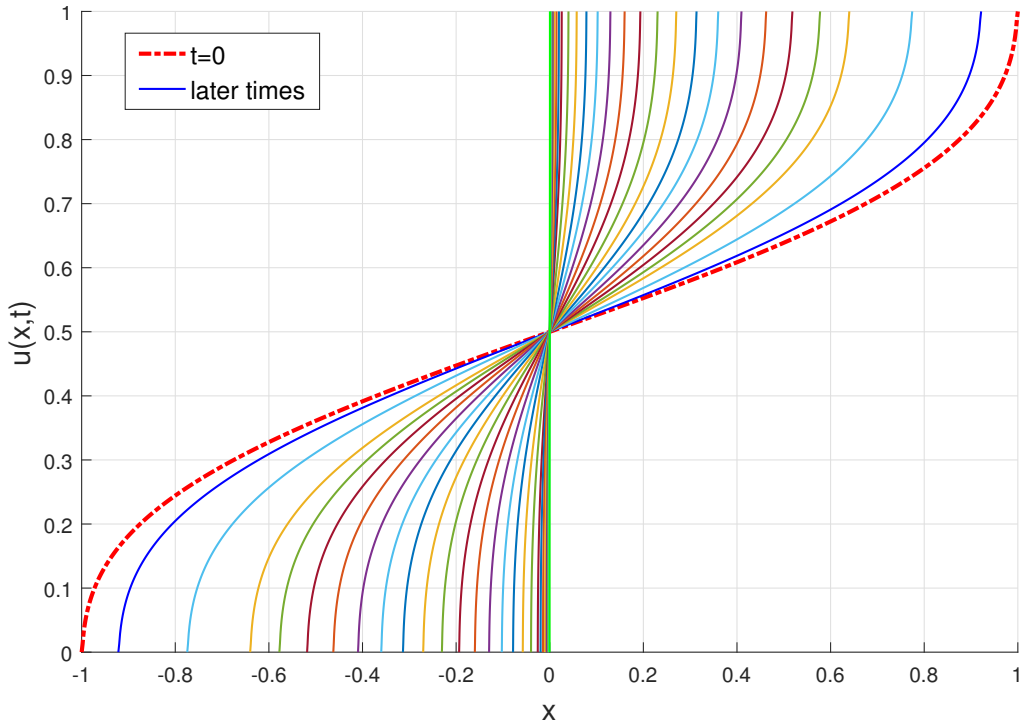


Figure 2.3: The evolution of the image intensity distribution $u(x,t)$ for $p+q=4$

We will see the constriction in the next, the free boundary problem later in the non-linear case.

## 2.3 Free boundary problem for contour enhancement

In this section, we present a free boundary problem aimed at determining the evolution of image intensity within a boundary layer. The problem is formulated as follows:

Given an increasing function $u_0(x)$ defined on an interval $I=(-a_1,a_2)$ with boundary values $u_0(-a_1)=0$ and $u_0(a_2)=1$, we seek to find a continuous function $u(x,t)$ and continuous curves $x=l(t)$ and $x=r(t)$ such that:

1. Initial Conditions: $l(0)=-a_1$ , $r(0)=a_2$ and $l(t)<r(t)$ for some time interval $t\in(0,T)$.

2. Domain of Interest: - The function $u$ solves the following problem in the domain $\Omega=\{(x,t):0<t<T,\, l(t)<x<r(t)\}$:

$$\begin{cases} \frac{\partial u}{\partial t}=\left(1-p\right)u_x^{-(q+p)}u_{xx}, & \text{in } \Omega \\ u\left(x,0\right)=u_0\left(x\right), & \text{for } -a_1\le x\le a_2 \\ u\left(l\left(t\right),t\right)=0, u_x(l\left(t\right),t)=+\infty & \text{for } 0<t<T \\ u\left(r\left(t\right),t\right)=1, u_x(r\left(t\right),t)=+\infty & \text{for } 0<t<T \end{cases}, \tag{2.23}$$

Here, $T$ can be either finite or infinite. The function $u(x,t)$ and the moving boundaries $l(t)$ and $r(t)$ are unknowns that must be determined by the over-specified conditions of the problem. This characteristic classifies the problem as a free boundary problem. Consequently, the interfaces $x=l(t)$ and $x=r(t)$ are referred to as "free boundaries."

The initial condition $u_0$ is monotonic on the interval $[-a_1, a_2]$ with $u_0(-a_1) = 0$ and $u_0(a_2) = 1$. As time $t$ progresses, the solution $u(x,t)$ becomes more refined. Notably, the two free boundaries $l(t)$ and $r(t)$ contract over time. When these moving boundaries intersect, a vertical front is formed, indicating that the enhancement process is complete. This phenomenon is illustrated in Figure 2.4.

Figure 2.4 visually represents the evolution of the solution to the free boundary problem. The left side of the figure depicts the initial state of the solution at time $t = 0$ and the state when complete enhancement is achieved at some later time $t$. The right side of the figure shows the corresponding sections of the grey region, specifically highlighting the transition domain. This transition domain illustrates how the boundaries $l(t)$ and $r(t)$ move and eventually converge, leading to the formation of a vertical front that signifies the completion of the enhancement process.

This problem is significant in the context of image processing, particularly in contour enhancement, where the evolution of image intensity plays a crucial role in defining and refining boundaries within an image. The mathematical formulation and the visual representation in Figure 2.4 provide a comprehensive understanding of the dynamics involved in this free boundary problem.

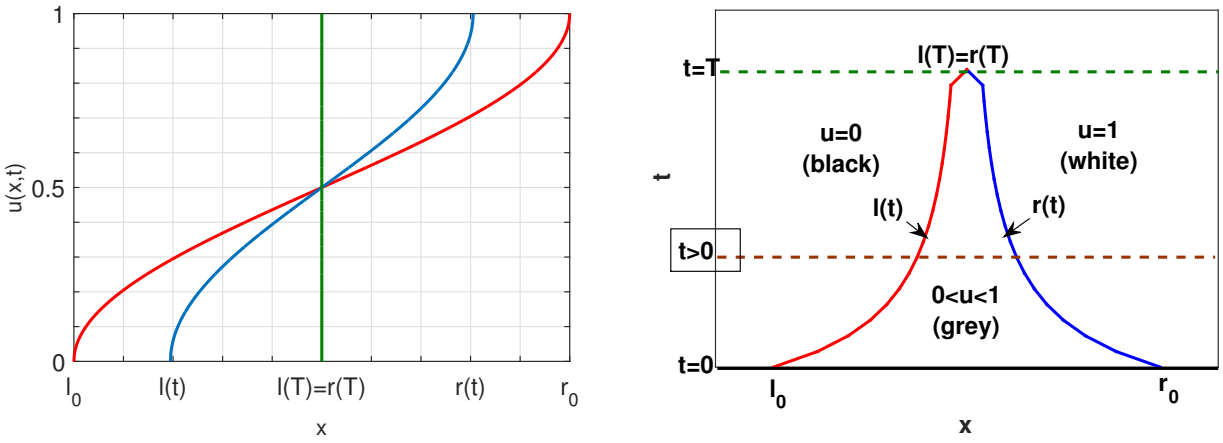


Figure 2.4: The left side illustrates the initial state of the solution to the free boundary problem at time 0, and the state when complete enhancement is achieved after some time $t$. On the right, the corresponding sections of the grey region, specifically the transition domain.

### 2.3.1 Initial condition and intermediate self-similar solution

In this section, we present a detailed analysis of the numerical computations performed to investigate the free-boundary problem associated with equation (2.9), with parameters set to $p = 0$ and $q = 4$, corresponding to the Beltrami flow. These computations were conducted following the methodologies described in [9, 10], where the evolution of the image intensity distribution over time was examined.

To gain deeper insight into the underlying dynamics, we conducted a thorough study of the evo-

lution of the initial condition over time within the framework of the free-boundary problem. Our numerical results reveal that for certain initial conditions particularly when the function $u_0(x)$ exhibits non-monotonic behaviour the solution transforms as time progresses. As shown in Figure 2.5, the solution follows the behaviour of self-similar solutions, where the function becomes monotonic and increasing over time, ultimately aligning with the general characteristics of such solutions.

In the context of the numerical simulations presented here, the self-similar solution emerges as an intermediate asymptotic solution . This means that, after an initial transient phase, the solution becomes independent of the fine details of the initial condition and follows a universal pattern dictated by the governing equation. This observation is crucial in understanding the long-term evolution of solutions within the free-boundary problem, as it suggests that the system naturally selects a self-similar form regardless of the complexity of the initial condition. Figure 2.5 illus-

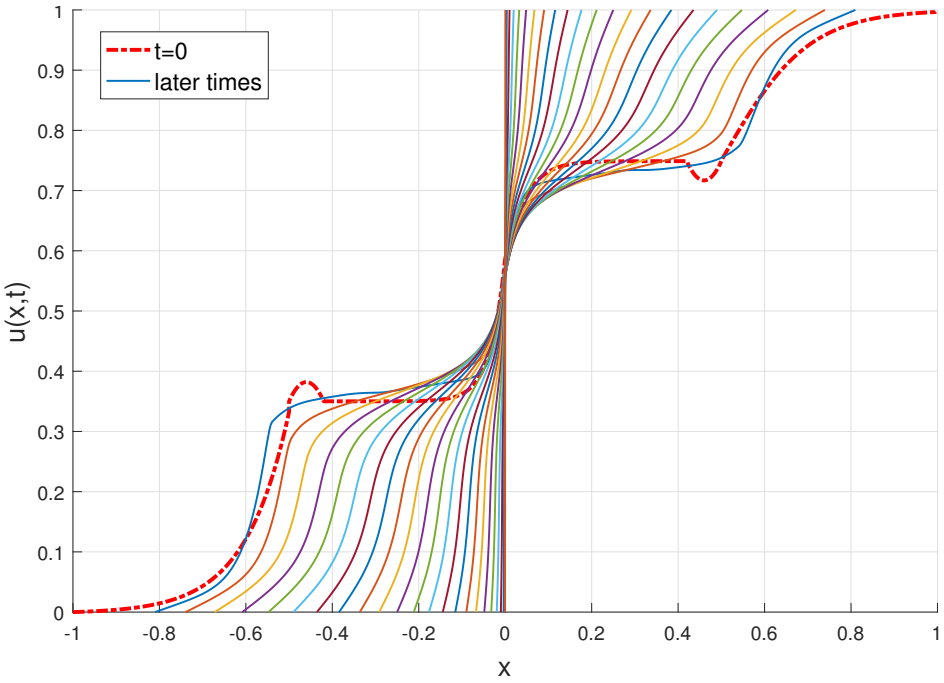


Figure 2.5: The evolution of the image intensity distribution for $p = 0$ and $q = 4$ (Beltrami flow), with non-monotonic initial condition.

trates the evolution of the image intensity distribution $u(x,t)$ over time. The red dashed curve represents the initial condition $u_0(x)$, which in this case exhibits a non-monotonic profile. As time progresses, our analysis of the free-boundary problem shows that the initial condition transitions from a non-monotonic state to a monotonic state, confirming that the solution gradually adopts the characteristics of a self-similar solution. This transition is particularly significant a regardless of the specific form of the initial condition, the solution eventually conforms to a self-similar behaviour, dictated by the governing equation. The numerical results further indicate that this self-similar regime is robust and independent of initial irregularities, suggesting that the long-term

behaviour of the system is inherently governed by self-similarity.
Our findings align with the theoretical framework established by Barenblatt [9].

## 2.4 Numerical resolution of PDEs

We begin by considering a function $u_0 : [a, b] \to \mathbb{R}$. The main idea behind nonlinear diffusion filtering is to derive a family of filtered versions of $u_0$, denoted as $u(x, t)$, by solving an appropriate diffusion process. This process is initialized with $u_0$ and subject to homogeneous Neumann boundary conditions.

### 2.4.1 Numerical processing

For the numerical solution of equation it is necessary to discretize the operators involved in the continuous problem; therefore we will first perform a spatial discretization and then a temporal discretization . These two kinds of approximation will lead us to the numerical problem to be solved.

### 2.4.2 Approximations of the partial derivatives

One possible spatial discretization in one dimensions. Assume that $u$ is a function of the independent variables $x$ and $t$. To discretize the domain, subdivide the $x-t$ plane into a grid consisting of equal rectangular cells with sides of length $\Delta x; \Delta t$, representing the spatial and temporal step sizes, respectively. Let

$$\begin{aligned} \Delta t = T/N, \quad t^n = n\Delta t, \quad n = 0, 1, ..., N \\ \Delta x = 1/M, \quad x_j = j\Delta x, \quad j = 0, 1, ..., M \end{aligned}$$

for some positive integers $N$ and $M$. Denote the value of $u$ at the representative mesh point by Define

$$u_j^n = u(x_j).$$

### 2.4.3 Spatial discretization

In the context of spatial discretization, it is necessary to approximate the first derivatives with respect to $x$, the second derivatives with respect to $x$, as well as the mixed second-order cross derivatives involving $x$. For the discretization of the first derivative of the intensity $u$ with respect to $x$, there are several finite difference schemes available. Specifically, the first derivative can be approximated using either a centered finite difference scheme or a decentered (upwind or downwind) finite difference scheme, both derived from classical finite difference methods, as described below

$$\frac{\partial u}{\partial x} \approx \begin{cases} \frac{u(x)-u(x-\Delta x)}{\Delta x} + O(\Delta x), \\ \frac{u(x+\Delta x)-u(x)}{\Delta x} + O(\Delta x), \\ \frac{u(x+\Delta x)-u(x-\Delta x)}{2\Delta x} + O\left(\Delta x^2\right), \end{cases}$$

where $\Delta x$ is the spatial discretization step along the $x - axis$.

To approximate the second derivative $\frac{\partial^2 u}{\partial x^2}$ using the classical finite difference method, we apply the standard three-point scheme, which relies on the values of the function at a grid point and its immediate neighbors.

$$\frac{\partial^2 u}{\partial x^2} \approx \frac{u(x+\Delta x) - 2u(x) + u(x-\Delta x)}{\Delta x^2} + O\left(\Delta x^2\right),$$

note that $\frac{\partial^2 u}{\partial x^2}$ is approximated accordingly.

Let $A$ represent the spatial discretization matrix for the problem. It is important to note that, due to the homogeneous Neumann boundary condition, we can simplify the discretization scheme near the boundary. Specifically, at the grid points close to the boundary, we can directly apply the fact that the intensity value at these points is equal to the intensity value at the adjacent grid points located at the boundary.

### 2.4.4 Time discretization

In terms of temporal discretization for the problem, we can consider three different approaches: an explicit time-marching scheme, an implicit time-marching scheme, or a semi-implicit time-marching scheme, which is often more convenient to implement due to its balance between stability and computational efficiency. The spatial and temporal derivatives are derived from Taylor series expansions evaluated at specific points $P(x_j)$.

$$\left(\frac{\partial^2 u}{\partial x^2}\right)_j \approx \frac{u\{(j+1)\Delta x\} - 2u\{j\Delta x\} + u\{(j-1)\Delta x\}}{\Delta x^2}$$

i.e.

$$\left(\frac{\partial^2 u}{\partial x^2}\right)_j \approx \frac{u_{j+1} - 2u_j + u_{j-1}}{\Delta x^2}$$

with a leading error of order $\Delta x^2$.

Progressive and regressive first order approimations can also be used the forward (resp. backward) difference approximation for at $P$ is

$$\left(\frac{\partial u}{\partial x}\right)_j^+ \approx \frac{u_{j+1} - u_j}{\Delta x}$$

$$\left(\frac{\partial u}{\partial x}\right)_j^- \approx \frac{u_j - u_{j-1}}{\Delta x}$$

with a leading error of $O(\Delta x)$.

The central difference method uses symmetric approximations:

$$\left(\frac{\partial u}{\partial x}\right)_j = \frac{u_{j+1} - u_{j-1}}{2\Delta x}$$

We put

$$g = u_x^m$$

### 2.4.5 The Semi-Implicit scheme

In this section, we present a semi-implicit numerical approximation scheme tailored for solving the governing equations under consideration. The proposed methodology leverages a semi-implicit Crank-Nicolson (CN) discretisation technique, which is particularly well-suited for addressing partial differential equations (PDEs) involving mixed derivative terms. This approach is widely recognised for its stability and second-order accuracy in time, making it a robust choice for handling complex temporal and spatial dynamics.

The semi-implicit Crank-Nicolson method is implemented as follows: the spatial derivative operators are discretised using a finite difference framework. Specifically, the mixed derivative terms are evaluated explicitly at the current time step, denoted as $t_n = n\Delta t$, where $n$ represents the time step index and $\Delta t$ is the temporal step size. Conversely, the non-mixed derivative terms are treated implicitly by computing their average across the current time step $t_n$ and the subsequent time step $t_{n+1} = (n+1)\Delta t$.

We start by marking the positions of the pixel of interest :

$$\frac{u_j^{n+1} - u_j^n}{\Delta t} = g^n \frac{u_{j-1}^{n+1} - 2u_j^{n+1} + u_{j+1}^{n+1}}{\Delta x^2}$$

After discretise we obtain the following:

$$u_j^n = -\frac{\Delta t}{\Delta x^2} g_j^n u_{j-1}^{n+1} + \left(1 + 2\frac{\Delta t}{\Delta x^2} g_j^n\right) u_j^{n+1} - \frac{\Delta t}{\Delta x^2} g_j^n u_{j+1}^{n+1}$$

with the Neumann boundary condition $u_1^{n+1} = u_2^{n+1}$ and $u_M^{n+1} = u_{M-1}^{n+1}$.

#### 2.4.5.1 Stability of Semi-Implicite scheme

To analyse the stability of the proposed semi-implicit numerical scheme, we employ von Neumann stability analysis, a widely used technique for examining the stability of finite difference methods. This approach involves assuming a solution of the form:

$$u_j^n = A^n e^{-ikj\Delta x},$$

where $u_j^n$ represents the numerical solution at spatial grid point $j$ and time step $n$, $A^n$ is the amplitude at time step $n$, $k$ is the wavenumber, $\Delta x$ is the spatial step size, and $i$ is the imaginary unit. This ansatz represents a Fourier mode, which allows us to study the growth or decay of the solution over time.

Substituting this assumed solution into the semi-implicit discretisation scheme yields the following relation:

$$A^n e^{-ikj\Delta x} = -\alpha_j A^{n+1} e^{-ik(j+1)\Delta x} + \left(1+2\alpha_j\right) A^{n+1} e^{-ikj\Delta x} - \alpha_j A^{n+1} e^{-ik(j-1)\Delta x}.$$

Here, $\alpha_j$ is a parameter that depends on the discretisation scheme and the problem's physical parameters. Simplifying this expression, we factor out $A^{n+1}e^{-ikj\Delta x}$ and use Euler's formula $e^{i\theta} + e^{-i\theta} = 2\cos(\theta)$ to rewrite the exponential terms. This leads to:

$$A^n = A^{n+1}\left[-\alpha_j e^{-ik\Delta x} + \left(1+2\alpha_j\right) - \alpha_j e^{ik\Delta x}\right].$$

Further simplification using trigonometric identities results in:

$$A^n = A^{n+1}\left[1 + 2\alpha_j - 2\alpha_j \cos(k\Delta x)\right].$$

Using the identity $1-\cos(k\Delta x) = 2\sin^2\left(\frac{k\Delta x}{2}\right)$, we obtain:

$$A^n = A^{n+1}\left[1 + 4\alpha_j \sin^2\left(\frac{k\Delta x}{2}\right)\right].$$

Rearranging this equation to solve for the amplification factor $A(k)$, defined as $A(k) = \frac{A^{n+1}}{A^n}$, we arrive at:

$$A(k) = \frac{1}{1 + 4\alpha_j \sin^2\left(\frac{k\Delta x}{2}\right)}.$$

The amplification factor $A(k)$ quantifies the growth or decay of the Fourier mode over a single time step. For the scheme to be stable, the magnitude of the amplification factor must satisfy $|A(k)| \leq 1$ for all wavenumbers $k$. Evaluating the magnitude of $A(k)$, we observe:

$$|A(k)| = \left|\frac{1}{1 + 4\alpha_j \sin^2\left(\frac{k\Delta x}{2}\right)}\right| \leq 1,$$

since $\alpha_j > 0$ and $\sin^2\left(\frac{k\Delta x}{2}\right) \geq 0$. This inequality holds for all values of $k$ and $\alpha_j$, indicating that the scheme is unconditionally stable. The semi-implicit scheme exhibits unconditional stability, ensuring that numerical solutions remain bounded regardless of the time step size $\Delta t$ or spatial step size $\Delta x$.

The semi-implicit discretisation scheme leads to a system of linear equations that can be expressed in matrix form. Specifically, the system is represented as:

$$\begin{pmatrix} 1+\alpha_2 & -\alpha_2 & 0 & \cdots & 0 \\ -\alpha_3 & 1+2\alpha_3 & -\alpha_3 & \cdots & 0 \\ \vdots & \ddots & \ddots & \ddots & \vdots \\ 0 & \cdots & -\alpha_{N-2} & 1+2\alpha_{N-2} & -\alpha_{N-2} \\ 0 & \cdots & 0 & -\alpha_{N-1} & 1+\alpha_{N-1} \end{pmatrix} \begin{pmatrix} u_2^{n+1} \\ u_3^{n+1} \\ \vdots \\ \vdots \\ u_{N-1}^{n+1} \end{pmatrix} = \begin{pmatrix} u_2^n \\ u_3^n \\ \vdots \\ \vdots \\ u_{N-1}^n \end{pmatrix},$$

where $\alpha_i = \frac{\Delta t}{\Delta x^2} g_i^n$. Here, $\Delta t$ and $\Delta x$ denote the temporal and spatial step sizes, respectively, and $g_i^n$ represents a function of the problem's parameters at spatial index $i$ and time step $n$. The matrix $A$ is a tridiagonal matrix, which arises naturally from the finite difference discretisation of the governing equations.

The problem is now reduced to solving the linear system:

$$A\mathbf{u}^{n+1} = \mathbf{u}^n,$$

where $A$ is the tridiagonal matrix defined above, $\mathbf{u}^{n+1}$ is the vector of unknown solution values at the next time step $n+1$, and $\mathbf{u}^n$ is the vector of known solution values at the current time step $n$.

The matrix $A$ exhibits a strictly diagonally dominant structure, which ensures its invertibility and the uniqueness of the solution. A matrix is strictly diagonally dominant if, for each row, the absolute value of the diagonal element is greater than the sum of the absolute values of the off-diagonal elements. Mathematically, this property is expressed as:

$$|1+2\alpha_i| > |-\alpha_i| + |-\alpha_i|,$$

or equivalently,

$$|1+2\alpha_i| > 2|\alpha_i|.$$

Since $\alpha_i > 0$, this inequality simplifies to:

$$1+2\alpha_i > 2\alpha_i,$$

This inequality holds trivially, confirming that the matrix $A$ is strictly diagonally dominant. As a consequence, $A$ is invertible, and the linear system $A\mathbf{u}^{n+1} = \mathbf{u}^n$ has a unique solution.

The semi-implicit scheme reduces the original problem to solving a tridiagonal linear system, which is both computationally efficient and numerically stable due to the strictly diagonally dominant nature of the matrix $A$. The invertibility of $A$ guarantees a unique solution, and the tridiagonal structure enables the use of the Thomas algorithm for efficient computation. This approach ensures robust and accurate numerical solutions, making it well-suited for solving partial differential equations in scientific and engineering applications.

### 2.4.6 Behaviour of Solutions in Free Boundary Problems for Monotonic and Non-Monotonic Initial Conditions

In this section, we provide a detailed example illustrating the behaviour of solutions under both monotonic and non-monotonic initial conditions. The analysis is conducted within the context of one-dimensional , specifically focusing on the evolution of image intensity distribution $u(x,t)$. The initial conditions are defined mathematically, and their evolution is visualised to demonstrate the impact of monotonicity on the solution's behaviour.

We defined function $u_0$ for the case initial condition monotone:

$$u(x,0) = \begin{cases} \frac{50}{1+e^{-10x}} - 0.0023, & x \in ]-1;-0.5[ \\ -20(x+0.46)^2 + 0.382, & x \in [-0.5;-0.42[ \\ \frac{5}{1+e^{-30(x-0.1)}} + 0.35, & x \in [-0.42;0[ \\ \frac{0.6}{1+4.5e^{-30(x-0.1)}} + 0.1504, & x \in [0;0.42[ \\ 10(x-0.5)^2 + 0.65, & x \in [0.42;0.5[ \\ \frac{0.9}{1+e^{-10(x-0.41)}} + 0.1022, & x \in [0.5;1[ \end{cases}$$

This piecewise function is designed to ensure a smooth transition between different regions of the domain while maintaining a monotonic increase or decrease in intensity. The monotonicity is crucial for understanding how the solution evolves over time, particularly in the context of image enhancement, where preserving or enhancing contours and gradients is often a primary objective.

We defined function $u_0$ for the case initial condition non-monotone:

$$u(x,0) = \begin{cases} \frac{50}{1+e^{-10x}} - 0.0023, & x \in ]-1;-0.5[ \\ \frac{5}{1+e^{-30(x-0.1)}} + 0.35, & x \in [-0.5;0[ \\ \frac{0.6}{1+4.5e^{-30(x-0.1)}} + 0.1504, & x \in [0;0.5[ \\ \frac{0.9}{1+e^{-10(x-0.41)}} + 0.1022, & x \in [0.5;1[ \end{cases}$$

In this case, the function is designed to introduce non-monotonic behaviour, including local maxima or minima. This is particularly relevant where the image contains noise or artifacts that disrupt the monotonicity of intensity gradients. Understanding the evolution of such initial conditions is essential for developing robust enhancement image .

Figure 2.6 presents the evolution of the one-dimensional image intensity distribution $u(x,t)$ for both monotonic and non-monotonic initial conditions. The figure is divided into two parts:

- Figure (a): Shows the evolution of the image intensity distribution for the monotonic initial condition. The smooth transitions and consistent gradients are evident, highlighting the preservation of monotonicity over time.

- Figure (b): Illustrates the evolution for the non-monotonic initial condition. Here, the presence of local variations and disruptions in the intensity gradient is clearly visible, demonstrating the challenges posed by non-monotonicity in image processing.

The comparison between the monotonic and non-monotonic cases provides valuable insights into the behaviour of solutions in one-dimensional image enhancement. The solution starts with

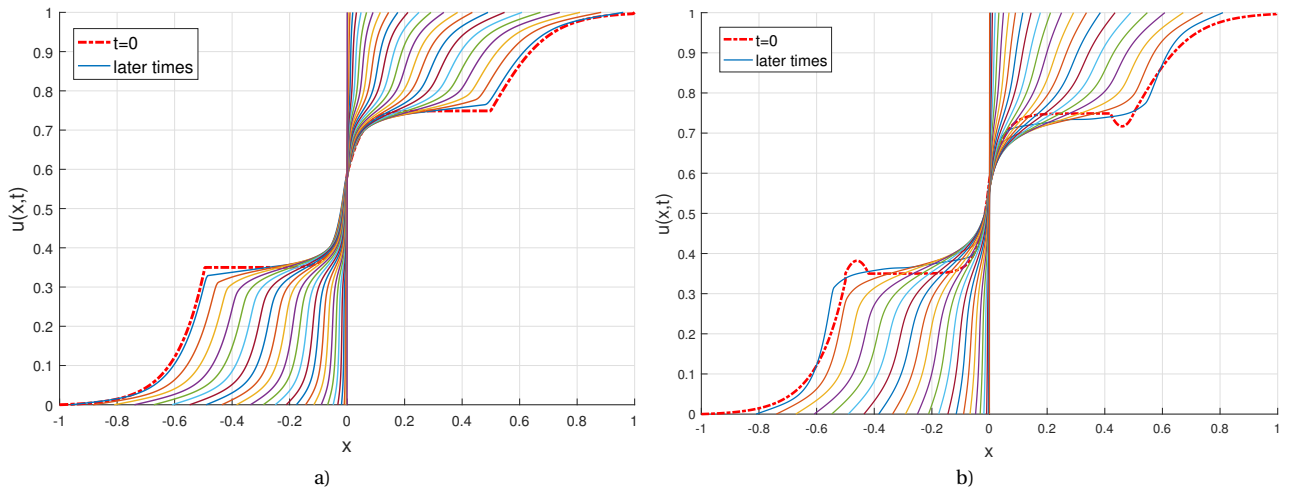


Figure 2.6: The evolution of the image intensity distribution $u(x,t)$. Top left: for initial condition monoton Top right : for initial condition non-monoton

either a monotonic or non-monotonic initial condition, as time progresses, the solution begins to exhibit self-similar behaviour, at large times, the solution converges to a completely monotonic function. Over time, the solution $u(x,t)$ evolves in such a way that it begins to exhibit self-similar behaviour.

## 2.5 Non-enhanced contour for $1-p \geq q$

In this section, we investigate the case where contour enhancement does not occur, corresponding to the case where $1-p \geq q$. The analysis is divided into two distinct cases based on the values of $q$ and $p$. The linear case, previously discussed in Section 2.1.1 (linear case), aligns with $q=-p$.

### Case for $1-p \geq q > -p$

To solve the governing equation (referenced as (2.23), we employ a self-similar solution of the form (2.12). Substituting (2.12) into (2.23) yields the following equation:

$$-\frac{\dot{a}}{a}\xi\frac{d\phi}{d\xi} = (1-p)\frac{1}{a^{-(q+p)+2}}\frac{d^2\phi}{d\xi^2}\left(\frac{d\phi}{d\xi}\right)^{-(q+p)}, \quad \text{for } 1-p \geq q > -p.$$

The separation of variables argument necessitates that the following condition is satisfied:

$$\frac{\dot{a}}{a} = -\alpha\frac{1}{a^{-(q+p)+2}}, \tag{2.24}$$

where $\alpha < 0$ is an arbitrary constant. Integrating this equation straightforwardly gives:

$$a(t) = \left[\alpha(q+p-2)t + A_0\right]^{\frac{-1}{q+p-2}}, \quad \text{for } 0 < t < \infty.$$

The equation for the profile $\phi$ then becomes:

$$\alpha\xi\frac{d\phi}{d\xi} = (1-p)\frac{d^2\phi}{d\xi^2}\left(\frac{d\phi}{d\xi}\right)^{-(q+p)}.$$

Upon integration, we obtain:

$$\frac{d\phi}{d\xi} = \left[\frac{-\alpha(q+p)}{2(1-p)}\right]^{\frac{-1}{q+p}} C^{\frac{-2}{q+p}}\left[1+\left(\frac{\xi}{C}\right)^2\right]^{\frac{-1}{q+p}}, \quad \text{for } 1-p \geq q > -p,$$

where $-\infty \leq \xi \leq +\infty$. Applying the boundary conditions $\phi(-\infty) = 0$ and $\phi(+\infty) = 1$, and integrating further, we arrive at:

$$\phi(\xi) = \left[\frac{-\alpha(q+p)}{2(1-p)}\right]^{\frac{-1}{q+p}} C^{\frac{q+p-2}{q+p}} \int_{-\infty}^{\frac{\xi}{C}} \left[1+\eta^2\right]^{\frac{-1}{q+p}} d\eta,$$

where

$$C = \left[\frac{-\alpha(q+p)}{2(1-p)}\right]^{\frac{-1}{q+p-2}} \left[2\int_0^{\infty}\left[1+\eta^2\right]^{\frac{-1}{q+p}} d\eta\right]^{\frac{-(q+p)}{q+p-2}}.$$

Thus, the self-similar solutions take the form:

$$u(x,t) = \left[\frac{-\alpha(q+p)}{2(1-p)}\right]^{\frac{-1}{q+p}} C^{\frac{q+p-2}{q+p}} \int_{-\infty}^{\frac{x-x_0}{Ca(t)}} \left[1+\eta^2\right]^{\frac{-1}{q+p}} d\eta.$$

In this case, where $1-p \geq q > -p$ and $p < 1$, as $t \to \infty$, $u_x \to 0$. For instance, when $q = 1-p$, the exact solution is expressed as:

$$u(x,t) = \frac{1}{\pi}\arctan\left(\frac{\alpha}{2\pi(1-p)}\frac{x-x_0}{t+A_0}\right) + \frac{1}{2}, \tag{2.25}$$

and its gradient is given by:

$$u_x = \frac{\alpha}{2(1-p)(t+A_0)}\left[1+\left(\frac{\alpha}{2\pi(1-p)}\frac{x-x_0}{t+A_0}\right)^2\right]^{-1}. \tag{2.26}$$

The solution (2.25) illustrates that the initially smoothed stepwise distribution expands over time, with its width increasing proportionally to $t + A_0$. The gradient (2.26) diminishes over time, approaching zero as $t \to \infty$ (see Figure 2.7).

Figure 2.7 illustrates the temporal evolution of the image intensity distribution for the specific case where $q = 1-p$. This figure visually represents the solution's behavior over time, highlighting key aspects of the diffusion process in the absence of contour enhancement.

As time progresses, the solution exhibits a broadening of the intensity distribution, indicating that the initially sharp contours of the image become increasingly diffuse. This broadening is a direct consequence of the purely diffusive nature of the governing equation under the condition $1-p \geq q$. The self-similar solutions derived in the previous section demonstrate that the width of

the intensity distribution expands proportionally with time, leading to a gradual loss of contour definition.

A critical observation from the figure is the asymptotic behavior of the first derivative of the solution, $u_x$, which tends to zero as $t \to \infty$. This behavior is mathematically expressed in Equation (2.26), where the gradient of the solution decays inversely with time. The diminishing gradient signifies the smoothing out of the intensity profile, resulting in the absence of sharp transitions or contour in the image.

The phenomenon observed in Figure 2.7 aligns with the theoretical predictions, confirming that the solutions in this regime do not exhibit contour enhancement. Instead, the diffusion process dominates, leading to the blurring of contours and a loss of detail in the image.

A similar outcome, albeit with potentially different rates, applies to more general parameter values where $1-p \geq q > -p$ and $p < 1$. These solutions are purely diffusive and exhibit no contour enhancement, leading to blurred contours in the image.

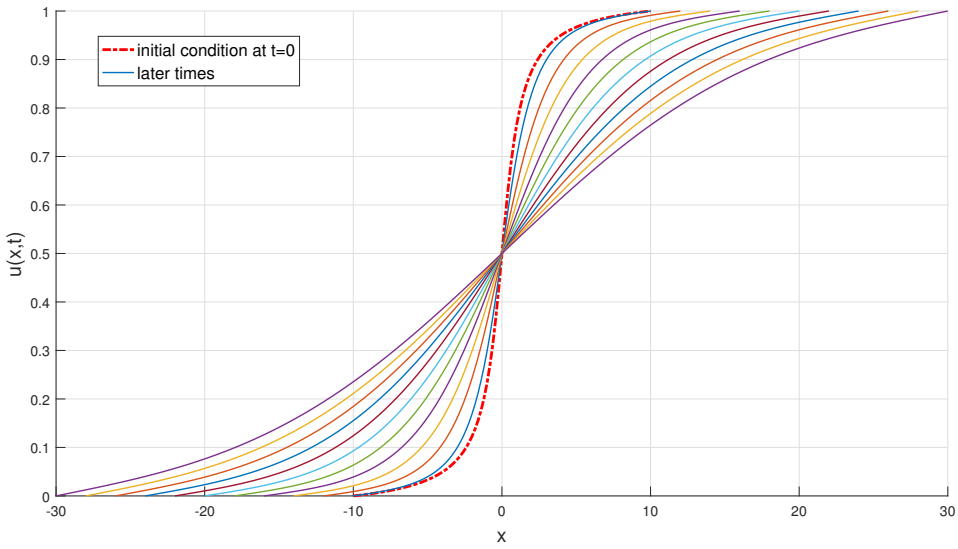


Figure 2.7: The evolution of the image intensity distribution for $q = 1-p$.

## Case for $q < -p$

The resolution of the (2.24) given equation yields the function $a(t)$ in the form:

$$a(t) = \left[\alpha(q+p-2)t + A_0\right]^{-\frac{1}{(q+p)-2}}, \quad 0 < t < \infty,$$

where $\alpha$ is a negative constant, $A_0 > 0$ is a constant.

The ordinary differential equation (ODE) for the profile $\phi$ is given by:

$$\alpha\xi\frac{d\phi}{d\xi} = (1-p)\frac{d^2\phi}{d\xi^2}\left(\frac{d\phi}{d\xi}\right)^{-(q+p)}.$$

This equation can be rewritten after integration as:

$$\left(\frac{d\phi}{d\xi}\right)^{-(q+p)} = \frac{-\alpha(q+p)}{2(1-p)}\xi^2 + C,$$

where $C$ is an integration constant. The equation can be further simplified to:

$$\left(\frac{d\phi}{d\xi}\right)^{-(q+p)} = \frac{\alpha(q+p)}{2(1-p)}\left[-\xi^2 + C^2\right].$$

This form highlights the dependence of $\frac{d\phi}{d\xi}$ on $\xi$.

The derivative $\frac{d\phi}{d\xi}$ is expressed as:

$$\frac{d\phi}{d\xi} = \left[\frac{\alpha(q+p)}{2(1-p)}\right]^{-\frac{1}{q+p-2}} C^{-\frac{2}{q+p}} \left[1 - \left(\frac{\xi}{C}\right)^2\right]^{-\frac{1}{q+p}}, \quad -C < \xi < +C.$$

This equation describes the spatial variation of the profile $\phi$.

Further integration, combined with boundary conditions, yields the profile $\phi(\xi)$:

$$\phi(\xi) = \left[\frac{\alpha(q+p)}{2(1-p)}\right]^{-\frac{1}{q+p}} C^{\frac{q+p-2}{q+p}} \int_{-1}^{\frac{\xi}{C}} \left[1-\eta^2\right]^{\frac{1}{q-p}} d\eta, \quad -C < \xi < +C.$$

The constant $C$ is determined by:

$$C = \left[\frac{\alpha(q+p)}{2(1-p)}\right]^{-\frac{1}{q+p-2}} \left[2\int_0^1 \left[1-\eta^2\right]^{-\frac{1}{q+p}} d\eta\right]^{-\frac{q+p}{q+p-2}}.$$

This ensures the consistency of the solution with the given boundary conditions.

The self-similar solution for the case $q < -p$ and $\alpha < 0$ is given by:

$$u(x,t) = \left[\frac{\alpha(q+p)}{2(1-p)}\right]^{-\frac{1}{q+p}} C^{\frac{q+p-2}{q+p}} \int_{-1}^{\frac{x-x_0}{Ca(t)}} \left[1-\eta^2\right]^{\frac{1}{q-p}} d\eta.$$

This represents the general solution in terms of the spatial variable $x$ and time $t$.

Finally, the partial derivative $\frac{\partial u}{\partial x}$ is computed as:

$$\frac{\partial u}{\partial x} = \frac{1}{Ca(t)}\left[\frac{\alpha(q+p)}{2(1-p)}\right]^{-\frac{1}{q+p}} C^{\frac{q+p-2}{q+p}} \left[1 - \left(\frac{x-x_0}{Ca(t)}\right)^2\right]^{\frac{1}{q-p}}$$

This derivative describes the rate of change of the solution $u(x,t)$ with respect to $x$.

Indicating that the derivative $\frac{\partial u}{\partial x}$ tends to zero as $t \to \infty$. This is because $a(t)$ tends to zero faster than the growth of $\frac{x-x_0}{Ca(t)}$.

As $t \to \infty$, $a(t)$ decays to zero because of the negative exponent. This decay implies that the spatial scale of the solution $u(x,t)$ expands over time, causing the solution to become increasingly "flattened" or "smoothed out" as $t$ grows.

The decay of $\frac{\partial u}{\partial x}$ to zero reflects the diffusive nature. As $t \to \infty$, the solution spreads out spatially, and any sharp features or contours in the initial profile are smoothed out. This is a hallmark of

diffusive processes, where gradients tend to diminish over time, leading to a more homogeneous state.

The phenomenon of contour enhancement typically refers to the sharpening of gradients or discontinuities in a solution over time. In this case, however, the opposite occurs: the derivative $\frac{\partial u}{\partial x}$ tends to zero, meaning that the solution becomes smoother and more uniform as $t \to \infty$. This behaviour is consistent with the solutions non-enhancement of contour.

In the following , we will explore specific examples that illustrate the concepts discussed earlier. These examples will provide exact solutions to the partial differential equation (PDE) under consideration, offering deeper insights into the behaviour for particular values of the parameters $q < -p$.

## Exemple1. $q + p = \frac{-2}{3}$

The equation (2.23) becomes:

$$u_t = (1-p)\, u_x^{\frac{2}{3}} u_{xx}$$

Substituting the solution (2.12) into this equation yields

$$\frac{-\dot{a}}{a}\xi\frac{d\phi}{d\xi} = \frac{1}{a^{\frac{8}{3}}}\frac{d^2\phi}{d\xi^2}\left(\frac{d\phi}{d\xi}\right)^{\frac{2}{3}}$$

A separation of variables approach indicates that the subsequent conditions, along with simple integration, yield:

$$a(t) = \left(-\frac{8}{3}\alpha t + A_0\right)^{\frac{3}{8}}, \quad 0 < t < \infty,$$

where $\alpha < 0$ is negative constant. The equation for the profile $\phi$, becomes:

$$-\alpha\xi\frac{d\phi}{d\xi} = (1-p)\frac{d^2\phi}{d\xi^2}\left(\frac{d\phi}{d\xi}\right)^{\frac{2}{3}}$$

After integration, the profile $\phi$ is given by

$$\phi(\xi) = \frac{8}{3\pi}\left[3\arcsin\left(\frac{\xi}{C}\right) + \frac{2\xi}{C}\left(1-\left(\frac{\xi}{C}\right)^2\right)^{\frac{3}{2}} + \frac{3\xi}{C}\sqrt{1-\left(\frac{\xi}{C}\right)^2} + \frac{3\pi}{16}\right].$$

The exact solution written under the form:

$$u(x,t) = \frac{8}{3\pi}\left[3\arcsin\left(\frac{x-x_0}{Ca(t)}\right) + 2\left(\frac{x-x_0}{Ca(t)}\right)\left(1-\left(\frac{x-x_0}{Ca(t)}\right)^2\right)^{\frac{3}{2}} + 3\left(\frac{x-x_0}{Ca(t)}\right)\sqrt{1-\left(\frac{x-x_0}{Ca(t)}\right)^2} + \frac{3\pi}{16}\right]. \tag{2.27}$$

The solution (2.27) demonstrates that the initially smoothed, stepwise intensity distribution undergoes temporal expansion, with its width increasing in direct proportion to $t + A_0$. This behaviour indicates a progressive broadening of the transition region over time. Concurrently, the

gradient $u_x$ exhibits a monotonic decrease, gradually tending towards zero as $t \to \infty$. This decline in gradient magnitude signifies a continuous attenuation of sharp variations in the distribution profile, ultimately leading to a more diffused state in the long-term evolution of the solution.
Figure 2.8 provides a visual representation of the temporal evolution of the image intensity distribution for the particular case where $p = 0$ and $q = -\frac{2}{3}$. This illustration effectively captures the key characteristics of the solutions dynamical behaviour, offering insights into the nature of the diffusion process in the absence of contour enhancement. Specifically, the figure highlights the gradual expansion of the intensity profile and the corresponding reduction in gradient magnitude, reinforcing the conclusion that no contour sharpening occurs within this parameter regime.

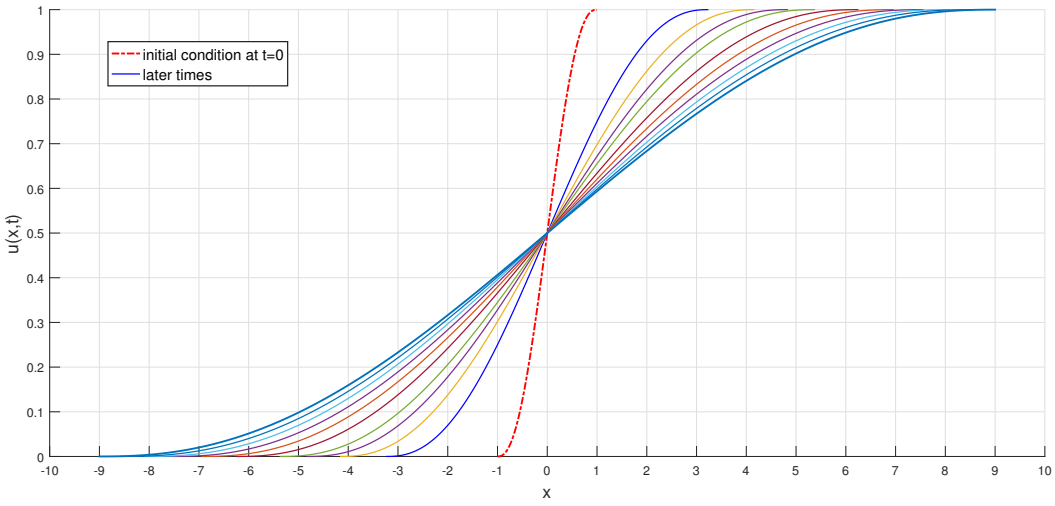


Figure 2.8: The evolution of the image intensity distribution for $p = 0$ and $q = -\frac{2}{3}$.

## Exemple2. $q + p = -1$

The equation (2.23) becomes:

$$u_t = (1-p)\, u_x u_{xx}$$

If we replace the solution (2.12) in this equation, we obtain

$$\frac{-\dot{a}}{a}\xi = \frac{1}{a^3}\frac{d^2\phi}{d\xi^2}$$

A separation of variables argument implies that the following conditions, and easy integration gives:

$$a(t) = (-3\alpha t + A_0)^{\frac{1}{3}}, \quad 0 < t < \infty,$$

where $\alpha < 0$ is negative constant. The equation for the profile $\phi$, becomes:

$$-\alpha\xi = (1-p)\frac{d^2\phi}{d\xi^2}$$

. After integration, the profile $\phi$ is given by

$$\phi(\xi) = \frac{3}{4}\left[\frac{\xi}{C} - \frac{1}{3}\left(\frac{\xi}{C}\right)^3 + \frac{2}{3}\right].$$

The exact solution written under the form:

$$u(x,t) = \frac{3}{4}\left[\frac{x-x_0}{Ca(t)} - \frac{1}{3}\left(\frac{x-x_0}{Ca(t)}\right)^3 + \frac{2}{3}\right]. \tag{2.28}$$

The solution (2.28) shows that the initially smoothed stepwise intensity distribution expands over time, with its width proportional to $t + A_0$. Simultaneously, the gradient $u_x$ decreases monotonically, approaching zero as $t \to \infty$, leading to a progressively diffused state.

Figure 2.9 illustrates the evolution of the intensity distribution for $p = 0$ and $q = -1$, highlighting the expansion of the profile and the decline in gradient, confirming the absence of contour enhancement.

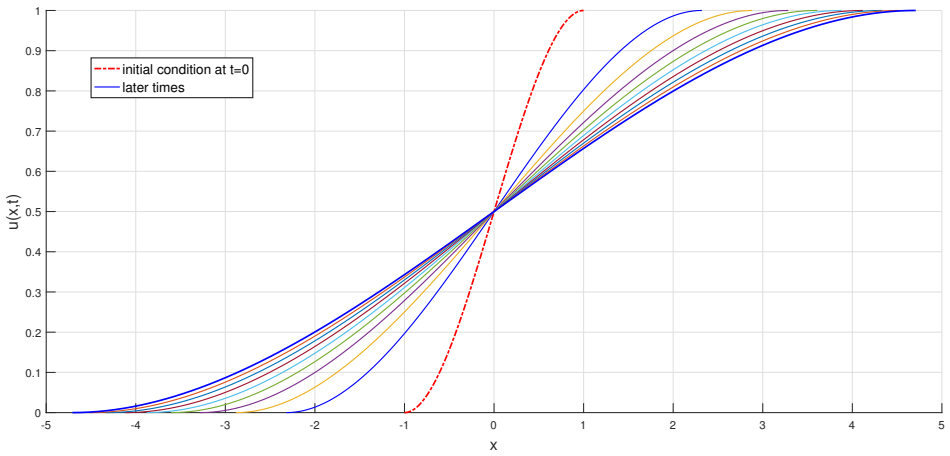


Figure 2.9: The evolution of the image intensity distribution for $p = 0$ and $q = -1$.

## Exemple3. $q + p = -2$

The equation (2.23) becomes:

$$u_t = (1-p)\, u_x^2 u_{xx}$$

By substituting the solution (2.12) into this equation, we derive

$$-\frac{\dot{a}}{a}\xi\frac{d\phi}{d\xi} = \frac{1}{a^4}\frac{d^2\phi}{d\xi^2}\left(\frac{d\phi}{d\xi}\right)^2$$

A separation of variables approach indicates that the subsequent conditions, along with straightforward integration, yield:

$$a(t) = (-4\alpha t + A_0)^{\frac{1}{4}}, \quad 0 < t < \infty,$$

where $\alpha < 0$ is negative constant. The equation for the profile $\phi$, becomes:

$$-\alpha\xi\frac{d\phi}{d\xi} = (1-p)\frac{d^2\phi}{d\xi^2}\left(\frac{d\phi}{d\xi}\right)^2$$

After integration, the profile $\phi$ is given by

$$\phi(\xi) = \frac{2}{\pi}\left[\frac{1}{2}\left(\frac{\xi}{C}\sqrt{1-\left(\frac{\xi}{C}\right)^2}\right) + \arcsin\left(\frac{\xi}{C}\right) + \frac{\pi}{4}\right].$$

The exact solution written under the form:

$$u(x,t) = \frac{2}{\pi}\left[\frac{1}{2}\left(\frac{x-x_0}{Ca(t)}\sqrt{1-\left(\frac{x-x_0}{Ca(t)}\right)^2}\right) + \arcsin\left(\frac{x-x_0}{Ca(t)}\right) + \frac{\pi}{4}\right]. \tag{2.29}$$

The solution presented in Equation (2.29) demonstrates that the initially smoothed stepwise distribution undergoes temporal broadening, with its width scaling proportionally to $t + A_0$. Concurrently, the gradient described in Equation $u_x$ decays over time, asymptotically approaching zero as $t \to \infty$ (see Figure 2.10).

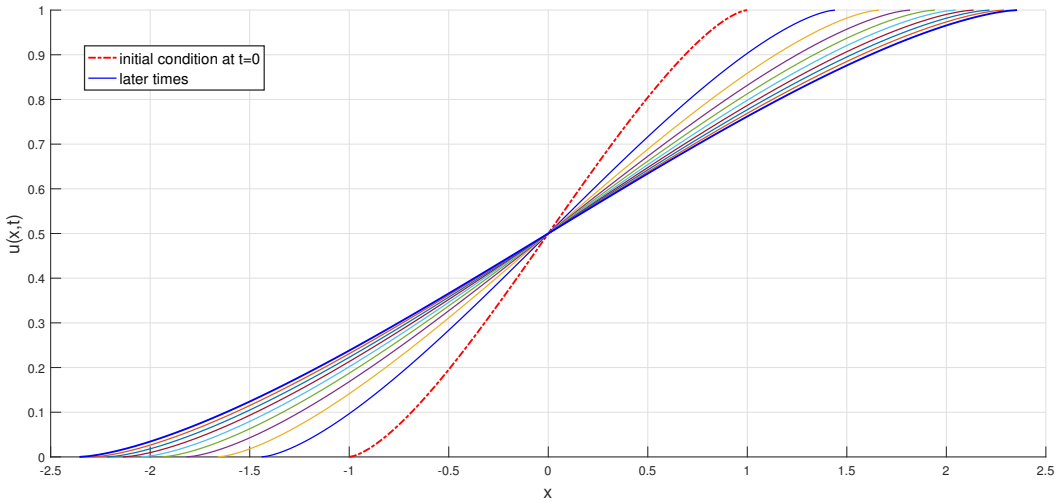


Figure 2.10: The evolution of the image intensity distribution for $p = 0$ and $q = -2$.

## 2.6 Conclusion and Comments

In conclusion, this chapter has presented a novel approach to image intensity evolution by introducing a new model based on nonlinear diffusion equations, which generalises mean curvature motion. The proposed model is particularly effective in describing intensity evolution within boundary layers near contours, where abrupt intensity changes occur. A significant contribution of this work is the formulation of a free boundary problem, which provides a more dynamic, flexible, and efficient framework for handling image contours compared to traditional methods. Through the analysis of a simplified one-dimensional case, we have explored the asymptotic behaviour of the model and investigated the influence of parameters $p$ and $q$ under the condition $1 - p \geq q$ and $p < 1$. This analysis has revealed specific , such as the extended case discussed in [1], where no improvement in the contour is observed. These findings offer valuable insights into the role of parameters in shaping the solution and highlight the potential of the proposed model for advancing the field of image processing.

Chapter 3

# *Self-similar solution for a new free-boundary problem and image contour enhancement*

In this chapter, we explore self-similar solutions for a newly formulated free-boundary problem in (2.23). Our analysis focuses on addressing the free-boundary problem and investigating the behaviour of solutions, particularly in relation to image contour enhancement. By studying the dynamics of this equation, we aim to establish a connection between the mathematical properties of the solutions and their ability to preserve and enhance image contour. Additionally, we conduct numerical simulations to validate the theoretical findings. These simulations are performed on grayscale two-dimensional images to assess the effectiveness of the proposed model in real-world applications. The experimental results demonstrate the models capability in maintaining and sharpening image contours, confirming the practical applicability of the theoretical insights. The results presented in this chapter are part of our research work published in [1].

## 3.1 Self-similar solutions to the free boundary problem

In this section, we aim to solve the problem described by equation (2.23) for the case where $q > 1-p$ and $p < 1$. To achieve this, we employ a self-similar solution of the form given by (2.12). By substituting this self-similar form into the original problem (2.23), we derive the following equation:

$$-\frac{\dot{a}}{a}\xi\frac{d\phi}{d\xi} = (1-p)\frac{1}{a^{-(q+p)+2}}\frac{d^2\phi}{d\xi^2}\left(\frac{d\phi}{d\xi}\right)^{-(q+p)}, \quad \text{for } q > 1-p. \tag{3.1}$$

Here, $\xi$ represents the similarity variable, and $\phi(\xi)$ is the profile function. The dot notation $\dot{a}$ denotes the time derivative of $a(t)$. The method of separation of variables requires that the following condition be satisfied:

$$\frac{\dot{a}}{a} = -\alpha\frac{1}{a^{-(q+p)+2}}, \tag{3.2}$$

where $\alpha$ is an arbitrary positive constant. This condition ensures that the time-dependent part of the solution can be separated from the spatial part, leading to a solvable ordinary differential equation for the profile function $\phi(\xi)$. The equation for the profile function $\phi(\xi)$ then becomes:

$$\alpha\xi\frac{d\phi}{d\xi} = (1-p)\frac{d^2\phi}{d\xi^2}\left(\frac{d\phi}{d\xi}\right)^{-(q+p)}.$$

Upon integrating the above equation, we obtain the following expression for the derivative of the profile function:

$$\frac{d\phi}{d\xi} = \left[\frac{\alpha\left(q+p\right)}{2\left(1-p\right)}\right]^{\frac{-1}{q+p}} C^{\frac{-2}{q+p}} \left[1-\left(\frac{\xi}{C}\right)^2\right]^{\frac{-1}{q+p}}, \tag{3.3}$$

where $C$ is a positive integration constant, and the solution is valid for:

$$-C \leq \xi \leq C.$$

By defining $\xi = \frac{x-x_0}{a(t)}$, the spatial domain is transformed to:

$$x_0 - Ca\left(t\right) \leq x \leq x_0 + Ca\left(t\right).$$

This suggests that the problem (2.23) can be interpreted as a free-boundary problem, where the boundaries $l(t)$ and $r(t)$ evolve over time. Specifically, $l(t) = x_0 - Ca(t)$ and $r(t) = x_0 + Ca(t)$, defining the region $l(t) \leq x \leq r(t)$ as the boundary layer. The resolution of equation (3.2) yields the time-dependent function $a(t)$:

$$a\left(t\right) = \left[\alpha\left(q+p-2\right)t + A_0\right]^{\frac{-1}{q+p-2}}, \quad \text{for } 0 < t < \infty \quad \text{if } q > 2-p, \tag{3.4}$$

and

$$a\left(t\right) = \left[\alpha\left(q+p-2\right)t + A_0\right]^{\frac{-1}{q+p-2}}, \quad \text{for } 0 < t < T \quad \text{if } 1-p < q < 2-p, \tag{3.5}$$

where $A_0 > 0$ is a constant, and $T$ is given by:

$$T = -\frac{A_0}{\alpha\left(q+p-2\right)}.$$

In the special case where $q = 2-p$, the solution simplifies to:

$$a\left(t\right) = e^{-(1-p)\pi^2 t}, \quad \text{for } 0 < t < \infty. \tag{3.6}$$

The values of the parameters $p$ and $q$ play a pivotal role in determining the nature of the self-similar solutions. These solutions can be classified into three distinct types based on the values of $p$ and $q$: Type I solutions occur when $q > 2-p$, Type II solutions arise when $1-p < q < 2-p$, and when $q = 2-p$, we recover the self-similar solutions of Type III.

Each type of solution exhibits unique characteristics, particularly in terms of their asymptotic behavior and the evolution of the boundary layer.

The asymptotic behavior of the self-similar solutions for equation (2.23) is closely tied to the values of $p$ and $q$. By examining these behaviors, we can gain insights into the phenomenon of contour enhancement, which is a key aspect of image evolution within the boundary layer.

To further analyse the solution, we integrate equation (3.3) and apply the boundary conditions $\phi(-C) = 0$ and $\phi(C) = 1$. This leads to the following expression for the profile function:

$$\phi(\xi) = \left[\frac{\alpha(q+p)}{2(1-p)}\right]^{\frac{-1}{q+p}} C^{\frac{q+p-2}{q+p}} \int_{-1}^{\frac{\xi}{C}} \left[1-\eta^2\right]^{\frac{-1}{q+p}} d\eta,$$

where the constant $C$ is determined by:

$$C = \left[\frac{\alpha(q+p)}{2(1-p)}\right]^{-\frac{1}{q+p-2}} \left[2\int_0^1 \left[1-\eta^2\right]^{\frac{-1}{q+p}} d\eta\right]^{\frac{-(q+p)}{q+p-2}},$$

for $q \neq 2-p$.

The self-similar solution $u(x,t)$ takes the form:

$$u(x,t) = \left[\frac{\alpha(q+p)}{2(1-p)}\right]^{\frac{-1}{q+p}} C^{\frac{q+p-2}{q+p}} \int_{-1}^{\frac{x-x_0}{Ca(t)}} \left[1-\eta^2\right]^{\frac{-1}{q+p}} d\eta, \tag{3.7}$$

and its spatial gradient is given by:

$$u_x = \frac{1}{a(t)} \left[\frac{\alpha(q+p)}{2(1-p)}\right]^{\frac{-1}{q+p}} C^{\frac{-2}{q+p}} \left[1-\left(\frac{x-x_0}{Ca(t)}\right)^2\right]^{\frac{-1}{q+p}}. \tag{3.8}$$

The gradient $u_x$ exhibits significant asymptotic characteristics, particularly in the boundary layer near the image contour. The width of the transition region, defined as $r(t)-l(t)$, is given by:

$$2Ca(t) = 2C\left[\alpha(q+p-2)t + A_0\right]^{\frac{-1}{q+p-2}}. \tag{3.9}$$

This width evolves over time and is influenced by the parameters $p$ and $q$, which in turn affect the phenomenon of contour enhancement. The next section will explore this phenomenon in greater detail for various values of $p$ and $q$.

### 3.1.1 Self-similar solution of type I

We begin by examining the case where $q > 2-p$ and $p < 1$. It is observed that the solution given in Equation (3.7) represents a local solution.

For the profile $\phi$, Equation (3.3) can be expressed as:

$$\frac{d\phi}{d\xi} = \left[\frac{\alpha(q+p)}{2(1-p)}\right]^{\frac{-1}{q+p}} C^{\frac{-2}{q+p}} \left[1-\left(\frac{\xi}{C}\right)^2\right]^{\frac{-1}{q+p}}, \text{with } q > 2-p \tag{3.10}$$

where $q > 2-p$, and $\xi$ is defined within the interval:

$$-C \leq \xi \leq C.$$

Here, $C$ is a positive integration constant. By defining $\xi = \frac{x-x_0}{a(t)}$, the spatial domain is constrained to:

$$x_0 - Ca(t) \leq x \leq x_0 + Ca(t). \tag{3.11}$$

This formulation, encompassing Equations (3.10)-(3.11), presents a free-boundary problem. The objective is to determine the evolution of image intensity within the boundary layer defined by $l(t)$ and $r(t)$ such that $l(t) \le x \le r(t)$, with $l(t) = x_0 - Ca(t)$ and $r(t) = x_0 + Ca(t)$.
Integrating Equation (3.10) and applying the boundary conditions $\phi(-C) = 0$ and $\phi(C) = 1$, we derive the following expression for $\phi(\xi)$:

$$\phi(\xi) = \left[\frac{\alpha(q+p)}{2(1-p)}\right]^{\frac{-1}{q+p}} C^{\frac{q+p-2}{q+p}} \int_{-1}^{\frac{\xi}{C}} \left[1-\eta^2\right]^{\frac{-1}{q+p}} d\eta,$$

where the constant $C$ is given by:

$$C = \left[\frac{\alpha(q+p)}{2(1-p)}\right]^{-\frac{1}{q+p-2}} \left[2\int_0^1 \left[1-\eta^2\right]^{\frac{-1}{q+p}} d\eta\right]^{\frac{-(q+p)}{q+p-2}},$$

The self-similar solution takes the form:

$$u(x,t) = \left[\frac{\alpha(q+p)}{2(1-p)}\right]^{\frac{-1}{q+p}} C^{\frac{q+p-2}{q+p}} \int_{-1}^{\frac{x-x_0}{Ca(t)}} \left[1-\eta^2\right]^{\frac{-1}{q+p}} d\eta, \tag{3.12}$$

At the free boundaries $x = l(t)$ and $x = r(t)$, the image intensity remains continuous. However, the spatial derivative $u_x$ exhibits a discontinuity, diverging to infinity at these boundaries. Initially, the transition region, as described by Equation (3.9), narrows over time, leading to a sharp localisation of the intensity change. This process results in the transformation of an initially smooth image $u_0$ into a step function, with contour enhancement becoming increasingly pronounced as time progresses.
As the system evolves, the behaviour of $u_x$ at a specific point $x = x_0$ is influenced by the dynamics of the boundary movement and the continuous reduction of the transition region. The sharpening of contour and the accompanying enhancement are direct consequences of this evolving behaviour, which progressively intensifies the contrast in image intensity at the boundaries. Specifically, the derivative $u_x$ at $x = x_0$ is given by:

$$u_x(x_0,t) = \frac{1}{a(t)}\left[\frac{\alpha(q+p)}{2(1-p)}\right]^{\frac{-1}{q+p}} C^{\frac{-2}{q+p}},$$

which grows over time and diverges as $O\left(t^{-\frac{1}{q+p-2}}\right)$ as $t \to \infty$. Consequently, the validity of the asymptotic equation (2.9) improves with time.
Figure 3.1 illustrates the evolution of the image intensity distribution $u(x,t)$ for two distinct parameter sets: $p = \frac{1}{2}$ and $q = \frac{5}{2}$ (top left), and $p = -1$ and $q = 4$ (top right). The figure demonstrates the process of contour enhancement through the dynamic behaviour of the intensity function $u(x,t)$. It is evident that $u$ remains continuous across the two delimiting curves $l(t)$ and $r(t)$, which define the boundaries of the transition region. However, the spatial derivative $u_x$ exhibits a significant discontinuity, characterised by an infinite jump at these boundaries. This behaviour is

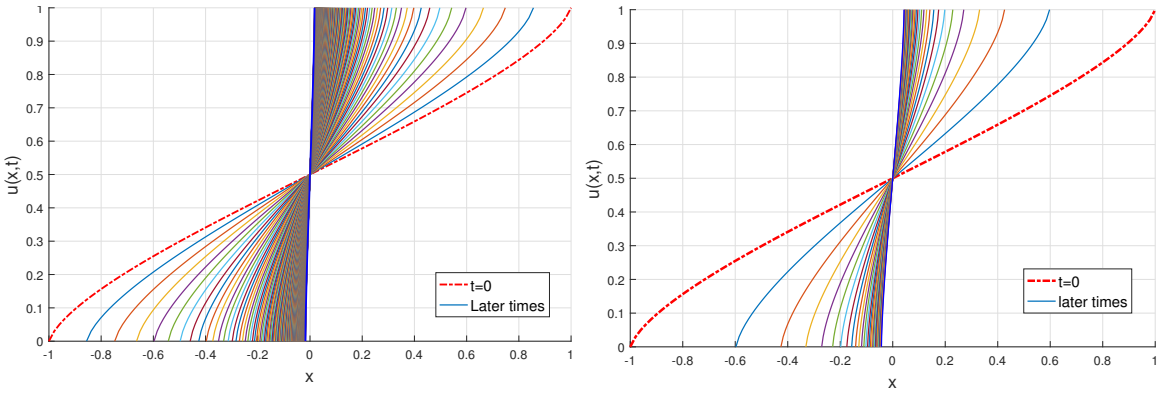


Figure 3.1: The evolution of the image intensity distribution $u(x,t)$. Top left: for $p=\frac{1}{2}$ and $q=\frac{5}{2}$. Top right : for $p=-1$ and $q=4$.

a direct consequence of the narrowing transition region, which sharpens the intensity profile over time.

The intensity function $u(x,t)$ develops a steep gradient near the boundaries, ultimately forming a vertical front. This sharpening effect is indicative of contour enhancement, where the contrast between adjacent regions of the image becomes increasingly pronounced. The formation of this vertical front highlights the transition from an initially smooth intensity distribution to a more defined, step-like profile. This phenomenon is consistent with the theoretical predictions outlined in the preceding analysis, where the derivative $u_x$ grows unbounded as time progresses, leading to the observed enhancement.

### 3.1.2 Self-similar solution of type II

In contrast to Type I solutions, which exist globally in time, Type II solutions are only defined within a finite time interval $0<t<T$. This class of solutions arises under the parameter constraint: $1-p<q<2-p$, with $\quad p<1$.

Our objective is to derive and analyse the behaviour of these solutions, particularly their role in contour enhancement within the framework of the free-boundary problem.

To construct the self-similar profile $\phi(\xi)$, we rewrite the governing equation in terms of the similarity variable $\xi$, yielding the ordinary differential equation:

$$\frac{d\phi}{d\xi}=\left[\frac{\alpha\left(q+p\right)}{2\left(1-p\right)}\right]^{\frac{-1}{q+p}}C^{\frac{-2}{q+p}}\left[1-\left(\frac{\xi}{C}\right)^2\right]^{\frac{-1}{q+p}},\text{with }\ 1-p<q<2-p \tag{3.13}$$

where the parameter $C$ is a positive integration constant, and the domain of the self-similar variable is constrained as:

$$-C\leq\xi\leq C.$$

Here, the self-similar transformation is defined by $\xi=\frac{x-x_0}{a(t)}$, where $a(t)$ represents a time-dependent scaling factor that governs the evolution of the intensity profile over time. Consequently, the spa-

tial boundaries of the solution are given by:

$$x_0 - Ca(t) \leq x \leq x_0 + Ca(t).$$

This formulation establishes a free-boundary problem where the image intensity evolves within the dynamically shrinking boundary layer $l(t)$ and $r(t)$, such that: $l(t) = x_0 - Ca(t), \quad r(t) = x_0 + Ca(t)$. By applying the appropriate boundary conditions and integrating the self-similar equation, we impose: $\phi(-C) = 0, \quad \phi(C) = 1$. From this, we derive the self-similar profile explicitly as:

$$\phi(\xi) = \left[\frac{\alpha(q+p)}{2(1-p)}\right]^{\frac{-1}{q+p}} C^{\frac{q+p-2}{q+p}} \int_{-1}^{\frac{\xi}{C}} \left[1-\eta^2\right]^{\frac{-1}{q+p}} d\eta,$$

The parameter $C$ is determined by:

$$C = \left[\frac{\alpha(q+p)}{2(1-p)}\right]^{-\frac{1}{q+p-2}} \left[2\int_0^1 \left[1-\eta^2\right]^{\frac{-1}{q+p}} d\eta\right]^{\frac{-(q+p)}{q+p-2}},$$

The full solution, incorporating the scaling law, takes the form:

$$u(x,t) = \left[\frac{\alpha(q+p)}{2(1-p)}\right]^{\frac{-1}{q+p}} C^{\frac{q+p-2}{q+p}} \int_{-1}^{\frac{x-x_0}{Ca(t)}} \left[1-\eta^2\right]^{\frac{-1}{q+p}} d\eta, \tag{3.14}$$

This self-similar solution reveals a crucial characteristic: as time progresses, the width of the transition region determined by equation (3.9) continually shrinks, leading to a progressive sharpening of the solution.

One of the most significant findings from this analysis is that the spatial derivative of the solution, $u_x$, undergoes an infinite jump at the boundaries defined by $l(t)$ and $r(t)$. More precisely:

$$u_x \sim O\left((T-t)^{\frac{-1}{q+p-2}}\right) \quad \text{as} \quad t \to T.$$

This implies that the gradient of the solution becomes unbounded over time, which results in contour enhancement. As the support of the solution contracts, the intensity function remains continuous, but the transition between intensity levels becomes increasingly steep.

Thus, the Type II self-similar solution naturally amplifies contrast in image intensity, forming sharp contours as $t \to T$. This behaviour is particularly relevant in image processing applications, where retaining and enhancing structural features such as contours is crucial.

Unlike Type I solutions, which persist indefinitely, Type II solutions exist only for $0 < t < T$, terminating in a finite-time singularity. The solution evolves within a narrowing free-boundary layer, continuously sharpening as time progresses. The function $u(x,t)$ remains continuous, but its gradient, $u_x$, diverges at the boundaries, leading to strong intensity contrasts.

This study confirms that self-similar solutions of Type II provide a natural mechanism for contour formation and enhancement, governed by the nonlinear diffusion process embedded in the governing equation.

Figure 3.2 illustrates the self-similar solutions to the problem described in equation (2.23) for different values of the parameters $p$ and $q$, specifically under the conditions $1-p<q<2-p$ and $p<1$. As previously discussed, the solution evolves towards the formation of a vertical front within a finite time interval.

The left of Figure 3.2 depicts the evolution of the image intensity distribution $u(x,t)$ for the parameter values $p=\frac{1}{2}$ and $q=1$. The right of Figure shows the corresponding evolution for $p=-1$ and $q=\frac{5}{2}$. These plots demonstrate how the intensity distribution changes over time, leading to the development of sharp contour or contours within the image. As time progresses, the solutions exhibit a significant enhancement of contours. This is evidenced by the steepening of the intensity gradients, which forms well defined contour. The transition region, where the intensity changes rapidly, narrows over time. This narrowing indicates that the image contour are becoming sharper and more pronounced.

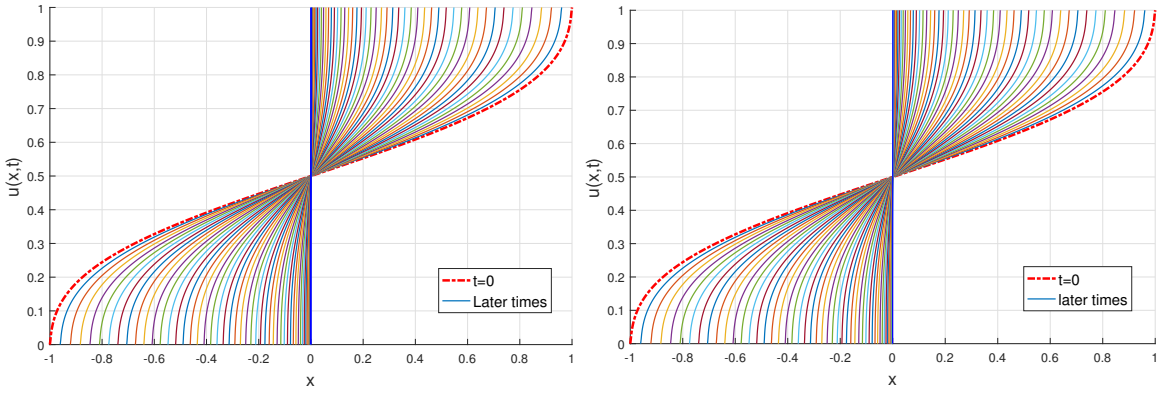


Figure 3.2: The evolution of the image intensity distribution $u(x,t)$. Top left : for value of $p=\frac{1}{2}$ and $q=1$. Top right : for value of $p=-1$, and $q=\frac{5}{2}$.

The behaviour of the solutions over time is characterised by the continuous intensification of the spatial derivative $u_x$. As $t$ approaches the finite time $T$, the gradient $u_x$ grows unboundedly, following the form $O\left((T-t)^{\frac{-1}{q+p-2}}\right)$. This unbounded growth signifies that the contour within the image are becoming increasingly sharp.

At the boundaries defined by $l(t)$ and $r(t)$, the intensity function $u$ remains continuous. However, the first derivative $u_x$ experiences an infinite jump at these boundaries. This discontinuity in the derivative is a key feature of the solution, indicating the presence of sharp transitions in the image intensity. As time progresses, this jump becomes more pronounced, further emphasising the sharpness of the contour.

### 3.1.3 Self-similar solution of type III

In this section, we explore the special case where $q=2-p$, with $p<1$. Under these conditions, we derive the self-similar solution of Type III. This solution is characterised by specific properties that

distinguish it from the previously discussed Type I and Type II solutions.

The profile $\phi$ for the Type III solution is governed by the following differential equation:

$$\frac{d\phi}{d\xi} = \frac{1}{\pi C}\left[1-\left(\frac{\xi}{C}\right)^2\right]^{\frac{-1}{2}}, \tag{3.15}$$

where $-C \le \xi \le C$. Here, $C$ is an arbitrary positive integration constant. This equation describes the rate of change of the profile $\phi$ with respect to the variable $\xi$.

To obtain the explicit form of the profile $\phi$, we integrate the above equation and apply the boundary conditions $\phi(-C) = 0$ and $\phi(C) = 1$. This integration yields the self-similar solution of Type III, which takes the form:

$$u(x,t) = \frac{1}{\pi}\arcsin\left(\frac{x-x_0}{Ca(t)}\right) + \frac{1}{2}.$$

This expression represents the image intensity distribution $u(x,t)$ as a function of spatial variable $x$ and time $t$.

The gradient of the image intensity, denoted by $u_x$, is given by:

$$u_x = e^{(1-p)\pi^2 t}\frac{1}{\pi C}\left[1-\left(\frac{x-x_0}{Ca(t)}\right)^2\right]^{\frac{-1}{2}}.$$

This equation indicates that the gradient $u_x$ grows exponentially as time $t$ increases. Specifically, for $q = 2-p$, the gradient blows up exponentially as $t \to \infty$. This exponential growth signifies a significant enhancement in the gradient over time.

The width of the transition region, defined as $r(t) - l(t)$, exhibits a decreasing trend over time. This reduction in width is indicative of the shrinking support of the solution. As the transition region narrows, the spatial gradient $u_x$ intensifies, leading to the phenomenon of gradient enhancement. In this case, the phenomenon of contour enhancement is observed. The solutions evolution results in forming a vertical front, where the image intensity $u(x,t)$ remains continuous at the free boundaries. However, the gradient $u_x$ increases significantly over time, leading to the sharpening of contour within the image. This enhancement becomes more pronounced after a larger time interval, as the gradient continues to grow exponentially.

Figure 3.3 illustrates the evolution of the image intensity distribution $u(x,t)$ for two distinct values of the parameter $p$: $p = \frac{1}{2}$ ( left) and $p = -1$ ( right). This figure provides a visual representation of the self-similar solution of Type III, particularly highlighting the phenomenon of contour enhancement and the behaviour of the solution over time.

The plots in Figure 3.3 demonstrate how the image intensity distribution $u(x,t)$ evolves as time progresses. For both values of $p$, the solution exhibits a clear trend towards the formation of a vertical front. This vertical front represents a sharp transition in the image intensity, which becomes more pronounced as time increases. The evolution towards this front is a key characteristic of the Type III self-similar solution.

The first derivative of the image intensity, $u_x$, plays a crucial role in understanding the contour enhancement phenomenon. As shown in the figure, the gradient $u_x$ intensifies over time, particularly near the boundaries of the transition region. This intensification is a direct consequence of the exponential growth of $u_x$.
The exponential term $e^{(1-p)\pi^2 t}$ indicates that the gradient grows rapidly as time $t$ increases, leading to a significant enhancement in the sharpness of the contours.

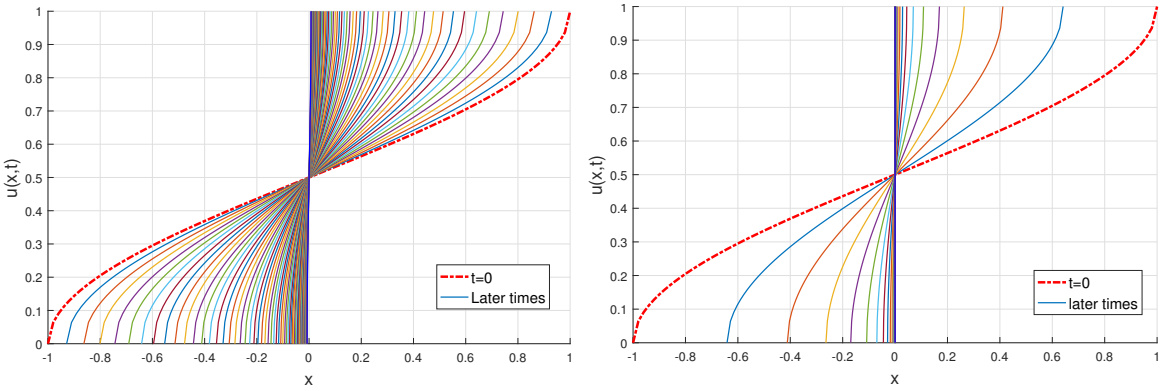


Figure 3.3: The evolution of the image intensity distribution $u(x,t)$. Top left : for value of $p = \frac{1}{2}$. Top right : for value of $p = -1$.

The phenomenon of contour enhancement is clearly observed in Figure 3.3. As the solution evolves, the transition region where the intensity changes rapidly becomes narrower. This narrowing is accompanied by an increase in the gradient $u_x$, resulting in the formation of sharp contour within the image. The enhancement of these contour becomes more noticeable after a larger time interval, as the gradient continues to grow exponentially.

## 3.2 Simulation Results for 2-D Gray Level Images

We now want to examine the validity of the theoretical results presented in the preceding sections for image enhancement. We will perform some numerical experiments on different types of images, such as gray-scale, to demonstrate the interest and efficiency of the proposed model (2.5). We will examine the efficiency of our model by performing some numerical experiments with different image types for certain values of the parameters $p$ and $q$, which correspond to the cases presented in the solutions of type I, type II, and type III.
For the numerical solution of equation (2.6) it is necessary to discretize the operators involved in the continuous problem.

### Spatial discretization

In the context of spatial discretisation, it is essential to approximate the first-order partial derivatives with respect to $x$ and $y$, alongside the second-order partial derivatives in both directions, as

well as the mixed second-order derivative with respect to $x$ and $y$. In the subsequent analysis, classical finite difference methods will be employed to approximate these derivatives. When discretising the first derivative of the intensity function $u$ with respect to $x$, several finite difference schemes are available. These schemes can be selected based on the specific requirements of the numerical method, with options including both centred and decentered (biased) finite difference approximations. The following section presents these schemes in detail, highlighting their respective properties and applications.

$$\frac{\partial u}{\partial x} \approx \begin{cases} \frac{u(x,y)-u(x-h_x,y)}{h_x} + O(h_x) \\ \frac{u(x+h_x,y)-u(x,y)}{h_x(x)} + O(h_x) \\ \frac{u(x+h_x,y)-u(x-h_x,y)}{2h_x} + O(h_x^2) \end{cases}$$

Here, $h_x$ denotes the spatial discretisation step along the $x$-axis. It is important to note that the first two finite difference schemes are decentered (or biased), while the final scheme is centred. Although the decentered schemes generally offer lower accuracy compared to the centred scheme, they can be particularly advantageous in scenarios involving boundary layers, where numerical stability and handling of sharp gradients are critical.

Similarly, for approximating the first derivative with respect to $y$, equivalent finite difference schemes can be derived. However, these will not be detailed in this context, as the approach follows the same principles outlined for the $x$-direction.

When approximating the second-order derivative $\frac{\partial^2 u}{\partial x^2}$ using classical finite difference methods, we adopt the well-established three-point central difference scheme. This approach is widely recognised for its balance between computational efficiency and accuracy in representing second-order derivatives.

$$\frac{\partial^2 u}{\partial x^2} \approx \frac{u(x+h_x,y) - 2u(x,y) + u(x-h_x,y)}{h_x^2} + O(h_x^2)$$

note that $\frac{\partial^2 u}{\partial y^2}$ is approximated accordingly. Lastly for the second cross derivative $\frac{\partial^2 u}{\partial x \partial y}$ with respect to $x$ and $y$, we can consider one of the following approximations

$$\begin{aligned} \frac{\partial^2 u}{\partial x \partial y} \approx & \frac{u(x+h_x,y+h_y) - u(x-h_x,y-h_y)}{2h_x h_y} \\ & + \frac{2u(x,y) - u(x+h_x,y) - u(x-h_x,y)}{2h_x h_y} \\ & - \frac{u(x,y+h_y) + u(x,y-h_y)}{2h_x h_y} + O(h_x h_y) \end{aligned}$$

or else a simpler approximation formula

$$\begin{aligned} \frac{\partial^2 u}{\partial x \partial y} \approx & \frac{u(x-h_x,y-h_y) - u(x-h_x,y+h_y)}{4h_x h_y} \\ & - \frac{u(x+h_x,y-h_y) - u(x+h_x,y+h_y)}{4h_x h_y} + O\left(h_x^2 h_y^2\right) \end{aligned}$$

Let $A$ denote the spatial discretisation matrix corresponding to problem (2.6). It is important to note that, due to the presence of homogeneous Neumann boundary conditions, the discretisation scheme can be readily simplified for grid points located near the boundary. This simplification arises from the fact that the intensity value at a boundary-adjacent grid point is equivalent to the intensity values at the neighbouring grid nodes situated on the boundary. By incorporating this condition, the discretisation scheme can be adjusted in a straightforward manner, thereby reducing computational complexity while preserving accuracy.

### Time discretization

For the temporal discretisation of problem (2.6), several approaches can be considered. These include the explicit time-marching scheme, the implicit time-marching scheme, or a semi-implicit scheme, which often proves to be more practical and convenient to implement. Each method presents distinct advantages in terms of stability, computational efficiency, and ease of implementation, depending on the specific characteristics of the problem at hand.

### Explicit time marching scheme

The solution of the time-dependent problem (2.6) using an explicit time-marching scheme is defined by the following formulation:

$$\frac{U^{q+1}-U^{q}}{dt}+A^{q}U^{q}=0, \quad q=1,2,\dots$$

In this context, $dt$ represents the discretisation step with respect to time. The previously described scheme can also be formulated inductively, which allows for a more systematic approach to the time-stepping process. This inductive form can be particularly useful for deriving the solution iteratively over discrete time intervals, facilitating the analysis and computation of the time-dependent problem in a structured manner. The formulation in an inductive style is as follows:

$$U^{q+1}=\left(Id-dt.A^{q}\right)U^{q}, \quad q=1,2,\dots$$

where $Id$ represents the identity matrix. However, it is well-established that the explicit time-marching scheme necessitates a stability condition to ensure the accuracy and reliability of the solution. This stability condition can be derived using the Von Neumann stability analysis, also known as Fourier analysis, which is a standard method for examining the stability of numerical schemes. By applying this analysis, one can obtain a condition for stability, typically expressed as follows:

$$dt<dt_{0}$$

where $dt_0$ is a given threshold.

### Implicit time marching scheme

In this approach, the temporal evolution of the system is computed iteratively by discretising the time variable. Unlike explicit methods, the implicit scheme involves solving a system of algebraic equations at each time step. This method is advantageous in terms of stability, as it does not impose the stringent stability conditions typically required by explicit schemes.
The solution to the time-dependent problem (2.6) using an implicit time-marching scheme is formulated as follows:

$$\left(Id + dt \cdot A^{q+1}\right) U^{q+1} = U^q, \quad q = 1, 2, \ldots$$

Note that at each time step, we have to solve a nonlinear algebraic system since in the implicit time discretization the components of the unknowns $U^{q+1}$ are involved in the entries of the matrix $A^{q+1}$. Such nonlinear problem can be solved by the iterative Newton method; but there is no assurance that this iterative method will converge since the entries of the matrix $A^{q+1}$ depend on the components of the unknown vector and, consequently, it is difficult to study the behaviour of this method. This is why for this kind of problem we prefer to use semi-implicit time marching methods where we use the components $U^q$ computed at the previous time step, in particular for the non-linearities that occur at the denominator of the problem (2.6).

### Semi-implicit time marching scheme

In this approach, the time-stepping method combines elements of both explicit and implicit schemes, striking a balance between computational efficiency and stability. The semi-implicit scheme typically involves updating some terms using explicit discretisation, while others are handled implicitly. This mixed method enables the scheme to achieve improved stability compared to purely explicit methods, particularly for stiff problems, while maintaining a lower computational cost compared to fully implicit methods.
The semi-implicit time-marching scheme is defined as follows:

$$\left(Id + dt.A^q\right) U^{q+1} = U^q, \quad q = 1, 2, \ldots$$

The matrix $A^q$ is computed as previously described, utilising the components of $U^q$ to evaluate the square of the second derivatives with respect to both $x$ and $y$, as well as the denominator and the product $u_x \cdot u_y$, which is the coefficient of $u_{xy}$. Consequently, at each time step, we must solve a large, sparse algebraic system, where the matrix $\left(Id + dt \cdot A^q\right)$ is irreducible and strictly diagonally dominant, thereby ensuring its invertibility. This system can be efficiently solved using an iterative method such as the Gauss-Seidel method, which, due to the aforementioned properties of the

matrix, guarantees convergence. Furthermore, by applying the Von-Neumann stability analysis once more, we can demonstrate that the semi-implicit time-marching scheme is unconditionally stable.

In contrast to the explicit scheme, the semi-implicit time-marching scheme will be the preferred method for numerical implementation. This preference arises primarily from the computational advantages it offers. The semi-implicit scheme strikes a balance between the stability of implicit methods and the efficiency of explicit ones. By handling some terms implicitly and others explicitly, it allows for larger time steps without compromising stability, making it particularly advantageous for problems that involve stiff equations or rapidly varying solutions. This combined approach enhances the overall efficiency and robustness of the numerical solution, making it a more suitable choice for the problem at hand.

## 3.3 Numerical experiments and discussion

We will now present numerical examples to demonstrate the behaviour of the equation in two dimensions, and compare them with the reduced equation in 1-D for different values of $q$ and $p$. The figures 3.4, 3.5, and 3.7 to 3.6 illustrate the evolution of image intensity distributions in both one-dimensional (1-D) and two-dimensional (2-D) contexts, related to the contour enhancement phenomenon governed by the generalization of mean curvature motion in (2.6).

This equation describes how the image intensity $u$ evolves over time $t$, with $p$ and $q$ being parameters that influence the contour enhancement process.

Figure 3.4: Case $1-p<q<2-p$ (Type II)

- 1-D Evolution: The first row demonstrates the evolution of the intensity distribution in one dimension. Over time, the domain contracts, and the first derivative diminishes, leading to sharper contours. This behavior is characteristic of contour enhancement, where the intensity function evolves to highlight boundaries more distinctly.

- 2-D Evolution: The second row shows the initial image and the results after 50, 100, and 200 iterations of filtering. The images exhibit progressive contour enhancement, with contours becoming more pronounced as the number of iterations increases.

Figure 3.5: Case $q=2-p$ (Type III)

- 1-D Evolution: In this scenario, the evolution in one dimension shows a balance between domain contraction and contours sharpening. The first derivative stabilizes, leading to a consistent enhancement of contours over time.

- 2-D Evolution: The filtered images after 50, 100, and 200 iterations reveal a steady improvement in contour clarity. The enhancement process is more uniform compared to Type II, with contours

becoming well-defined without excessive domain contraction.

Figure 3.6: Case $q > 2 - p$ (Type I)

- 1-D Evolution: Here, the domain contracts more rapidly, and the first derivative decreases significantly. This results in a more aggressive contour enhancement, where contours become very sharp, but the overall domain may shrink excessively.

- 2-D Evolution: The images filtered after 50, 100, and 200 iterations show a pronounced contour enhancement. However, the rapid domain contraction can lead to a loss of detail in regions away from the contours.

- Parameter $p$: Controls the diffusion rate. A higher $p$ value leads to slower diffusion, preserving contours better but potentially slowing down the enhancement process.

- Parameter $q$: Influences the ontour enhancement strength. A higher $q$ value results in more aggressive contour sharpening but may cause excessive domain contraction.

In summary, the interplay between $p$ and $q$ determines the balance between contour enhancement and domain preservation. The evolution of the intensity distribution in both 1-D and 2-D contexts demonstrates how these parameters affect the contour enhancement phenomenon over time, with each case (Type I, II, III) showcasing different characteristics in the enhancement process.

The proposed generalisation of mean curvature motion in (2.6) is a significant advancement in the study of contour enhancement phenomena. By incorporating the parameters $p$ and $q$, the equation offers a versatile and robust framework for controlling the contour enhancement process. The evolution of the intensity distribution, as demonstrated in the figures, underscores the effectiveness of this generalised equation in achieving precise and controlled contour enhancement over time.

Figures 3.7 to 3.11, illustrate the results of the application of equation (2.6) to 2-D gray level images. By comparing between the images, display the results obtained by using different values of parameters $p$ and $q$ for a large stopping time and the evolution of equation (2.9) corresponding.

In Figure 3.7 we can see that the linear filter has blurred contours after a number of steps. In contrast, in figure 3.7(a) dot-dash correspond the image original (initial condition), the width of the transition region $r(t) - l(t)$ which increases with time, this yields to blurred results at the contours of image.

A similar result with the linear case, for $q = 1 - p$, we see that in Figure 3.8 this yields to blurred results at the contours of image with large time.

On the other hand, Figures 3.4 to 3.6, shows the results of the application to the same test image. We see that the values of $q > 1 - p$ has done a superior job of preserving contours even for a larger stopping, leads to sharp contours and enhancement image. It also can be observed from the 1-D ,

the curves are parametrized by time, evolving with increasing $t$ towards the sharp front, the width of the transition region decreases with time, the spatial gradient of the solution $u_x$, increases with time, so the contour enhancement takes place.

Our numerical experience which is also confirm the self-similar approach is valid for the study of contour enhancement.

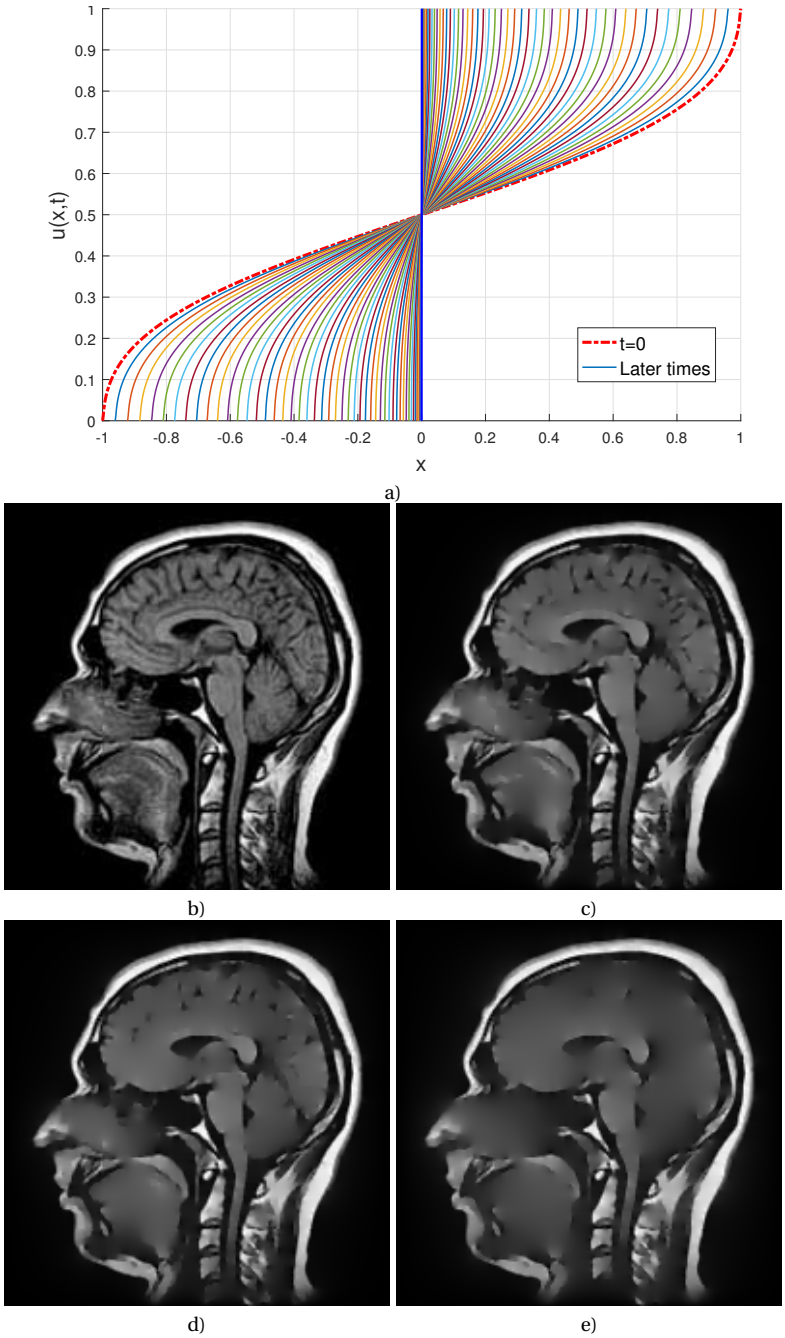


Figure 3.4: Comparison of the evolution of the image intensity distribution corresponding in 1-D i the case $1-p<q<2-p$ (type II), and the evolution of equation corresponding in 2-D (2.6). For $p=\frac{1}{2}$ and $q=1$, the first row the evolution in 1D. Second row shows the initial image and results with image filtred after (50,100,200) iteration.

## 3.4 Conclusion and comments

In this chapter, we explore self-similar solutions for a newly formulated free-boundary problem in (2.23). Our analysis focuses on addressing the free-boundary problem and investigating the behaviour of solutions, particularly in relation to image contour enhancement. By studying the dynamics of this equation, we aim to establish a connection between the mathematical properties of the solutions and their ability to preserve and enhance image contours. Additionally, we conduct numerical simulations to validate the theoretical findings. These simulations are performed on grayscale two-dimensional images to assess the effectiveness of the proposed model in real-world applications. The experimental results demonstrate the model's capability in maintaining and sharpening image contours, confirming the practical applicability of the theoretical insights. The results presented in this chapter are part of our research work published in [1].

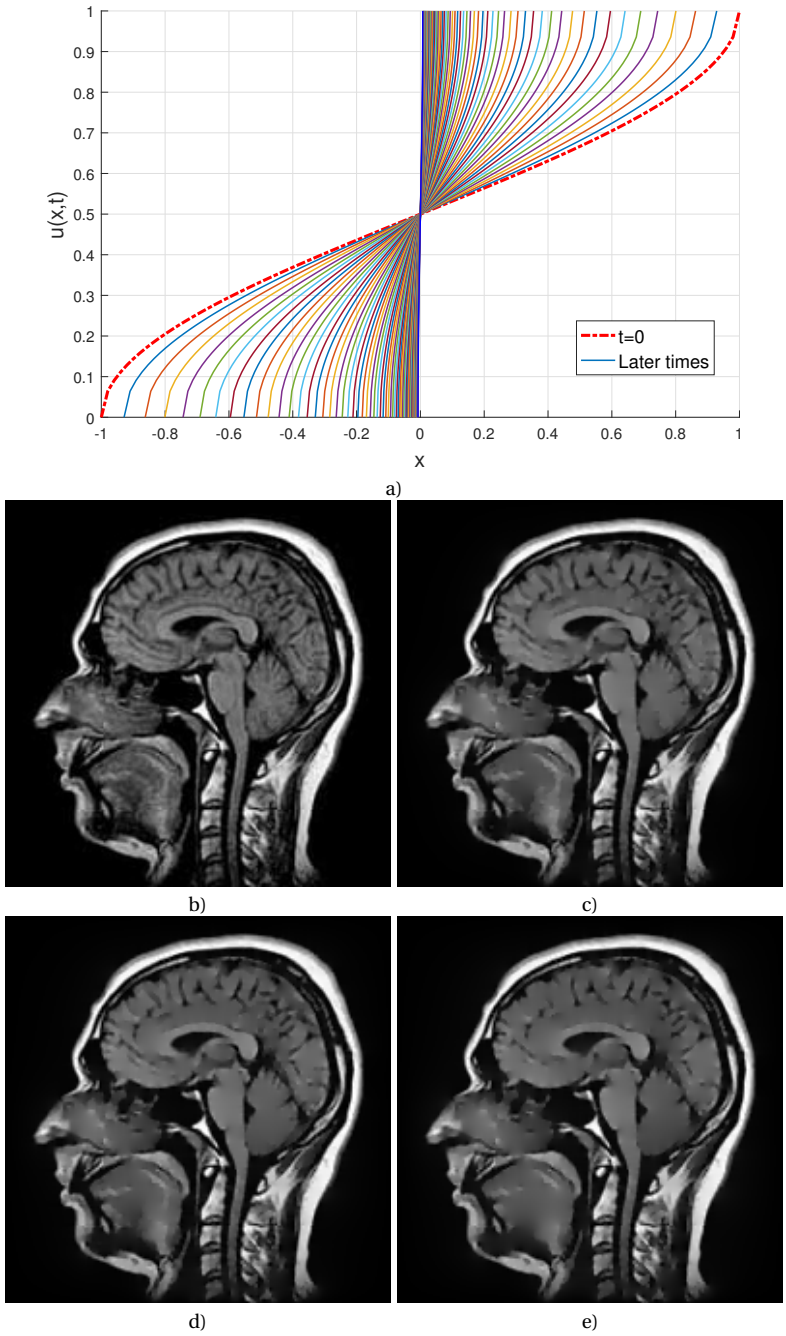


Figure 3.5: Comparison of the evolution of the image intensity distribution corresponding in 1-D in the case $q = 2 - p$ (type III), and the evolution of equation corresponding in 2-D (2.6). For $p = \frac{1}{2}$ and $q = \frac{3}{2}$, the first row the evolution in 1D. Second row shows the initial image and results with image filtred after (50,100,200) iteration.

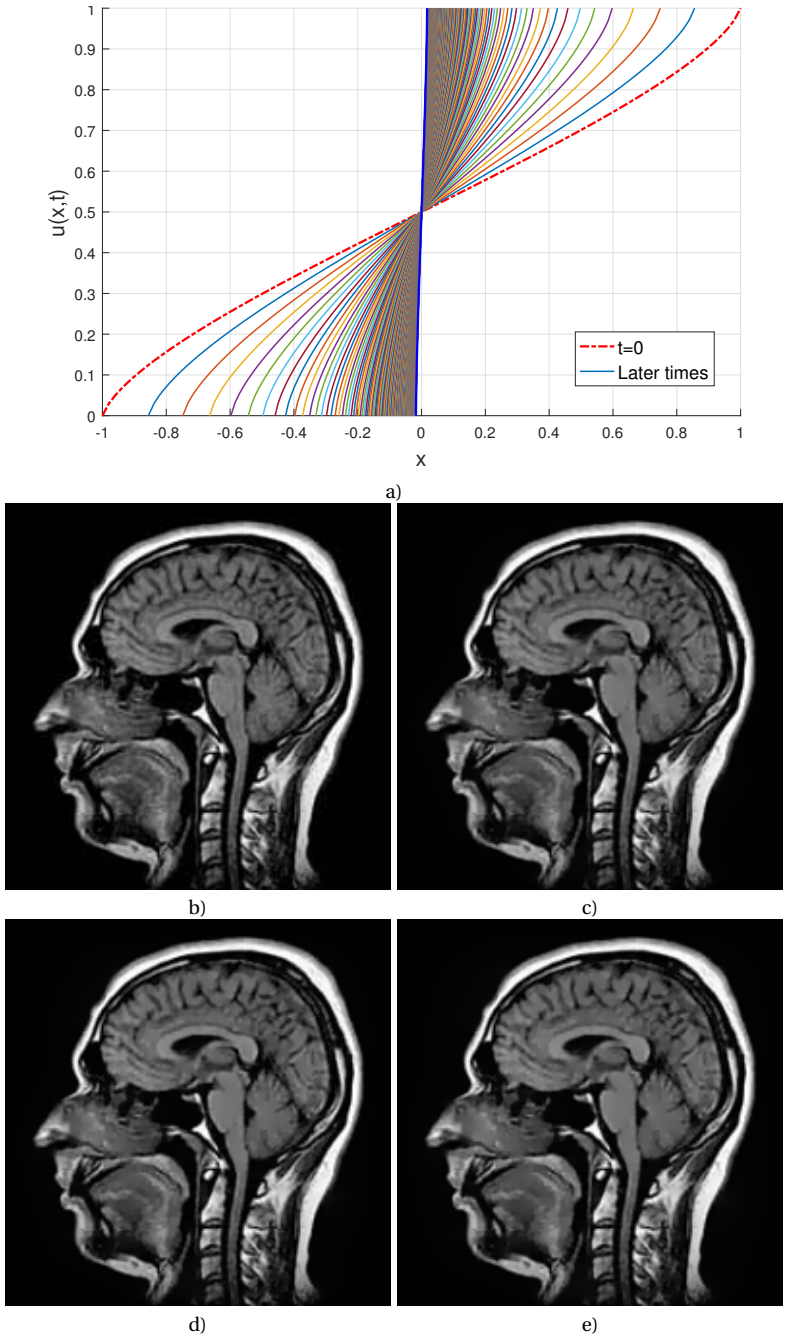


Figure 3.6: Comparison of the evolution of the image intensity distribution corresponding in 1-D in the case $q > 2 - p$ (type I), and the evolution of equation corresponding in 2-D (2.6). For $p = \frac{1}{2}$ and $q = \frac{5}{2}$, the first row the evolution in 1D. Second row shows the initial image and results with image filtred after (50,100,200) iteration.

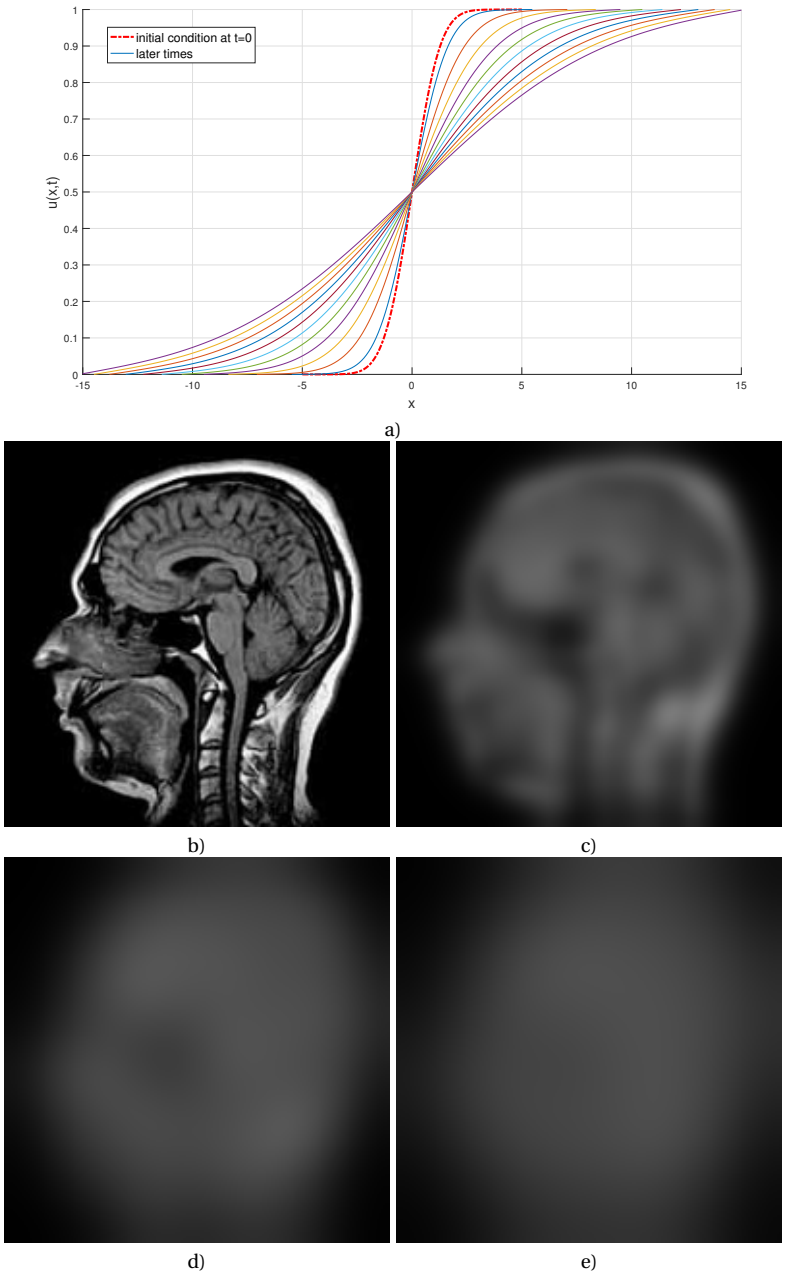


Figure 3.7: Comparison of the evolution of the image intensity distribution in 1-D (heat eqution) for $p = q = 0$, and the evolution of equation in 2-D (2.6). The first row corresponds the evolution of the image intensity in 1D. Second row shows the initial image and results with image filtred after (20,50,100) iteration, the resulting image is blurred.

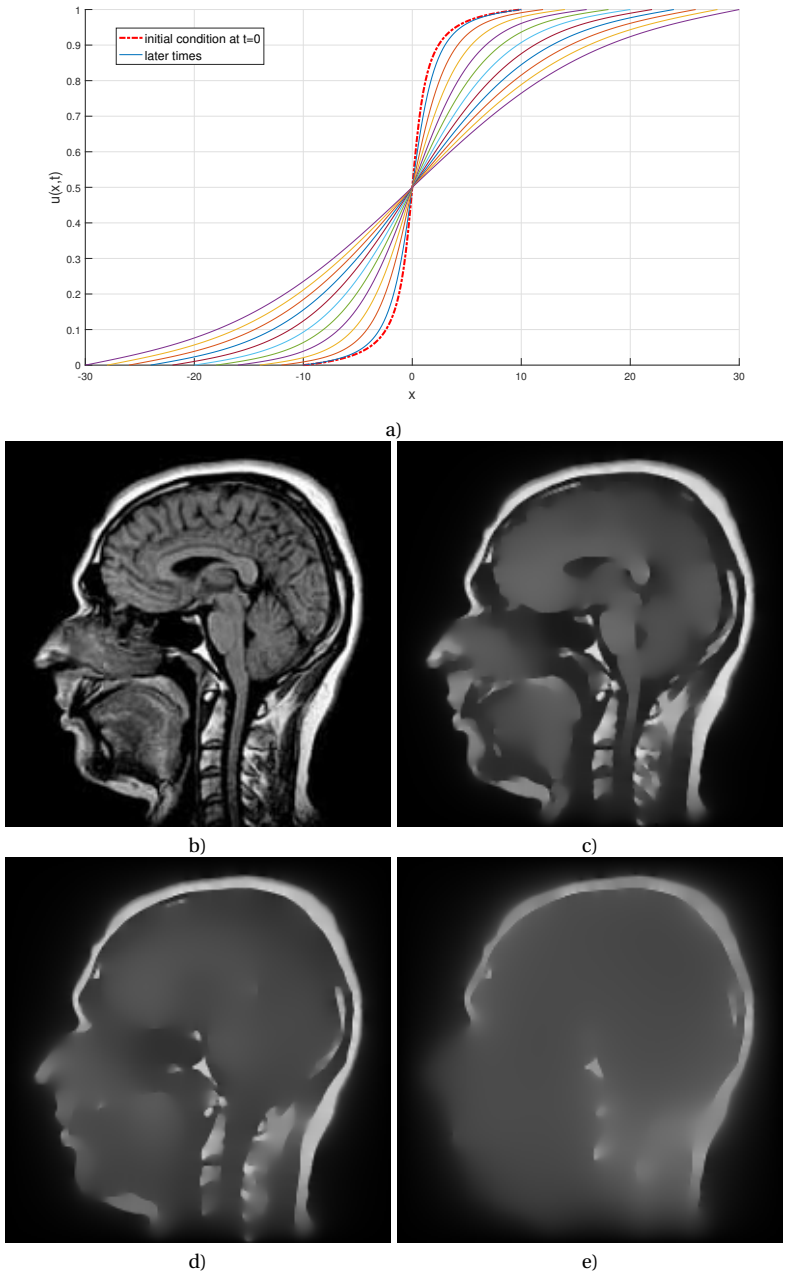


Figure 3.8: Comparison of the evolution of the image intensity for the special case $q = 1 - p$ in 1-D, and the evolution of equation corresponding in 2-D (2.6). For $p = \frac{1}{2}$ and $q = \frac{1}{2}$, the first row shows the evolutio in 1-D. Second row corresponds the initial image and results with image filtred after (50,100,200) iteration, the resulting image is blurred.

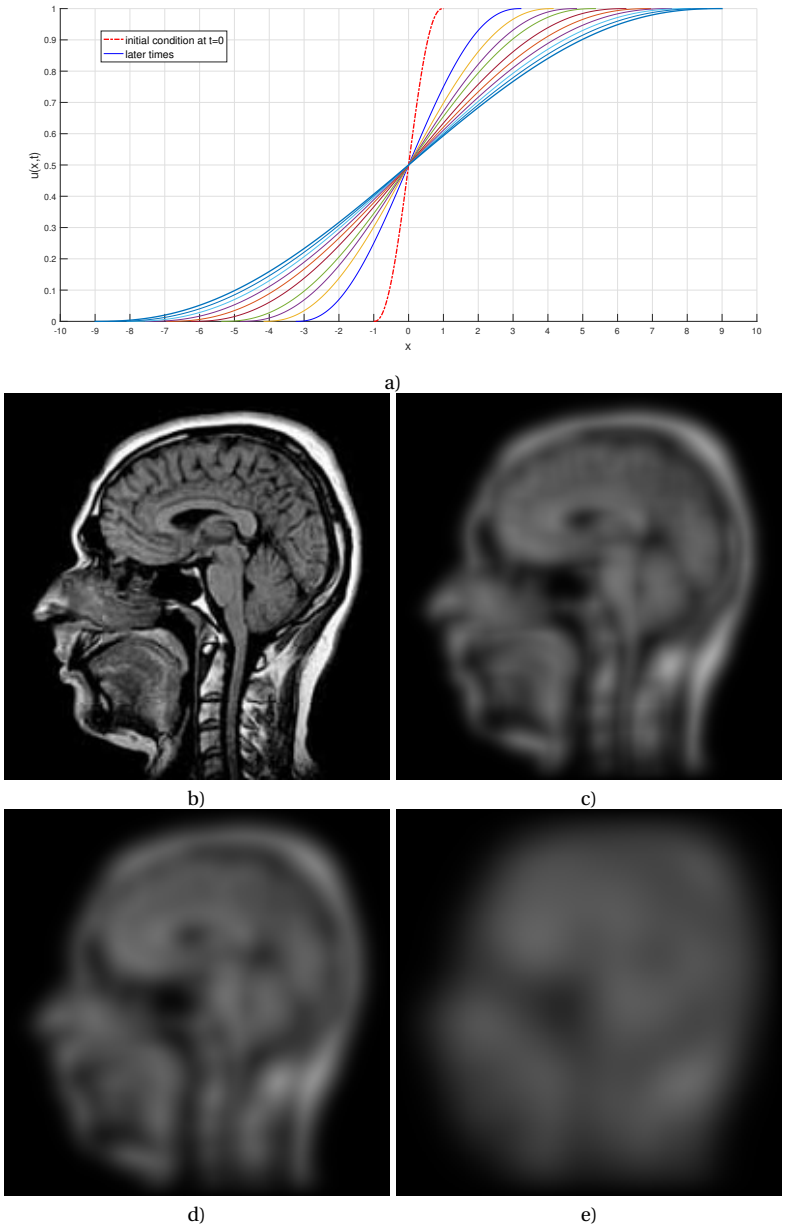


Figure 3.9: Comparison of the evolution of the image intensity for the special case $q < 1 - p$ in 1-D, and the evolution of equation corresponding in 2-D (2.6). For $p = 0$ and $q = \frac{-2}{3}$, the first row shows the evolutio in 1-D. Second row corresponds the initial image and results with image filtred after (5,20,50) iteration, the resulting image is blurred.

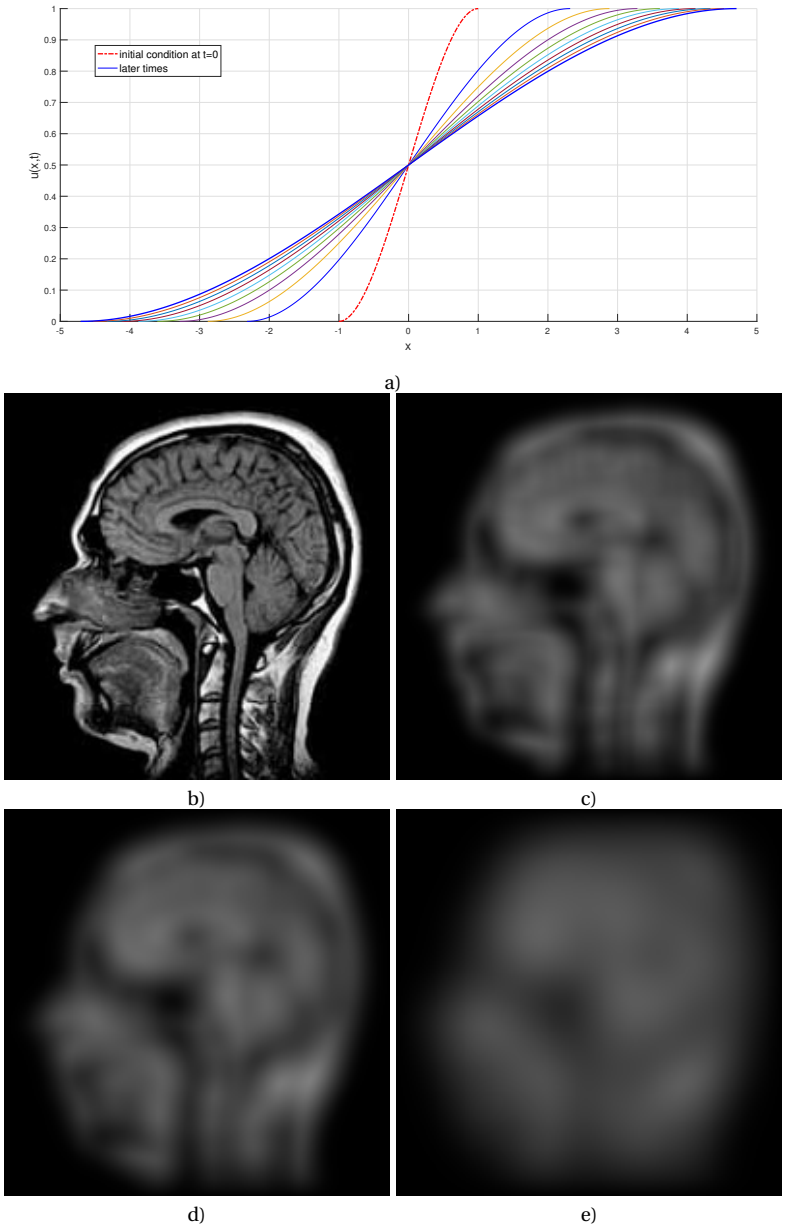


Figure 3.10: Comparison of the evolution of the image intensity for the special case $q < 1 - p$ in 1-D, and the evolution of equation corresponding in 2-D (2.6). For $p = 0$ and $q = -1$, the first row shows the evolutio in 1-D. Second row corresponds the initial image and results with image filtred after (5,20,50) iteration, the resulting image is blurred.

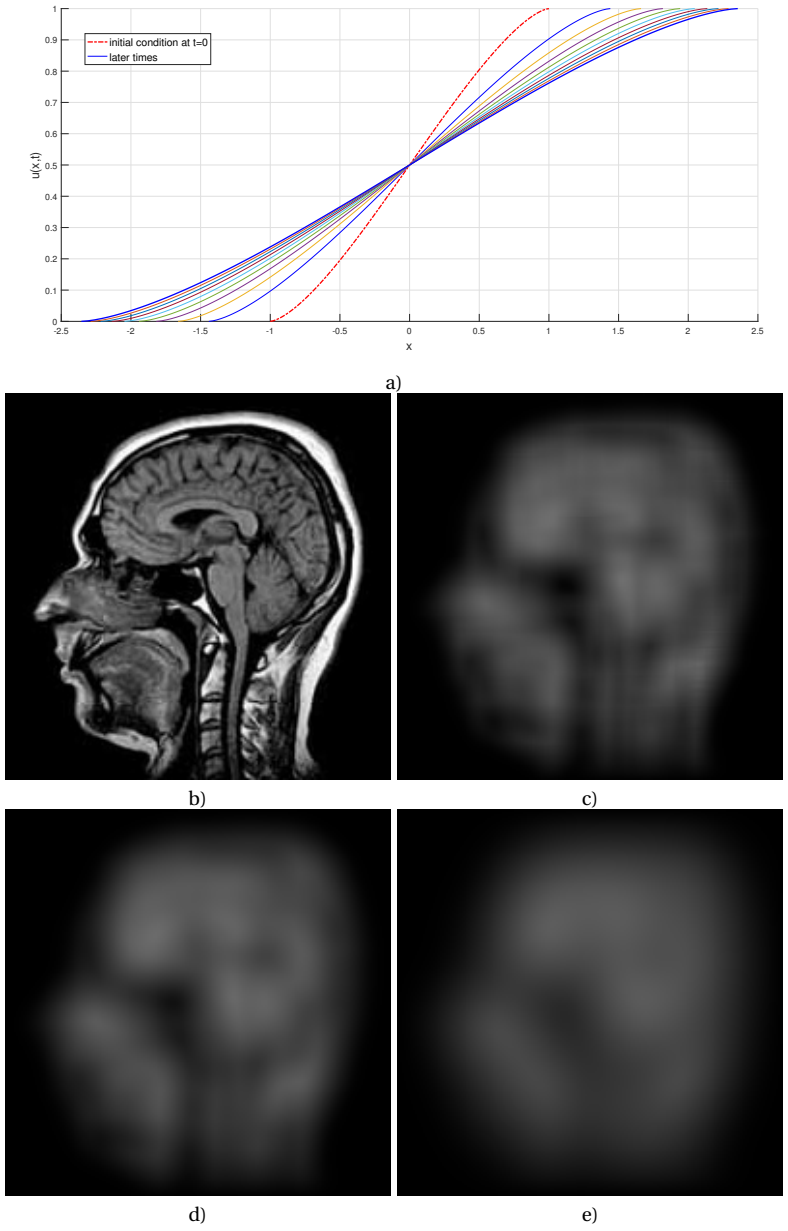


Figure 3.11: Comparison of the evolution of the image intensity for the special case $q < 1 - p$ in 1-D, and the evolution of equation corresponding in 2-D (2.6). For $p = 0$ and $q = -2$, the first row shows the evolutio in 1-D. Second row corresponds the initial image and results with image filtred after (5,20,50) iteration, the resulting image is blurred.

Chapter 4

# *Contour enhancement with inverse degenerate parabolic equation*

In this chapter, we consider a new model arising from the main problem is also addressed, it is related to the class of inverse problems with free boundaries. We present in this chapter an analysis on the improvement of the image contour and which could be interesting and a future contribution in the development of the so-called "Schock filter" models, which are very effective in the phenomenon of image restoration.

*Our model.* In a natural way we propose as a model the equation

$$\frac{\partial u}{\partial t} = (1-p)\,|u_x|^{-(q+p)}\,u_{xx}, \quad \text{for } p>1. \tag{4.1}$$

Gives the problem of shock filter. We present the solutions for (4.1) by using self-similar solutions according to the enhancement parameters of $p$ and $q$. Then we discus the asymptotics behaviours of these solutions, in order to illustrat the phenomenon of contour enhancement in image processing.

## 4.1 Self-Similar Solutions for Inverse Nonlinear Free Boundary and Boundary Value Problem

We get this type for $q \le 1-p$ and $p>1$. We present the subsequent boundary problem (2.23), for determining the evolution of image intensity within the boundary layer. We try now to solve problem by introducing the the self-similar solution written under the form (2.12).

We should first deduce the equation satisfied by the function $\phi$ used for the definition of self-similar solutions.

### 4.1.1 Contour Enhancement with a Nonlinear Boundary Value Problem

#### Case for $1-p \ge q > -p$

We aim to solve equation (2.23) using the self-similar solution method, where the solution is assumed to take the form (2.12). Substituting equation (2.12) into the original equation (2.23) leads

to a modified equation that is often more manageable analytically:

$$-\frac{\dot{a}}{a}\xi\frac{d\phi}{d\xi}=(1-p)\frac{1}{a^{-(q+p)+2}}\frac{d^2\phi}{d\xi^2}\left(\frac{d\phi}{d\xi}\right)^{-(q+p)},\ \text{for } 1-p\geq q>-p. \tag{4.2}$$

The separation of variables argument necessitates that the subsequent conditions are satisfied:

$$\frac{\dot{a}}{a}=-\alpha\frac{1}{a^{-(q+p)+2}}, \tag{4.3}$$

where $\alpha>0$ is arbitrary positif constant.

Easy integration gives:

$$a(t)=\left[\alpha(q+p-2)\,t+A_0\right]^{\frac{-1}{q+p-2}},\quad \text{for } 0<t<T.$$

where $A_0>0$, is a constant, and $T$ is obtained as

$$T=-\frac{A_0}{\alpha(q+p-2)}.$$

The equation for the profile $\phi$, becomes:

$$\alpha\xi\frac{d\phi}{d\xi}=(1-p)\frac{d^2\phi}{d\xi^2}\left(\frac{d\phi}{d\xi}\right)^{-(q+p)}. \tag{4.4}$$

After easy integration, we get:

$$\frac{d\phi}{d\xi}=\left[\frac{-\alpha(q+p)}{2(1-p)}\right]^{\frac{-1}{q+p}}C^{\frac{-2}{q+p}}\left[1+\left(\frac{\xi}{C}\right)^2\right]^{\frac{-1}{q+p}},\ \text{for } 1-p\geq q>-p, \tag{4.5}$$

where

$$-\infty\leq\xi\leq+\infty.$$

By using the boundary condition $\phi(-\infty)=0$, $\phi(+\infty)=1$, These conditions model a system where the solution transitions smoothly from one steady state to another, resembling a sharp interface or transition front. The problem is formulated on an unbounded domain, capturing the asymptotic behaviour of the solution as $\xi\to\pm\infty$.

we obtain, after integration:

$$\phi(\xi)=\left[\frac{-\alpha(q+p)}{2(1-p)}\right]^{\frac{-1}{q+p}}C^{\frac{q+p-2}{q+p}}\int_{-\infty}^{\frac{\xi}{C}}\left[1+\eta^2\right]^{\frac{-1}{q+p}}d\eta,$$

where

$$C=\left[\frac{-\alpha(q+p)}{2(1-p)}\right]^{-\frac{1}{q+p-2}}\left[2\int_0^{\infty}\left[1+\eta^2\right]^{\frac{-1}{q+p}}d\eta\right]^{\frac{-(q+p)}{q+p-2}},$$

Thus, we obtain self-similar solutions, with the form

$$u(x,t)=\left[\frac{-\alpha(q+p)}{2(1-p)}\right]^{\frac{-1}{q+p}}C^{\frac{q+p-2}{q+p}}\int_{-\infty}^{\frac{x-x_0}{Ca(t)}}\left[1+\eta^2\right]^{\frac{-1}{q+p}}d\eta. \tag{4.6}$$

The problem (4.6) has a solution in a self-similar form that exhibits a blow-up in finite time. The solution is established for all $t \in (0,T)$ ; where $T$ denotes the blow-up time of the solution such that:

$$\forall x \in \mathbb{R}_+,\ \lim_{t\to T^-} u(x,t) = +\infty \text{ and } \forall x \in \mathbb{R}_-,\ \lim_{t\to T^-} u(x,t) = -\infty$$

and

$$\forall x \in \mathbb{R},\ \lim_{t\to T^-} u_x(x,t) = +\infty$$

In this case, a token that the contour enhancement is taking place: Across the two delimiting curves $(l(t)\ ,\ r(t))$, the intensity function $u$ is continuous, but its derivative $u_x$ suffers an infinite jump. The spatial gradient of the solution $u_x$ increases with time and blows up like "$O\left((T-t)^{\frac{1}{q+p-2}}\right)$ " as $t \to T$, its support shrinks. This leads to sharp contours in the image.
In order to illustrate the utilization of the technique to obtain contour enhancement , we present the following examples.

***Exemple 1.*** $q+p=\frac{1}{2}$

In this case, The equation (4.5) for the profile $\phi$, can be written as :

$$\frac{d\phi}{d\xi} = \left[\frac{-\alpha}{4(1-p)}\right]^{-2} C^{-3}\left[1+\left(\frac{\xi}{C}\right)^2\right]^{-2}, \tag{4.7}$$

Further integration and using the boundary conditions $\phi(-\infty)=0$, $\phi(+\infty)=1$, then we obtain

$$\phi(\xi) = \frac{1}{\pi}\left[\arctan\left(\frac{\xi}{C}\right) + \frac{\xi}{C\left(\left(\frac{\xi}{C}\right)^2+1\right)} + \frac{\pi}{2}\right],$$

for

$$\xi \in \left]-\infty;+\infty\right[$$

where

$$C = \left(\frac{\pi}{2}\right)^{\frac{1}{3}}\left(\frac{4(1-p)}{\alpha}\right)^{\frac{2}{3}}$$

In this case, the self similar solutions of (4.7) assumes the form

$$u(x,t) = \frac{1}{\pi}\left[\arctan\left(\frac{x}{C(T-t)^{\frac{2}{3}}}\right) + \frac{x}{C(T-t)^{\frac{2}{3}}\left(\left(\frac{x}{C(T-t)^{\frac{2}{3}}}\right)^2+1\right)} + \frac{\pi}{2}\right],$$

The gradients are given by

$$u_x(x,t) = \frac{36}{(18\pi)^{\frac{4}{3}}}\left[1+\left(\frac{x}{C(T-t)^{\frac{2}{3}}}\right)^2\right]^{-2},$$

The solution is established for all $t \in (0, T)$ ; where $T$ represents the blow-up time of the solution such that:

$$\forall x \in \mathbb{R}_+, \lim_{t \to T^-} u(x,t) = +\infty \text{ and } \forall x \in \mathbb{R}_-, \lim_{t \to T^-} u(x,t) = -\infty$$

and

$$\forall x \in \mathbb{R}, \lim_{t \to T^-} u_x(x,t) = +\infty$$

The contour enhancement by evolution of image intensity function $u(x,t)$ illustrated in the Figure 4.1, It is seen that the intensity function $u$ is continuous over the two delimiting curves; nevertheless, its derivative $u_x$ suffers an infinite jump. Moreover, the evolution arrives at a vertical front, so the enhancement happens.

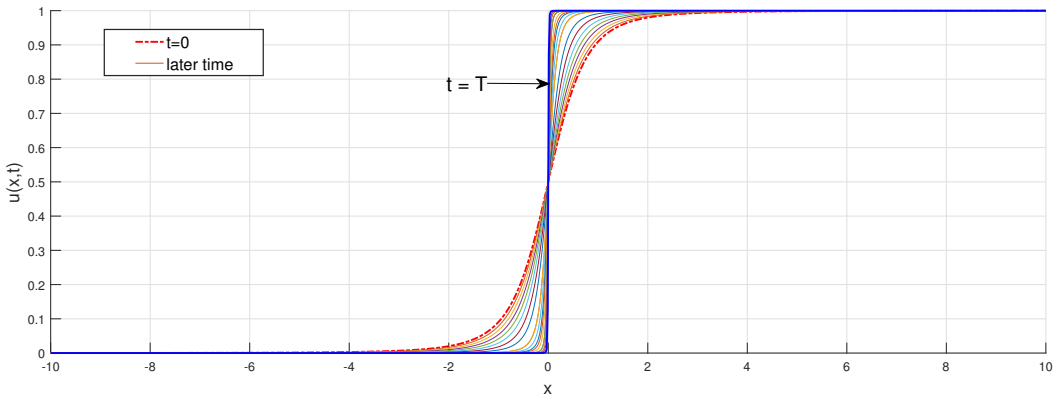


Figure 4.1: The evolution of the image intensity distribution $u(x,t)$. For value of $p = 2$ and $q = -\frac{3}{2}$.

***Exemple 2*** $q + p = \frac{2}{3}$

In this case, The equation (4.5) for the profile $\phi$, can be written as:

$$\frac{d\phi}{d\xi} = \left[\frac{-\alpha}{3(1-p)}\right]^{-\frac{3}{2}} C^{-3} \left[1 + \left(\frac{\xi}{C}\right)^2\right]^{-\frac{3}{2}}, \tag{4.8}$$

Additional integration applying the boundary constraints. $\phi(-\infty) = 0$, $\phi(+\infty) = 1$, then we obtain

$$\phi(\xi) = \frac{1}{2}\left[\frac{\xi}{\left(\left(\frac{\xi}{C}\right)^2 + 1\right)^{\frac{1}{2}}} + 1\right],$$

for

$$\xi \in ]-\infty; +\infty[$$

where

$$C = \sqrt{2}\left(\frac{3(p-1)}{\alpha}\right)^{\frac{4}{3}}$$

In this case, the self similar solutions of (4.8) assumes the form

$$u(x,t)=\frac{1}{2}\left[\frac{x}{C(T-t)^{\frac{3}{4}}\left(\left(\frac{x}{C(T-t)^{\frac{3}{4}}}\right)^{2}+1\right)^{\frac{1}{2}}}+1\right],$$

The solution is established for all $t\in(0,T)$ ; where $T$ represents the blow-up time of the solution such that:

$$\forall x\in\mathbb{R}_{+},\ \lim_{t\to T^{-}}u(x,t)=+\infty \text{ and } \forall x\in\mathbb{R}_{-},\ \lim_{t\to T^{-}}u(x,t)=-\infty$$

and

$$\forall x\in\mathbb{R},\ \lim_{t\to T^{-}}u_{x}(x,t)=+\infty$$

in the Figure 4.2, It is seen that the intensity function $u$ is continuous over the two delimiting curves; nevertheless, its derivative $u_x$ suffers an infinite jump. Moreover, the evolution arrives at a vertical front, so the enhancement happens.

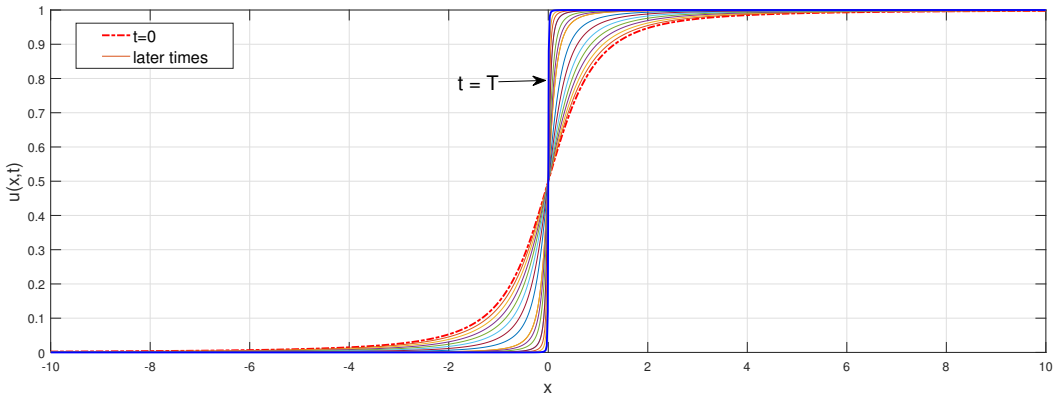


Figure 4.2: The evolution of the image intensity distribution $u(x,t)$. For value of $p=2$ and $q=-\frac{4}{3}$.

**The Case $q=-p$**

The equation (4.1) becomes

$$u_{t}(x,t)=-u_{xx}. \tag{4.9}$$

In this case, The equation (4.9) for the profile $\phi$, can be written as:

$$\frac{d\phi}{d\xi}=ke^{-\frac{\xi^{2}}{4}} \quad \text{, with } k \text{ is an integral constant.} \tag{4.10}$$

Subsequent integration and the application of the boundary conditions $\phi(-\infty)=0$, $\phi(+\infty)=1$, then we obtain

$$\phi(\xi)=\frac{1}{2}\left[erf\left(\frac{\xi}{2}\right)+1\right] \tag{4.11}$$

for

$$-\infty<\xi<+\infty.$$

The self-similar solution assume the form

$$u(x,t) = \frac{1}{2}\left[erf\left(\frac{x}{2(T-t)^{\frac{1}{2}}}\right)+1\right].$$

where

$$k = \frac{1}{2\sqrt{\pi}}$$

The gradients are given by

$$u_x(x,t) = \frac{1}{2\sqrt{\pi}} e^{-\frac{x^2}{4(T-t)}},$$

The solution is established for all $t \in (0,T)$ ; where $T$ represents the blow-up time of the solution such that:

$$\forall x \in \mathbb{R}_+, \lim_{t\to T^-} u(x,t) = +\infty \text{ and } \forall x \in \mathbb{R}_-, \lim_{t\to T^-} u(x,t) = -\infty$$

and

$$\forall x \in \mathbb{R}, \lim_{t\to T^-} u_x(x,t) = +\infty$$

The figure 4.3 illustrates the evolution of the solution $u(x,t)$ governed by the backward diffusion equation: Unlike the standard heat equation, this ill-posed equation leads to the enhancement of gradients over time instead of smoothing them. This results in the amplification of small differences, creating sharper transitions as $t$ increases.

At the initial time $t = 0$ (shown with the red dashed curve), the solution displays a smooth gradient. However, as time progresses, the curvature of the solution intensifies near the origin $x = 0$, reflecting the reverse diffusive process.

At the critical time $t = T$, the first derivative of the solution which represents the gradient terminates abruptly. This indicates the formation of a sharp interface where the gradient becomes discontinuous, a phenomenon known as gradient catastrophe or shock-like formation.

The final profile at $t = T$ resembles a step function, where the transition between states is nearly discontinuous. This behaviour mirrors shock wave formation in fluid dynamics, though here it emerges from the mathematical instability inherent in the backward diffusion process rather than physical discontinuities.

In the Figure 4.3, It is seen that the intensity function $u$ is continuous over the two delimiting curves; nevertheless, its derivative $u_x$ suffers an infinite jump. Moreover, the evolution arrives at a vertical front, so the enhancement happens.

### 4.1.2 Contour Enhancement with a Nonlinear Free-Boundary Value Problem

In this study, we aim to investigate the given differential equation for the parameter range $q < -p$. The primary objective of this investigation is to explore the mathematical properties of the

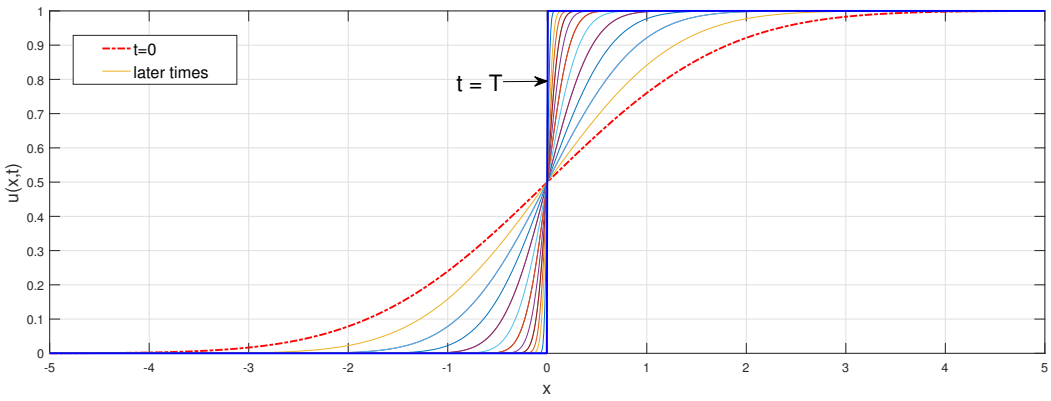


Figure 4.3: The evolution of the image intensity distribution $u(x,t)$. For value of $p=2$ and $q=-2$.

equation under these conditions and to assess its significance in the context of image contour enhancement. We get this type for $q<-p$ and $p>1$. We present the subsequent free boundary problem (2.23), for determining the evolution of image intensity within the boundary layer.

We aim to solve equation (2.23) for $q<-p$ and $p>1$, using the self-similar solution method, where the solution is assumed to take the form (2.12). Substituting equation (2.12) into the original equation (2.23) leads to a modified equation that is often more manageable analytically, we obtain, the equation:

$$-\frac{\dot{a}}{a}\xi\frac{d\phi}{d\xi}=(1-p)\frac{1}{a^{-(q+p)+2}}\frac{d^2\phi}{d\xi^2}\left(\frac{d\phi}{d\xi}\right)^{-(q+p)},\quad \text{for } q<-p \text{and} p>1. \tag{4.12}$$

The argument of separation of variables necessitates that the subsequent conditions be satisfied:

$$\frac{\dot{a}}{a}=-\alpha\frac{1}{a^{-(q+p)+2}}\ , \tag{4.13}$$

where $\alpha$ is arbitrary positive constant.

The equation for the profile $\phi$, becomes:

$$\alpha\xi\frac{d\phi}{d\xi}=(1-p)\frac{d^2\phi}{d\xi^2}\left(\frac{d\phi}{d\xi}\right)^{-(q+p)}.$$

After easy integration, we get:

$$\frac{d\phi}{d\xi}=\left[\frac{\alpha(q+p)}{2(1-p)}\right]^{\frac{-1}{q+p}}C^{\frac{-2}{q+p}}\left[1-\left(\frac{\xi}{C}\right)^2\right]^{\frac{-1}{q+p}}, \tag{4.14}$$

for

$$-C\le\xi\le C.$$

Here, $C$ is a positive integration constant. For $\xi=\frac{x-x_0}{a(t)}$, we have:

$$x_0-Ca(t)\le x\le x_0+Ca(t).$$

The problem (4.12) suggests a free-boundary problem specifically to determine the evolution of the image intensity in the boundary layer $l(t)$ and $r(t)$ such that $l(t) \le x \le r(t)$, with $l(t) = x_0 - Ca(t)$ and $r(t) = x_0 + Ca(t)$.

The resolution of (4.13) gives,

$$a(t) = \left[\alpha\left(q+p-2\right)t + A_0\right]^{\frac{-1}{q+p-2}}, \quad \text{for } 0 < t < T \quad \text{if } q < -p \text{and} p > 1, \tag{4.15}$$

where $A_0 > 0$, is a constant, and $T$ is obtained as

$$T = -\frac{A_0}{\alpha\left(q+p-2\right)}.$$

Furthermore, by integrating equation (4.14) and applying the appropriate boundary conditions, we can derive the following results: $\phi(-C) = 0$ and $\phi(C) = 1$. This leads to the subsequent solution:

$$\phi(\xi) = \left[\frac{\alpha\left(q+p\right)}{2\left(1-p\right)}\right]^{\frac{-1}{q+p}} C^{\frac{q+p-2}{q+p}} \int_{-1}^{\frac{\xi}{C}} \left[1-\eta^2\right]^{\frac{-1}{q+p}} d\eta,$$

where

$$C = \left[\frac{\alpha\left(q+p\right)}{2\left(1-p\right)}\right]^{-\frac{1}{q+p-2}} \left[2\int_0^1 \left[1-\eta^2\right]^{\frac{-1}{q+p}} d\eta\right]^{\frac{-(q+p)}{q+p-2}},$$

for $q \neq 2-p$.

The self-similar solution takes the following form

$$u(x,t) = \left[\frac{\alpha\left(q+p\right)}{2\left(1-p\right)}\right]^{\frac{-1}{q+p}} C^{\frac{q+p-2}{q+p}} \int_{-1}^{\frac{x-x_0}{Ca(t)}} \left[1-\eta^2\right]^{\frac{-1}{q+p}} d\eta, \tag{4.16}$$

and its gradient is given by

$$u_x = \frac{1}{a(t)}\left[\frac{-\alpha\left(q+p\right)}{2\left(1-p\right)}\right]^{\frac{1}{q+p}} C^{\frac{-2}{q+p}} \left[1-\left(\frac{x-x_0}{Ca(t)}\right)^2\right]^{\frac{-1}{q+p}}. \tag{4.17}$$

The relation in equation (4.17) demonstrates significant asymptotic characteristics of image evolution within the boundary layer at the image contour. The width of the transition region is given by $r(t) - l(t)$ equal to:

$$2Ca(t) = 2C\left[\alpha\left(q+p-2\right)t + A_0\right]^{\frac{-1}{q+p-2}}. \tag{4.18}$$

The phenomenon of contour enhancement is discussed in the next for various values of parameters $p$ and $q$.

We now present a set of examples that include exact solutions to illustrate the phenomenon of contour enhancement and its connection to our current study for values where $q < -p$. These examples demonstrate how the mathematical framework under investigation governs the behaviour of contour structures, providing deeper insight into the role of the parameters $p$ and $q$ in shaping the enhancement process.

***Exemple 1.*** $q+p=-\frac{1}{2}$

The equation (4.14) for the profile $\phi$, can be written as :

$$\frac{d\phi}{d\xi}=\left[\frac{\alpha}{4(p-1)}\right]^2\left[1-\left(\frac{\xi}{C}\right)^2\right]^2, \tag{4.19}$$

Continued integration, as well as the use of the boundary conditions $\phi(-C)=0$, $\phi(C)=1$, then the solution of the problem is written as

$$u(x,t)=\frac{15}{16}\left[\frac{1}{5}\left(\frac{x}{C(T-t)^{\frac{2}{5}}}\right)^5-\frac{2}{3}\left(\frac{x}{C(T-t)^{\frac{2}{5}}}\right)^3+\frac{x}{C(T-t)^{\frac{2}{5}}}+\frac{8}{15}\right],$$

The gradients are given by

$$u_x(x,t)=\frac{C^4}{100(T-t)^{\frac{2}{5}}}\left[1-\left(\frac{x}{C(T-t)^{\frac{2}{5}}}\right)^2\right]^2,$$

The solution is established for all $t\in(0,T)$ ; where $T$ represents the blow-up time of the solution such that:

$$\forall x\in\mathbb{R}_+,\ \lim_{t\to T^-}u(x,t)=+\infty \text{ and } \forall x\in\mathbb{R}_-,\ \lim_{t\to T^-}u(x,t)=-\infty$$

and

$$\forall x\in\mathbb{R},\ \lim_{t\to T^-}u_x(x,t)=+\infty$$

From the given Figure in 4.4. In the given example for $q+p=-\frac{1}{2}$, we observe the evolution of the intensity function $u(x,t)$ over time. As $t$ increases, the function $u$ remains continuous, while its first derivative $u_x$ experiences a significant change. Specifically, as $t\to T$, the derivative undergoes an infinite discontinuity, resulting in the formation of a nearly vertical front at $x=0$. This phenomenon illustrates the process of contour enhancement, where the gradient of the function becomes extremely steep, effectively sharpening the transition between different intensity regions. Such behaviour highlights the impact of the governing equation in enhancing contour definition within the image.

***Exemple 2.*** $q+p=-1$

In this case, The equation (4.14) for the profile $\phi$, can be written as :

$$\frac{d\phi}{d\xi}=\frac{C^2}{6}\left[1-\left(\frac{\xi}{A}\right)^2\right], \tag{4.20}$$

Additional integration applying the boundary constraints $\phi(-C)=0$, $\phi(C)=1$, then the solution of the problem is written as

$$u(x,t)=-\frac{1}{4}\left(\frac{x}{C(T-t)^{\frac{1}{3}}}\right)^3+\frac{3}{4}\frac{x}{C(T-t)^{\frac{1}{3}}}+\frac{1}{2},$$

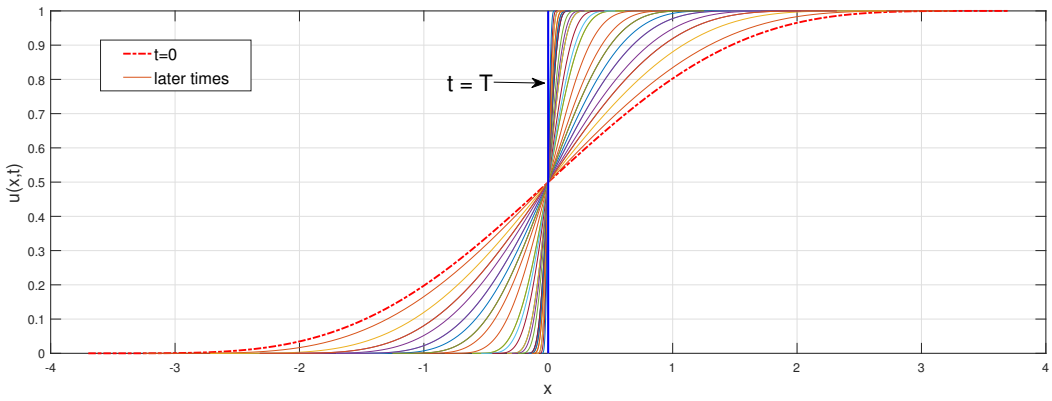


Figure 4.4: The evolution of the image intensity distribution $u(x,t)$. For value of $p=2$ and $q=\frac{5}{2}$.

The gradients are given by

$$u_x(x,t) = \frac{C^2}{6\,(T-t)^{\frac{1}{3}}}\left[1-\left(\frac{x}{C\,(T-t)^{\frac{1}{3}}}\right)^2\right],$$

we can see that if $t \to T^-$, then we obtain $u_x(x,t) \to \infty$, and

$$\forall x \in \mathbb{R}_+,\ \lim_{t\to T^-} u(x,t) = +\infty \text{ and } \forall x \in \mathbb{R}_-,\ \lim_{t\to T^-} u(x,t) = -\infty$$

From the provided figure in 4.5, the evolution of the intensity function $u(x,t)$ is examined for the case where $q+p=-1$. As time $t$ progresses, the function $u$ maintains its continuity, whereas its first derivative $u_x$ undergoes a notable transformation. In particular, as $t$ approaches $T$, the derivative $u_x$ develops an infinite discontinuity, leading to the creation of an almost vertical front at $x=0$. This behavior demonstrates contour enhancement, where the function gradient becomes exceedingly steep, thereby sharpening the transition between distinct intensity regions. Such dynamics underscore the influence of the governing equation in improving the definition of contours within the image.

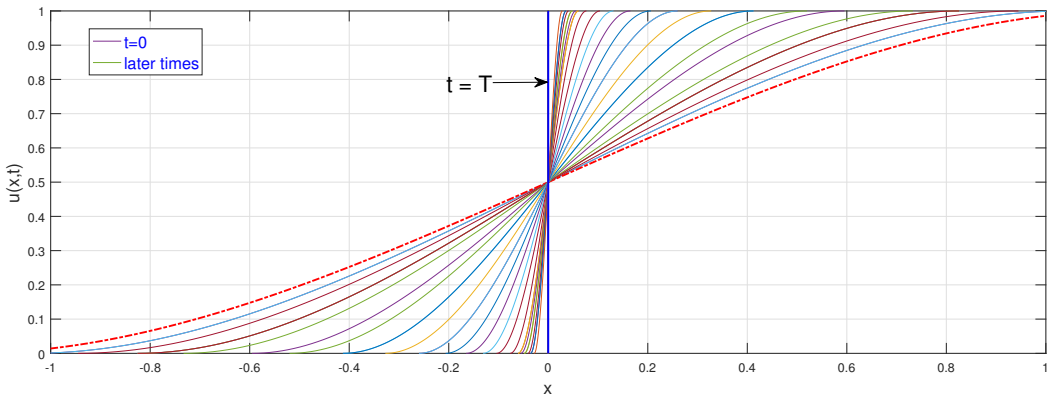


Figure 4.5: The evolution of the image intensity distribution $u(x,t)$. For value of $p=2$ and $q=-3$.

***Exemple 3.*** $q+p=-2$

In this case, The equation (4.14)for the profile $\phi$, can be written as :

$$\frac{d\phi}{d\xi}=\frac{C}{2}\left[1-\left(\frac{\xi}{C}\right)^2\right]^{\frac{1}{2}}, \tag{4.21}$$

Subsequent integration and the application of the boundary conditions $\phi(-C)=0$, $\phi(C)=1$, then the solution of the problem is written as

$$u(x,t)=\frac{1}{\pi}\left(\arcsin\left(\frac{x}{C(T-t)^{\frac{1}{4}}}\right)+\frac{x}{C(T-t)^{\frac{1}{4}}}\sqrt{1-\left(\frac{x}{C(T-t)^{\frac{1}{4}}}\right)^2}\right)+\frac{1}{2},$$

The gradients are given by

$$u_x(x,t)=\frac{C}{2(T-t)^{\frac{1}{4}}}\left[1-\left(\frac{x}{C(T-t)^{\frac{1}{4}}}\right)^2\right]^{\frac{1}{2}},$$

In the Figure 4.6, It is seen that the intensity function $u$ is continuous over the two delimiting curves; nevertheless, its derivative $u_x$ suffers an infinite jump. Moreover, the evolution arrives at a vertical front, so the enhancement happens. we can see that if $t\to T^-$, then we obtain $u_x(x,t)\to\infty$.

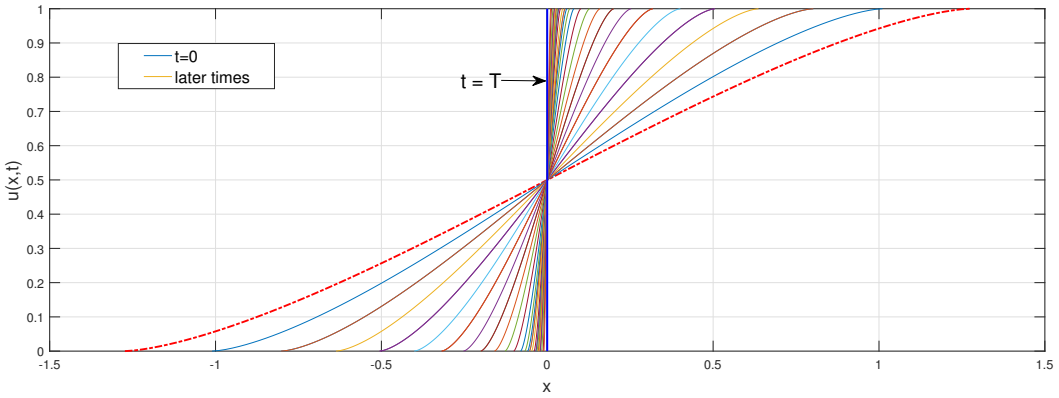


Figure 4.6: The evolution of the image intensity distribution $u(x,t)$. For value of $p=2$ and $q=-4$.

## 4.2 Cases of Free Boundary Problems and Contour Non-Enhancement

We try now to solve problem (2.23) for $q>1-p$ and $p<1$, by using the self-similar solution under the form (2.12). Taking account this form, substituting (2.12) into problem (2.23), we obtain, the equation:

$$-\frac{\dot{a}}{a}\xi\frac{d\phi}{d\xi}=(1-p)\frac{1}{a^{-(q+p)+2}}\frac{d^2\phi}{d\xi^2}\left(\frac{d\phi}{d\xi}\right)^{-(q+p)},\quad \text{for } q>1-p. \tag{4.22}$$

The argument of separation of variables necessitates that the subsequent conditions be satisfied:

$$\frac{\dot{a}}{a} = -\alpha \frac{1}{a^{-(q+p)+2}} \ , \tag{4.23}$$

where $\alpha < 0$ is arbitrary negative constant.

The equation for the profile $\phi$, becomes:

$$\alpha\xi \frac{d\phi}{d\xi} = (1-p) \frac{d^2\phi}{d\xi^2} \left(\frac{d\phi}{d\xi}\right)^{-(q+p)} .$$

After easy integration, we get:

$$\frac{d\phi}{d\xi} = \left[\frac{\alpha(q+p)}{2(1-p)}\right]^{\frac{-1}{q+p}} C^{\frac{-2}{q+p}} \left[1 - \left(\frac{\xi}{C}\right)^2\right]^{\frac{-1}{q+p}} , \tag{4.24}$$

for

$$-C \le \xi \le C.$$

Here, $C$ is a positive integration constant. For $\xi = \frac{x-x_0}{a(t)}$, we have:

$$x_0 - Ca(t) \le x \le x_0 + Ca(t).$$

The problem (4.24)-(4.2) suggests a free-boundary problem specifically to determine the evolution of the image intensity in the boundary layer $l(t)$ and $r(t)$ such that $l(t) \le x \le r(t)$, with $l(t) = x_0 - Ca(t)$ and $r(t) = x_0 + Ca(t)$.

The resolution of (4.23) gives,

$$a(t) = \left[\alpha(q+p-2)t + A_0\right]^{\frac{-1}{q+p-2}}, \quad \text{for } 0 < t < \infty \quad \text{if } q > 2-p, \tag{4.25}$$

and

$$a(t) = \left[\alpha(q+p-2)t + A_0\right]^{\frac{-1}{q+p-2}}, \quad \text{for } 0 < t < T \quad \text{if } 1-p < q < 2-p, \tag{4.26}$$

where $A_0 > 0$, is a constant, and $T$ is obtained as

$$T = -\frac{A_0}{\alpha(q+p-2)}.$$

In the particular case $q = 2-p$, we have:

$$a(t) = e^{(p-1)\pi^2 t}, \quad \text{for } 0 < t < \infty. \tag{4.27}$$

Furthermore, by integrating equation (4.24) and applying the appropriate boundary conditions, we can derive the following results: $\phi(-C) = 0$ and $\phi(C) = 1$. This leads to the subsequent solution:

$$\phi(\xi) = \left[\frac{\alpha(q+p)}{2(1-p)}\right]^{\frac{-1}{q+p}} C^{\frac{q+p-2}{q+p}} \int_{-1}^{\frac{\xi}{C}} \left[1-\eta^2\right]^{\frac{-1}{q+p}} d\eta,$$

where

$$C = \left[\frac{\alpha\left(q+p\right)}{2\left(1-p\right)}\right]^{-\frac{1}{q+p-2}} \left[2\int_0^1 \left[1-\eta^2\right]^{\frac{-1}{q+p}} d\eta\right]^{\frac{-(q+p)}{q+p-2}},$$

for $q \neq 2-p$.

The self-similar solution takes the following form

$$u\left(x,t\right) = \left[\frac{\alpha\left(q+p\right)}{2\left(1-p\right)}\right]^{\frac{-1}{q+p}} C^{\frac{q+p-2}{q+p}} \int_{-1}^{\frac{x-x_0}{Ca(t)}} \left[1-\eta^2\right]^{\frac{-1}{q+p}} d\eta, \tag{4.28}$$

and its gradient is given by

$$u_x = \frac{1}{a(t)} \left[\frac{\alpha\left(q+p\right)}{2\left(1-p\right)}\right]^{\frac{-1}{q+p}} C^{\frac{-2}{q+p}} \left[1-\left(\frac{x-x_0}{Ca(t)}\right)^2\right]^{\frac{-1}{q+p}}. \tag{4.29}$$

The relation in equation (4.29) demonstrates significant asymptotic characteristics of image evolution within the boundary layer at the image contour. The width of the transition region is given by $r\left(t\right) - l\left(t\right)$ equal to:

$$2Ca\left(t\right) = 2C\left[\alpha\left(q+p-2\right)t + C_0\right]^{\frac{-1}{q+p-2}}. \tag{4.30}$$

The phenomenon of contour enhancement is discussed in the next for various values of parameters $p$ and $q$.

**Exemple.** $q = 2-p$

$$u_t(x,t) = -u_x^{-2} u_{xx}. \tag{4.31}$$

We try now to solve problem (4.31) by introducing the the self-similar solution written under the form :

$$u\left(x,t\right) = \phi\left(xe^{-\pi^2 t}\right) \quad x \in \mathbb{R},\ t > 0. \tag{4.32}$$

The equation for the profile $\phi$, becomes:

$$\left(\frac{d\phi}{d\xi}\right)^{-2} = -\pi^2\xi^2 + k, \tag{4.33}$$

which can be written after integration as

$$\frac{d\phi}{d\xi} = \frac{1}{\pi} C^{-1} \left[1-\left(\frac{\xi}{C}\right)^2\right]_+^{-\frac{1}{2}}, \tag{4.34}$$

for

$$-C \leq \xi \leq C$$

then we obtain, after integration and using the boundary conditions$\phi(-C) = 0$, $\phi(C) = 1$

$$\phi\left(\xi\right) = \frac{1}{\pi}\arcsin\left(\frac{\xi}{C}\right) + \frac{1}{2}, \tag{4.35}$$

The self-similar solution assume the form

$$u(x,t) = \frac{1}{\pi}\arcsin\left(\frac{x}{Ce^{\pi^2 t}}\right) + \frac{1}{2}, \tag{4.36}$$

The gradients are given by

$$u_x(x,t) = \frac{1}{\pi}C^{-1}\left[1 - \left(\frac{x}{Ce^{\pi^2 t}}\right)^2\right]^{-\frac{1}{2}},$$

Solution (4.36) demonstrates that , the smoothed stepwise initial distribution extends with time; its properly defined width increases with time proportionally to $e^{\pi^2 t}$, and the maximum of the derivative modulus $|\partial_x u|$ , decreases with time as $e^{-\pi^2 t}$. this yields to blurred contours.

So, qualitatively the situation for any $q > 1 - p$ is the same as in the case of $q = 2 - p$: this type of equations leads blurred contours of images.

Based Figure 4.7 , we analyse the evolution of the image intensity distribution $u(x,t)$ for the given parameter values $p = 2$ and $q = 0$.

At $t = 0$, the function $u(x,0)$ (depicted by the dashed red line) is smooth and continuous, representing the initial intensity distribution. As time progresses, the solution evolves according to the governing equation, leading to changes in the function's shape.

As $t \to T$, we observe that $u(x,t)$ remains continuous across the domain. However, its first derivative $u_x$ does not exhibit an infinite discontinuity or steepening effect. Instead of forming a sharp transition or an enhanced contour, the function undergoes a gradual smoothing process, indicating the absence of contour enhancement. This behaviour is fundamentally different from cases where the evolution sharpens image contours, suggesting that for $p = 2 - p$, the governing equation leads to contour diffusion rather than enhancement.

This result highlights the influence of parameter selection on the contour dynamics and confirms that under these conditions, the model does not enhance contour but rather contributes to their smoothing over time.

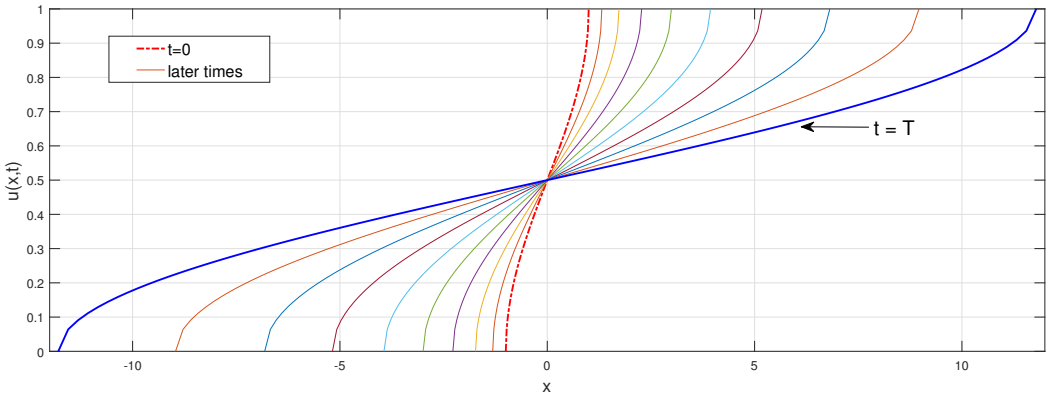


Figure 4.7: The evolution of the image intensity distribution $u(x,t)$. For value of $p = 2$ and $q = 0$.

## 4.3 Conclusion and Comments

This chapter has explored cases where $p > 1$, introducing a novel model derived from the principal problem under investigation. This model is closely associated with inverse problems involving free boundaries or boundary value problems. A detailed analysis has been conducted on the enhancement of image contours, demonstrating significant potential for future advancements in "Schocfilter" models, which are renowned for their efficacy in image restoration. The findings presented herein offer valuable insights and contribute to the ongoing evolution of image processing and restoration techniques. This study underscores the importance of the proposed approach and its potential to drive further progress in this field.

# *Conclusion*

This thesis introduce a new evolution model that generalizes mean curvature motion and provides a comprehensive study of contour enhancement via the formulation of a free boundary problem. We addressed a free boundary problem related to contour enhancement in image processing, modeled through a partial differential equation. The primary objective was to explore and construct general self-similar solutions to describe the dynamics of contour enhancement and its underlying mechanisms. This approach provides a deeper mathematical framework for understanding how image contours evolve over time, particularly under the influence of specific parameters. The methodology employed in this study involves the pursuit of general self-similar solutions to elucidate the phenomenon of contour enhancement within the realm of image processing.

The originality of this work lies in extending and generalizing the results of Barenblatt and Vásquez [9][55], who previously tackled similar problems in the context of free boundary phenomena. Our work introduces significant advancements. By seeking more generalized self-similar solutions, we provide a broader understanding of the contour enhancement process, allowing the model to be applied to more complex and realistic scenarios in image processing. The results highlight how the evolution of contours is driven by specific parameter values, which control the balance between noise reduction and contour sharpening. This insight not only confirms the effectiveness of the proposed mathematical model but also opens the door for future applications in contour detection, image segmentation, and visual data analysis. We also presented some numerical simulations for the proposed model on 2-D gray-level images to validate the theoretical findings. The numerical experiments demonstrate the effectiveness of the model in preserving and enhancing contours, confirming the practical applicability of the theoretical results.

Looking ahead, we aim to expand this study by systematically examining the behaviour of the equation in broader image processing. This will involve exploring its relationship with image restoration tasks, particularly in cases involving noise reduction, contour preservation, and texture enhancement. Furthermore, we intend to investigate the generalisation of Schoc filter models to more complex imaging problems. By doing so, we hope to contribute to the development of more efficient and adaptive image restoration techniques, while deepening the theoretical understanding of PDE-based models in this field.

# Bibliography


[1] Achour, H., Chouder, R., and Benhamidouche, N.(2024). *Self-Similar Solutions for a New Free-Boundary Problem and Image Contour Enhancement*. Dynamics of Continuous, Discrete and Impulsive Systems Series B: Applications and Algorithms, 31, 321-337.

[2] Alvarez, L., Guichard, F., Lions, P. L., and Morel, J. M. (1993). *Axioms and fundamental equations of image processing*. Archive for rational mechanics and analysis, 123, 199-257.

[3] Alvarez, L., Lions, P. L., and Morel, J. M. (1992). *Image selective smoothing and edge detection by nonlinear diffusion. II*. SIAM Journal on numerical analysis, 29(3), 845-866.

[4] Alvarez, L., and Mazorra, L. (1994). *Signal and image restoration using shock filters and anisotropic diffusion*. SIAM journal on numerical analysis, 31(2), 590-605.

[5] Angenent, S. (1988). *Local existence and regularity for a class of degenerate parabolic equations*. Mathematische Annalen, 280, 465-482.

[6] Arehart, A. B., Vincent, L., and Kimia, B. B. (1993, May). *Mathematical morphology: The hamilton-jacobi connection*. In 1993 (4th) International Conference on Computer Vision, 215-219. IEEE.

[7] Aronson, D. G., and Vázquez, J. L. (1987). *Eventual $C^{\infty}$-regularity and concavity for flows in one-dimensional porous media*. Archive for Rational Mechanics and Analysis, 99, 329-348.

[8] Aubert, G., and Kornprobst, P. (2006). *Mathematical problems in image processing: partial differential equations and the calculus of variations* (Vol. 147, p. 1). New York, NY: Springer.

[9] Barenblatt, G. I. (2001). *Self-similar intermediate asymptotics for nonlinear degenerate parabolic free-boundary problems that occur in image processing*. Proceedings of the National Academy of Sciences, 98(23), 12878-12881.

[10] Barenblatt, G. I., Bertsch, M., Chertock, A. E., and Prostokishin, V. M. (2000). *Self-similar intermediate asymptotics for a degenerate parabolic filtration-absorption equation*. Proceedings of the National Academy of Sciences, 97(18), 9844-9848.

[11] Barenblatt, GI and Višik, MI. (1956). *On finite velocity of propagation in problems of non-stationary filtration of a liquid or gas*. Prikladnaja Matematika i Mehanika, 20, 411-417.

[12] Basti, B., and Benhamidouche, N. (2020). *Global existence and blow-up of generalized self-similar solutions to nonlinear degenerate diffusion equation not in divergence form*. Appl. Math. E-Notes, 20, 367-387.

[13] Benhamidouche, N. (2008). *Exact solutions to some nonlinear PDEs, travelling profiles method*. Electronic Journal of Qualitative Theory of Differential Equations, 2008(15), 1-7.

[14] Bertero, M., Poggio, T. A., and Torre, V. (1988). *Ill-posed problems in early vision*. Proceedings of the IEEE, 76(8), 869-889.

[15] Black, M. J., Sapiro, G., Marimont, D. H., and Heeger, D. (1998). *Robust anisotropic diffusion*. IEEE Transactions on image processing, 7(3), 421-432.

[16] Caselles, V., and Morel, J. (1998). *Introduction to the special issue on partial differential equations and geometry-driven diffusion in image processing and analysis*. IEEE transactions on image processing, 7(3), 269-273.

[17] Catté, F., Lions, P. L., Morel, J. M., and Coll, T. (1992). *Image selective smoothing and edge detection by nonlinear diffusion*. SIAM Journal on Numerical analysis, 29(1), 182-193.

[18] Chan, T. F., and Shen, J. (2005). *Image processing and analysis: variational, PDE, wavelet, and stochastic methods*. Society for Industrial and Applied Mathematics.

[19] Charbonnier, P., Blanc-Feraud, L., Aubert, G., and Barlaud, M. (1994, November). *Two deterministic half-quadratic regularization algorithms for computed imaging*. In Proceedings of 1st international conference on image processing (Vol. 2, pp. 168-172). IEEE.

[20] Chouder, R., and Benhamidouche, N. (2019). *New exact solutions to nonlinear diffusion equation that occurs in image processing*. International Journal of Computing Science and Mathematics, 10(4), 364-374.

[21] Chouder, R., and Benhamidouche, N. (2018). *Travelling profile solutions for nonlinear degenerate parabolic equation and contour enhancement in image processing*. Applied Mathematics E-Notes, 18, 1-12.

[22] DiBenedetto, E. (2012). *Degenerate parabolic equations*. Springer Science and Business Media.

[23] Didas, S., and Weickert, J. (2007, May). *Combining curvature motion and edge-preserving denoising*. In International Conference on Scale Space and Variational Methods in Computer Vision (pp. 568-579). Berlin, Heidelberg: Springer Berlin Heidelberg.

[24] Fischl, B., and Schwartz, E. L. (1997). *Learning an integral equation approximation to nonlinear anisotropic diffusion in image processing*. IEEE Transactions on Pattern Analysis and Machine Intelligence, 19(4), 342-352.

[25] Gage, M. E. (1984). *Curve shortening makes convex curves circular*. Inventiones mathematicae, 76, 357-364.

[26] Gage, M., and Hamilton, R. S. (1986). *The heat equation shrinking convex plane curves*. Journal of Differential Geometry, 23(1), 69-96.

[27] Galić, I., Weickert, J., Welk, M., Bruhn, A., Belyaev, A., and Seidel, H. P. (2005, October). *Towards PDE-based image compression*. In International Workshop on Variational, Geometric, and Level Set Methods in Computer Vision (pp. 37-48). Berlin, Heidelberg: Springer Berlin Heidelberg.

[28] Gilboa, G., Sochen, N. A., and Zeevi, Y. Y. (2002). *Regularized shock filters and complex diffusion*. In Computer Vision-ECCV 2002: 7th European Conference on Computer Vision Copenhagen, Denmark, May 28-31, 2002 Proceedings, Part I 7 (pp. 399-413). Springer Berlin Heidelberg.

[29] Guichard, F., and Morel, J. M. (2001, June). *A note on two classical shock filters and their asymptotics*. In International Conference on Scale-Space Theories in Computer Vision (pp. 75-84). Berlin, Heidelberg: Springer Berlin Heidelberg.

[30] Huisken, G., *Flow by mean curvature of convex surfaces into spheres*. Journal of Differential Geometry, 20, 237–266 (1984).

[31] Iijima, T.: *Basic equation of figure and observational transformation*. Systems, Computers, Controls 2(4), 70–77 (1971)

[32] Joo, K., and Kim, S. (2003). *PDE-based image restoration, I: antistaircasing and anti-diffusion*. preprint.

[33] Kalashnikov, A. S. (1987). *Some problems of the qualitative theory of non-linear degenerate second-order parabolic equations*. Russian Mathematical Surveys, 42(2), 169-222.

[34] Kimmel, R. (2003). *Numerical Geometry of Images: Theory, Algorithms, and Applications*. Springer Verlag, New York, 50-60.

[35] Kimmel, R., Sochen, N., and Malladi, R. (1997). *From high energy physics to low level vision*. In Scale-Space Theory in Computer Vision: First International Conference, Scale-Space'97 Utrecht, The Netherlands, July 2-4, 1997 Proceedings 1 (pp. 236-247). Springer Berlin Heidelberg.

[36] Koenderink, J. J. (1984). *The structure of images*. Biological cybernetics, 50(5), 363-370.

[37] Kornprobst, P., Deriche, R., and Aubert, G. (1997, June). *Nonlinear operators in image restoration*. In Proceedings of IEEE Computer Society Conference on Computer Vision and Pattern Recognition (pp. 325-330). IEEE.

[38] Kramer, H. P., and Bruckner, J. B. (1975). *Iterations of a non-linear transformation for enhancement of digital images*. Pattern recognition, 7(1-2), 53-58.

[39] Malladi, R., and Sethian, J. A. (1995). *Image processing via level set curvature flow*. proceedings of the National Academy of sciences, 92(15), 7046-7050.

[40] Malladi, R., and Sethian, J. A. (1996). *Image processing: Flows under min/max curvature and mean curvature*. Graphical models and image processing, 58(2), 127-141.

[41] Marquina, A., and Osher, S. (2000). *Explicit algorithms for a new time dependent model based on level set motion for nonlinear deblurring and noise removal*. SIAM Journal on Scientific Computing, 22(2), 387-405.

[42] Marr, D., and Hildreth, E. (1980). *Theory of edge detection. Proceedings of the Royal Society of London*. Series B. Biological Sciences, 207(1167), 187-217.

[43] Morel, J. M., and Solimini, S. (2012). *Variational methods in image segmentation*: with seven image processing experiments (Vol. 14). Springer Science and Business Media.

[44] Osher, S., and Rudin, L. I. (1991, December). *Shocks and other nonlinear filtering applied to image processing*. In Applications of Digital Image Processing XIV (Vol. 1567, pp. 414-431). SPIE.

[45] Osher, S., and Rudin, L. I. (1990). *Feature-oriented image enhancement using shock filters*. SIAM Journal on numerical analysis, 27(4), 919-940.

[46] Osher, S., and Sethian, J. A. (1988). *Fronts propagating with curvature-dependent speed: Algorithms based on Hamilton-Jacobi formulations*. Journal of computational physics, 79(1), 12-49.

[47] Perona, P., and Malik, J. (1990). *Scale-space and edge detection using anisotropic diffusion*. IEEE Transactions on pattern analysis and machine intelligence, 12(7), 629-639.

[48] Schavemaker, J. G., Reinders, M. J., Gerbrands, J. J., and Backer, E. (2000). *Image sharpening by morphological filtering*. Pattern Recognition, 33(6), 997-1012.

[49] Sethian, J. A. (1982). *An Analysis of Flame Propagation [Ph. D. dissertation]*. Department of Mathematics, University of California, USA.

[50] Sochen, N., Kimmel, R., and Malladi, R. (1998). *A general framework for low level vision*. IEEE transactions on image processing, 7(3), 310-318.

[51] Schönlieb, C. B. (2015). *Partial differential equation methods for image inpainting*. (Vol. 29). Cambridge University Press.

[52] Strong, D., and Chan, T. (2003). *Edge-preserving and scale-dependent properties of total variation regularization*. Inverse problems, 19(6), S165.

[53] Terebes, R. M. (2004). *Diffusion directionnelle: applications à la restauration et à l'amélioration d'images de documents anciens* .(Doctoral dissertation), Université Bordeux I - France.

[54] Van Den Boomgaard, R., and Smeulders, A. (1994). *The morphological structure of images: The differential equations of morphological scale-space*. IEEE transactions on pattern analysis and machine intelligence, 16(11), 1101-1113.

[55] Vázquez, J. L., and Barenblatt, G. I. (2004). *Nonlinear diffusion and image contour enhancement*. Interfaces and Free Boundaries, 6(1), 31-54.

[56] Weickert, J. (1998). *Anisotropic diffusion in image processing*. (Vol. 1, pp. 59-60). Stuttgart: Teubner.

[57] Weickert, J. (2003, September). *Coherence-enhancing shock filters*. In Joint Pattern Recognition Symposium (pp. 1-8). Berlin, Heidelberg: Springer Berlin Heidelberg.

[58] Welk, M., Breuß, M., and Vogel, O. (2011). *Morphological amoebas are self-snakes*. Journal of Mathematical Imaging and Vision, 39, 87-99.

[59] Witkin, A. P. (1987). *Scale-space filtering*. In Readings in computer vision (pp. 329-332). Morgan Kaufmann.

[60] Yezzi, A. (1998). *Modified curvature motion for image smoothing and enhancement*. IEEE Transactions on Image Processing, 7(3), 345-352.

***Abstract***

The nonlinear diffusion equation is used to analyze the process of edge enhancement in image processing, based on a new evolution model considered as a generalization of mean curvature motion. A free boundary problem is formulated describing the image intensity evolution in the boundary layers around the edges of the image. An asymptotic self-similar solutions to this nonlinear diffusion equation is obtained in explicit forms. The solutions demonstrated that the edge enhancement and its rates depends on the parameters of equation. The experimental results demonstrate the effectiveness of the model in edge preservation.
**Key words:** Nonlinear diffusion equations - Mean curvature motion - Image processing- contour enhancement - Free boundaries - Self-similar solutions.

***Résumé***

L´equation de diffusion non linéaire est utilisée pour analyser le processus de rehaussement des contours en traitement d'image, en se basant sur un nouveau modèle d'évolution considéré comme une généralisation du mouvement de courbure moyenne. Un problème de frontière libre est formulé décrivant l'évolution de l'intensité de l'image dans les couches limites autour des bords de l'image. Une solution auto-similaire asymptotique à cette équation de diffusion non linéaire est obtenue sous des formes explicites. Les solutions ont démontré que le rehaussement des contours et ses taux dépendent des paramètres de l'équation. Les résultats expérimentaux démontrent l'efficacité du modèle dans la préservation des contours.
**Mots-clés:** Equations de diffusion non linéaires - Mouvement de courbure moyenne - Traitement de l' image -Amélioration de contour. - Frontières libres - Solutions auto-similaires.

**ملخص**

تُستخدم معادلة الانتشار غير الخطية لتحليل عملية تعزيز الحافة في معالجة الصور، استنادًا إلى نموذج تطور جديد يُعتبر تعميمًا لحركة الانحناء المتوسط. يتم صياغة مشكلة حدودية حرة تصف تطور شدة الصورة في طبقات الحدود حول حواف الصورة. يتم الحصول على حلول مقاربة ذاتية التشابه لهذه المعادلة الانتشارية غير الخطية في أشكال صريحة. أظهرت الحلول أن تعزيز الحافة ومعدلاته يعتمد على معلمات المعادلة. توضح النتائج التجريبية فعالية النموذج في الحفاظ على الحافة.
**الكلمات المفتاحية:** معادلات الانتشار غير الخطية ـ حركة الانحناء المتوسط ـ معالجة الصور ـ تحسين الحواف ـ الحدود الحرة ـ الحلول ذاتية التشابه.